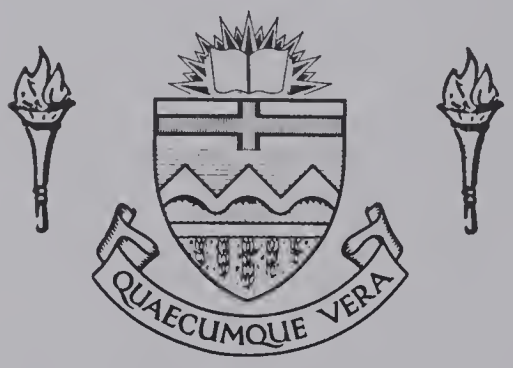

The University of Alberta
Printing Department
Edmonton, Alberta

THE UNIVERSITY OF ALBERTA

PRANDTL NUMBER DEPENDENCE OF THE UNSTEADY COMPRESSIBLE BOUNDARY LAYER

BY

© BERNARD LUFT

A THESIS

SUBMITTED TO THE FACULTY OF GRADUATE STUDIES

IN PARTIAL FULFILMENT OF THE REQUIREMENTS FOR THE DEGREE OF

MASTER OF SCIENCE

DEPARTMENT OF MECHANICAL ENGINEERING

EDMONTON, ALBERTA

SPRING, 1971

UNIVERSITY OF ALBERTA

FACULTY OF GRADUATE STUDIES

The undersigned certify that they have read, and recommend to the faculty of Graduate Studies for acceptance, a thesis entitled "PRANDTL NUMBER DEPENDENCE OF THE UNSTEADY COMPRESSIBLE BOUNDARY LAYER" submitted by BERNARD LUFT in partial fulfilment of the requirements for the degree of Master of Science.

ABSTRACT

The unsteady compressible laminar boundary layer on a stepwise accelerated semi-infinite flat plate at zero incidence is investigated for Prandtl numbers different from unity. A semi-similarity transformation is employed to transform the pertinent boundary layer equations such that the new independent variables become

$$\eta = \left(\sqrt{\frac{(m+1)\,U_e}{2\nu_{ref}\,Cx}}\right) Y \text{ , and } \tau = \frac{U_e t}{x} .$$

The equations are uncoupled for the case of a zero pressure gradient and are further linearized before a numerical solution is obtained. The energy equation with Pr = 0.72 is solved in two different ways. First, an initial condition is obtained by assuming that $\frac{\partial g}{\partial \tau}(\eta,0) = 0$, where $g(\eta,\tau) \equiv \frac{h}{h_e}(\eta,\tau)$ and second, by employing an empirical steady state enthalpy distribution as a solution for the unsteady case. For a range of Mach numbers $5 \leq M_e \leq 10$ the transient wall shear stress, heat transfer and weak-interaction induced pressure are obtained for both the isothermal and insulated wall.

ACKNOWLEDGEMENTS

The author wishes to express his thanks and acknowledgements to the following:

(i) Dr. C.M. Rodkiewicz for his guidance, encouragement and supervision of the thesis.

(ii) Prof. W. Jackson, from the Department of Computing Science, for his helpful discussions.

(iii) Miss Helen Wozniuk for her excellent typing of the thesis.

(iv) My wife, Audrey, for her patience, encouragement, typing of the first draft and proof reading the manuscript for grammar and spelling.

TABLE OF CONTENTS

TABLE OF CONTENTS (continued)

LIST OF FIGURES

LIST OF FIGURES (continued)

LIST OF FIGURES (continued)

LIST OF SYMBOLS

a	velocity of sound
a	coefficient in the recurrence relations (3.9) and (3.31)
A	a constant
b	coefficient in the recurrence relations (3.9) and (3.31)
c	coefficient in the recurrence relations (3.9) and (3.31)
C	a function of η and ξ defined by (3.13) or (3.38)
C	a constant or function of x in (2.11)
C_f	skin friction coefficient defined by (4.7)
c_p	specific heat at constant pressure
c_v	specific heat at constant volume
C_1	a constant defined by (3.47)
d	coefficient in the recurrence relations (3.9) and (3.31)
E	Eckert number
e	coefficient in the recurrence relation (3.9)
e	a constant in expression (2.19)
f	dimensionless stream function defined by (2.20)
g	dimensionless enthalpy ratio defined by (2.21)
G	scaling function in similarity transformation (2.21)
h	unsteady enthalpy
H	stepsize in the space (η) direction
I	integral in the displacement thickness defined by (4.23)

J	integral in the displacement thickness defined by (4.24)
k	thermal conductivity
m	a constant in (2.19)
m	time index corresponding to ξ in the numerical solution
M	Mach number
n	space index corresponding to η in the numerical solution
N	value of n corresponding to the free stream
Nu_x	local instantaneous Nusselt number
p	thermodynamic pressure in the equation of state (2.13)
Pr	Prandtl number defined by (4.4a)
q	instantaneous heat transfer per unit area defined by (4.1)
r	a function of η defined by (3.44)
R	a function of η and ξ defined by (3.12) or (3.37)
R	gas constant
Re_x	local Reynolds number defined by (4.46)
s	a function of η defined by (3.45)
s	representation of stream function increment Δf in the recurrence relation (3.11) and also in the computer program
S	a constant in (2.10)
St	Stanton number defined by (4.5)
t	time
T	stepsize in the time (τ or ξ) direction
T	temperature
u	velocity component in the x-direction parallel to the plate
U	free stream velocity

U	representation of enthalpy ratio increment Δg in the recurrence relation (3.31) and also in the computer program
v	velocity component in the y-direction normal to the plate
W_p	instantaneous piston velocity in expression (1.9)
x	Cartesian co-ordinate parallel to the plate
y	Cartesian co-ordinate normal to the plate
Y	"transformed coordinate" normal to the plate defined by (2.7)
α	instantaneous local heat-transfer coefficient defined by (4.3)
β	pressure gradient parameter
γ	ratio of specific heats c_p/c_v
δ	boundary layer thickness
δ^*	displacement thickness defined by (1.1)
δ_ρ	density defect thickness as defined by (4.16)
Δ	unsteady displacement thickness in (4.13)
ε	velocity-increase parameter defined by (2.37)
ζ	dummy variable of integration
η	independent space similarity variable defined by (2.17)
θ	steady body inclination to the free stream direction
θ	dummy variable of integration
μ	dynamic viscosity coefficient
ν	kinematic viscosity coefficient
ξ	independent time and space variable defined by (3.1)
ρ	density

τ	independent time and space similarity variable defined by (2.18)
τ	shear stress
χ	hypersonic pressure-interaction parameter defined by (4.25)
ψ	stream function

Subscripts

e	conditions prevailing in the free stream ($y = y_e$)
raw	evaluation at reference adiabatic wall conditions
ref	evaluation at suitable reference conditions
w	evaluation at the plate ($y = 0$)
x	evaluation at station x downstream from leading edge
0	initial steady state ($\tau<0$)
1	state at instant of change ($\tau=0$)
2	final steady state ($\tau>>0$)
∞	conditions prevailing upstream of the shock wave

CHAPTER I

STATEMENT OF THE PROBLEM AND ASSOCIATED LITERATURE

1.1 Introduction

From boundary layer theory, one effect of the viscous boundary layer on the remaining inviscid flow is an outward deflection of the streamlines near the body such that the effective shape of the body is changed due to the reduced mass flow within this boundary layer. A measure of this displacement of the external flow is given by the displacement thickness defined, for compressible flows, as [1,2]*

$$\delta^* = \int_0^y \left(1 - \frac{\rho u}{\rho_e U_e}\right) dy \ , \quad y \to \infty \ . \tag{1.1}$$

For slender bodies, such as a flat plate, moving at subsonic or low supersonic speeds, δ^* is of the order of $1/\sqrt{Re_x}$ so that for high local Reynolds numbers the manifestations of streamline displacement, such as induced pressures for example, can usually be neglected. For the same body flying at hypersonic speeds, however, the temperature in the boundary layer will be extremely high due to frictional heating and consequently the density will be very low. Thus, as equation (1.1) dictates, the displacement thickness will be large and in fact, the resulting streamline deflection will be of the order of $M_e^2/\sqrt{Re_x}$

---

*Numbers within square brackets refer to corresponding references.

and the induced pressure due to the interaction of this thick boundary layer with the Mach waves in the free stream is of the order of $M_e^3/\sqrt{Re_x}$ [3]. It becomes clear, then, that at hypersonic speeds viscous-inviscid interactions must be taken into account and aside from obtaining the magnitudes of the induced pressure it is desirable to determine what effect such interaction would have upon the surface skin friction and heat transfer coefficients.

In order to study and formulate the above phenomenon the following hypothetical problem is posed. Figure 1.1 depicts a semi-infinite flat plate with a "sharp" leading edge moving in air at hypersonic speeds. The word "sharp" is used in the same sense as in

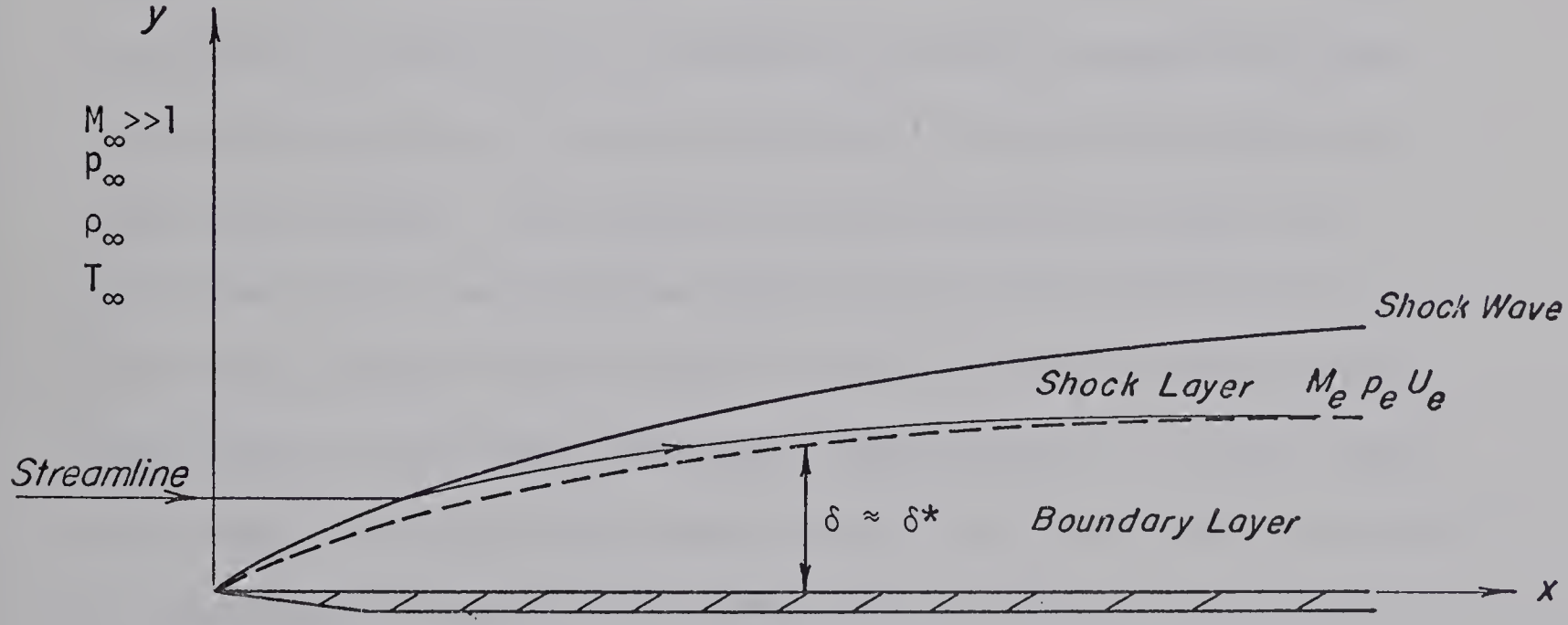

Fig. 1.1 Flat Plate at Hypersonic Speed

Reference [3] and that is to mean that the leading edge of the plate has essentially no effect on the inviscid pressure distribution along the surface. A blunted slender body, for example, would give rise to another interaction phenomenon usually referred to as vorticity interaction but we wish to concern ourselves only with the generally more important type of "self induced" interaction commonly referred to as a pressure interaction. The plate is assumed to be at some arbitrary hypersonic Mach number and zero angle of attack with temperature and velocity profiles at their corresponding initial steady states. The plate's velocity, U_e, is then impulsively increased by a small amount of the order of 1%.

Because of the presence of the boundary layer the external flow near the leading edge must turn as is illustrated by the sketch of a typical streamline. The result is an initial compression leading to the formation of a shock wave which, at high Mach numbers becomes quite strong. The viscous-inviscid interaction comes into play because the flow expansion following the shock determines the free stream pressure which affects the redistribution of the boundary layer which in turn affects the free stream pressure. For the steady states approximate relations governing the free stream induced pressure, p_e, have already been derived and these will be discussed briefly in the following section. Of prime importance also, however, are the problems of maneuverability and control of hypersonic vehicles and these are entirely dependent upon the temporal variations of induced

pressures, shearing stresses and heat transfer. The research in this direction has so far been scarce and in particular all available solutions have involved the common assumption that the Prandtl number is equal to unity. The mathematical formulation and pertinent assumptions used in this work are exactly the same as found in Reference [4]. That is, the two-dimensional, non-steady, compressible boundary layer equations are transformed by the use of the Dorodnitsyn-Howarth variable and the non-steady stream function. A semi-similarity transformation reduces the number of independent variables from three to two. The resulting momentum and energy equations are uncoupled by considering only the so called "weak interaction" region which is the region far downstream from the leading edge where the free stream velocity U_e can be considered a constant and thereby causing the pressure gradient to vanish. The momentum equation is linearized using the method of small perturbations and the resulting linear equation is solved with the aid of a digital computer employing a recurrence type numerical procedure which was also used in Reference [4]. The solution to the momentum equation obtained in this work is slightly more accurate since discretization errors have been reduced by using more nodal values in the computational molecule, reducing the step sizes in the space and time directions and employing double precision for all numerical work.

The major concern of the present analysis is to obtain the solution to the energy equation for any arbitrary Prandtl number and in particular for Pr = .72 which corresponds more closely to the value

for air. The solutions are obtained numerically using a similar recurrence technique as was used for the momentum equation. The effects of this change on the induced pressures, skin friction and heat transfer are discussed and compared with those results for Pr = 1 given in Reference [4]. For the case of Pr = 1 a closed form solution is available both for the insulated wall and the isothermal wall [4]. However, for Pr $\neq$ 1 an initial condition on $g \equiv h/h_e$ is required for the numerical solution of the unsteady energy equation since the condition at infinity cannot be satisfied due to the fact that a solution to the unsteady momentum equation cannot be developed beyond values of $\tau = 1/f_2'$. Thus, it will be demonstrated that by making the reasonable assumption $\partial g/\partial\tau(\eta,0) = 0$, a plausible initial condition on g can be derived.

In Section 3.5 an alternative candidate for a solution to the unsteady energy equation will be introduced. This solution will be in the form of an empirical enthalpy distribution for Prandtl numbers differing only slightly from unity. The empirical distribution will also be seen to reduce to the closed form solutions mentioned above when Pr = 1.

1.2 Review of Associated Literature

The unsteady problem of a sudden increase in velocity of a body already in motion with established velocity and temperature profiles in the boundary layer is quite similar to the problem of impulsive start from rest. In fact, it has been shown (see Sears [5] for example)

that at the time of change and except at the solid boundary (i.e. the plate surface in our case) the new velocity distribution is obtained simply by superimposing the suddenly created velocity on the established velocity profile existing in the boundary layer just before the change. Hence, some of the arguments pertaining to the transient velocity distribution in the boundary layer of a body starting impulsively from rest can equally well be applied to the problem under consideration here. The difference, however, being that the secondary boundary layer, which at the instant of the impulsive motion is in the form of a vortex sheet of zero thickness at the plate surface, grows in thickness and interacts in a non-linear way with the original or primary boundary layer already in existence before the impulsive change [6]. Because of the variation of both velocity and temperature normal to the plate within the primary boundary layer, it would not be reasonable to suppose that the entire time history of the growth of the secondary layer interacting with the primary layer and ultimately reaching a new steady state, would be quite similar to the complete development of a boundary layer from start of motion to the final steady state resulting from impulsive motion from rest.

The study of boundary-layer formation on an infinite flat plate after an impulsive start of motion dates back as far as Stokes, 1901 [2]. The solution to this problem for small times (sometimes referred to as the "Rayleigh problem") is

$$u = U \operatorname{erf}_c \left(\frac{y}{2\sqrt{\nu t}}\right) \tag{1.2}$$

with

$$u(0,t) = U \ .$$

The solution (1.2) is derived from the fact that at the start of boundary layer development the effects of diffusion far outweigh those of convection. At larger times from the start of motion the rate of diffusion balances the rate of convection and the flow field closely approximates a Blasius type of flow which is independent of time. J.T. Stuart (see Chapter VII of Reference [6]) offers an enlightening analysis of bodies starting from rest from a dimensional analysis point of view. For a semi-infinite flat plate impulsively started from rest it turns out that $\tau = Ut/x$ becomes a key variable in the mathematical formulation of the flow. If t is the elapsed time from start, x the distance measured from the leading edge of the plate and U the constant "step input" velocity then for τ very large the flow becomes independent of time and closely assumes the form of a Blasius flow. This flow occurs for a certain distance downstream from, but not including, the leading edge. For τ small the flow is of the Rayleigh type and is not affected by the leading edge. This flow occurs in a region extending from some point downstream from the leading edge to infinity. A transition region must therefore exist between the two types of dominant flows and this region depends on τ. As time increases, the Blasius region extends farther and farther down the plate and as $t \to \infty$, this region dominates everywhere whereas for t

very small, the Rayleigh flow was dominant almost everywhere.

Stewartson [7] obtained extreme solutions to the momentum equation simplified to

$$\frac{\partial u}{\partial t} + U_e \frac{\partial u}{\partial x} = \nu \frac{\partial^2 u}{\partial y^2} \tag{1.3}$$

where Rayleigh's analogy was used to replace the convection terms

$$u \frac{\partial u}{\partial x} + v \frac{\partial u}{\partial y} \quad \text{by} \quad U_e \frac{\partial u}{\partial x} \ .$$

The solutions obtained are

$$u = U_e \operatorname{erf} \left\{ \frac{y}{2\sqrt{\nu t}} \right\} \quad \tau < 1 \tag{1.4}$$

and

$$u = U_e \operatorname{erf} \left\{ \frac{y}{2} \sqrt{\frac{U_e}{\nu x}} \right\} \quad \tau > 1.$$

Strictly speaking these solutions are valid only near the boundary layer edge where $u \approx U_e$ but they do show qualitatively the motion of the Blasius to Rayleigh transition region down the plate as time increases. Using the momentum-integral method as an alternative approximation, Stewartson obtained for the shear stress at the wall

$$\left(\mu \frac{\partial u}{\partial y}\right)_{y=0} = 0.534 \, \rho \, U_e \sqrt{\frac{\nu}{t}} \qquad \tau \leq 2.65 \tag{1.5}$$

$$\left(\mu \frac{\partial u}{\partial y}\right)_{y=0} = 0.328\ \rho\ U_e \sqrt{\frac{U_e \nu}{x}} \qquad \tau \geq 2.65\ . \qquad (1.6)$$

Again an abrupt change from a time dependence to an x-dependence at some definite value of τ is indicated which does not seem physically reasonable. It was further shown by Stewartson that a power series in τ to account for gradual decreasing time dependence and increasing x-dependence cannot be constructed and this is also indicated in the discussion by Stuart.

Many investigators including S.I. Cheng, F.K. Moore, Simon Ostrach and others have studied similar problems and a resumé of their works may be found in Reference [4]. In each case a singularity was encountered in the neighbourhood of $\tau = 1$. Rodkiewicz and Reshotko [4] solved numerically the unsteady momentum equation describing the present problem but the solution could not be generated very far beyond $\tau = 1$. Rodkiewicz and Gupta [8] extended the solution slightly to $\tau = 1.3$ by use of double precision but the apparent success is misleading since the present writer has solved the same equation using double precision as well but reducing discretization errors by including extra nodal values in the computational molecule and reducing both stepsizes in space and time to 1/10th of the values used in both [4] and [8]. The results show a discontinuity beginning at a value of τ only slightly greater than unity. However, no serious attempt has been made in this work to resolve this problem.

The effects of Prandtl number variation on steady laminar

compressible flows have been quite thoroughly discussed by several authors. Flügge-Lotz and Arlo F. Johnson [9], for example, concluded that the drag of an insulated flat plate at zero angle of attack is unaffected by Mach and Prandtl numbers and that Prandtl number variation appears to create a significant change only in the enthalpy profile. They do not, however, consider boundary-layer shock-wave interaction. For unsteady flows the results of Ostrach [10], for example, are for a Prandtl number of .72 but do not lend themselves for direct comparison with this work since the plate is assumed to have a continuous time-dependent velocity. For the problem to be considered in this research, the author has not been able to find any solutions for Prandtl numbers different from unity.

Estimates of the steady state induced pressure are usually obtained with quite accurate results from the "tangent-wedge" method [3,11]. The resulting expression is

$$\frac{p_e}{p_\infty} = 1 + \gamma M_\infty \frac{d\delta^*}{dx} + \frac{\gamma(\gamma+1)}{4} \left(M_\infty \frac{d\delta^*}{dx}\right)^2 + \cdots \qquad (1.7)$$

with $M_\infty > 1$ and $M_\infty(d\delta^*/dx) \ll 1$.

Thus for the weak interaction case one might simply say $p_e/p_\infty \approx 1$ as a first approximation. Such a simplifying approximation would, however, defeat the basic purpose of an interaction study and hence we will concern ourselves with the transient contribution to the induced pressure. In Moore [12] the outward displacement of the boundary layer is likened to a mild constant-pressure explosion after the in-

stant of the impulsive change and associated with the resulting "sound" waves sent out into the inviscid stream is a pressure rise which from the acoustic approximation is given by $\rho_e\, a_e\, v_e$.

The acoustic approximation may be derived from Lighthill's piston theory [13] as discussed in a paper by J.W. Miles [14]. The perturbation pressure may be regarded as resulting from the motion of a piston normal to the plate and this disturbance may be treated as a simple wave. The perturbation pressure is then given by the relation

$$\Delta p_v = \rho a v' \tag{1.8}$$

where ρ and a are the local density and speed of sound and v' is the unsteady perturbation velocity normal to the perturbation wave front. The pressure, density and sonic speed at the piston thus depend only on the instantaneous piston velocity, W_p say, and are given by

$$\frac{p}{p_e} = \left(\frac{a}{a_e}\right)^{\frac{2\gamma}{\gamma-1}}, \quad \frac{\rho}{\rho_e} = \left(\frac{a}{a_e}\right)^{\frac{2}{\gamma-1}}, \quad \frac{a}{a_e} = 1 + \frac{\gamma-1}{2}\left(\frac{W_p}{a_e}\right). \tag{1.9}$$

Writing $W_p = W + v'$ with $W = U_e\theta$ and θ representing the local steady inclination of the surface to the free stream, and using $W_p = W$ in (1.9) for the calculation of ρ and a, we obtain

$$\Delta p_v = \rho_e\, a_e\, v' \left[1 + \frac{\gamma-1}{2} M_e\, \theta\right]^{\frac{\gamma+1}{\gamma-1}}$$

$$= \rho_e a_e v'[1 + \frac{\gamma-1}{2} M_e\theta + \frac{\gamma+1}{4} M_e^2 \theta^2 + O(M_e^3\theta^3)] . \qquad (1.10)$$

Since for our problem $\theta \equiv d\delta^*/dx << 1$ and $v' \equiv v_e$ expression (4.11) for the induced pressure follows. The normal component of velocity v_e is obtained from the expression for the unsteady displacement thickness given by Moore and Ostrach in Reference [15], and the result is an expression for the transient contribution to the induced pressure given by equation (4.28).

The usual Prandtl boundary layer assumptions have been adopted in the works cited above and will also be used in the present research. Although the boundary layer in hypersonic flow will be quite thick it has been pointed out by Shen [16] that the assumptions remain valid for δ^*/x sufficiently small. For the weak interaction region, x will be large so that this condition will be met in the present work. Also, it is shown by Butler [17] from a detailed investigation that the pressure across the hypersonic boundary layer tends to vary less (i.e. remain fairly constant) at increasing values of x, where x is measured from the leading edge of the plate.

Finally we note that the boundary layer under investigation is assumed to be laminar. For a typical cruise altitude of a hypersonic vehicle, say 90,000 ft. slightly above the stratosphere, the free stream temperature is approximately - 58°F (402°R). The corresponding sonic speed is then approximately 985 ft/sec. Hence the free stream velocity for a Mach number of 10 would be 9850 ft/sec. This would give

a local Reynolds number based on a nominal distance of 10 ft. from the leading edge of about 9.85×10^8 which is by far above the critical Reynolds number for a flat plate. Other effects on the laminar to turbulent transition such as pressure gradient, for example, must also be considered. In our case the effect of heat transfer and compressibility is a favourable one since it is known that transfer of heat from the boundary layer to the wall exerts a stabilizing influence by increasing the critical Reynolds number [2]. In fact, there appear to be certain combinations of Mach number and wall enthalpies (g_w) for which the boundary layer is completely stable i.e. for which the critical Reynolds number becomes infinite. We therefore retain our mathematical model on the assumption of a laminar, compressible, unsteady two-dimensional boundary layer.

CHAPTER II

THE GOVERNING BOUNDARY LAYER EQUATIONS

2.1 Unsteady Prandtl Boundary Layer Equations

The general form of the unsteady, compressible, laminar, two-dimensional boundary layer equations with the adoption of Prandtl's boundary layer assumptions for hypersonic flow are as follows [12,18]:

$$\frac{\partial \rho}{\partial t} + \frac{\partial}{\partial x}(\rho u) + \frac{\partial}{\partial y}(\rho v) = 0 \tag{2.1}$$

$$\rho\left(\frac{\partial u}{\partial t} + u\frac{\partial u}{\partial x} + v\frac{\partial u}{\partial y}\right) = -\frac{\partial p}{\partial x} + \frac{\partial}{\partial y}\left(\mu\frac{\partial u}{\partial y}\right) \tag{2.2}$$

$$\frac{\partial p}{\partial y} = 0 \tag{2.3}$$

$$\rho\left(\frac{\partial h}{\partial t} + u\frac{\partial h}{\partial x} + v\frac{\partial h}{\partial y}\right) = \frac{\partial p}{\partial t} + u\frac{\partial p}{\partial x} + \frac{\partial}{\partial y}\left(\frac{\mu}{Pr}\frac{\partial h}{\partial y}\right) + \mu\left(\frac{\partial u}{\partial y}\right)^2 . \tag{2.4}$$

The boundary conditions are:

at $y = 0$

$$u = v = 0$$

$$h = h_w(x,t)$$

(2.5)

at $y = y_e$

$$u = U_e(x,t)$$

$$h = h_e(x,t)$$

The pressure, being assumed independent of y, imposed on the plate is given by its free stream value according to the solution of

$$-\frac{1}{\rho_e}\frac{\partial p_e}{\partial x} = \frac{\partial U_e}{\partial t} + U_e\frac{\partial U_e}{\partial x} \tag{2.6a}$$

which is the Eulerian equation of motion [19] and follows immediately from (2.2) when specialized to the inviscid free stream flow. Similarly, specializing (2.4) to the free stream one obtains

$$\rho_e\left(\frac{\partial h_e}{\partial t} + U_e\frac{\partial h_e}{\partial x}\right) = \frac{\partial p_e}{\partial t} + U_e\frac{\partial p_e}{\partial x} \tag{2.6b}$$

where $U_e(x,t)$ represents the prescribed non-steady potential motion.

2.2 The Dorodnitsyn-Howarth Variable and the Non-Steady Stream Function

It is possible to rewrite the equations (2.1) through (2.4) in a form similar to that for the incompressible boundary layer by adopting the Dorodnitsyn-Howarth variable [18]

$$Y = \int_0^y \frac{\rho}{\rho_{ref}}\,dy \tag{2.7}$$

and introducing the stream function $\psi(x,y,t)$ so that the velocity components are related to it by the equations

$$u = \frac{\rho_{ref}}{\rho}\frac{\partial \psi}{\partial y} = \frac{\partial \psi}{\partial Y} \tag{2.8}$$

$$v = - \frac{\rho_{ref}}{\rho} \left(\frac{\partial \psi}{\partial x} + \frac{\partial Y}{\partial t} \right) . \qquad (2.9)$$

The equation of continuity (2.1) is then automatically satisfied.

Because of the high temperature rise in the boundary layer at high Mach number flows, it becomes necessary to take into account the effect of temperature on the properties of the gas and in particular its viscosity. An accurate relation between viscosity and temperature is given by Sutherland's equation

$$\frac{\mu}{\mu_{ref}} = \left(\frac{T}{T_{ref}} \right)^{3/2} \frac{T_{ref} + S}{T + S} \qquad (2.10)$$

where S is Sutherland's constant which for air is approximately 110°K [2]. Following Chapman and Rubesin [20] equation (2.10) may be approximated by the relation

$$\frac{\mu}{\mu_{ref}} = C(x) \frac{T}{T_{ref}} \qquad (2.11)$$

where C(x) is fixed so that the viscosity is accurately determined in the more important region near the surface of the plate. If, for example, equations (2.10) and (2.11) are matched at a temperature corresponding to the average surface temperature, $\bar{T}_w$, then [20]

$$C(x) = \left(\sqrt{\frac{\bar{T}_w}{T_{ref}}} \right) \frac{T_{ref} + S}{T_w + S} . \qquad (2.12)$$

Finally, assuming a perfect gas with thermal equation of state

$$p = \rho RT \tag{2.13}$$

the viscosity relation becomes as in [12]

$$\frac{\mu}{\mu_{ref}} = C(x) \frac{\rho_{ref}}{\rho} \quad . \tag{2.14}$$

Substituting equations (2.7), (2.8), (2.9) and (2.14) into equations (2.2) and (2.4), the momentum and energy equations become respectively [4]

$$\frac{\partial^2 \psi}{\partial Y \partial t} + \frac{\partial \psi}{\partial Y} \frac{\partial^2 \psi}{\partial x \partial Y} - \frac{\partial \psi}{\partial x} \frac{\partial^2 \psi}{\partial Y^2} = \frac{\rho_e}{\rho} U_e \frac{\partial U_e}{\partial x} + C \nu_{ref} \frac{\partial^3 \psi}{\partial Y^3} \tag{2.15}$$

$$\frac{\partial h}{\partial t} + \frac{\partial \psi}{\partial Y} \frac{\partial h}{\partial x} - \frac{\partial \psi}{\partial x} \frac{\partial h}{\partial Y} = - \frac{\rho_e}{\rho} \frac{\partial \psi}{\partial Y} U_e \frac{\partial U_e}{\partial x} + \nu_{ref} \frac{C}{Pr} \frac{\partial^2 h}{\partial Y^2} + \nu_{ref} C \left(\frac{\partial^2 \psi}{\partial Y^2}\right)^2 \tag{2.16}$$

It has been further assumed that the Prandtl number Pr is constant for air.

2.3 Boundary Layer Equations in Similarity Form

As demonstrated by Rodkiewicz and Reshotko [4] equations (2.15) and (2.16) may be further simplified by the introduction of two similarity variables which reduce the number of independent variables from three (x,Y,t) to two (η,τ). The following transformation of variables was used:

$$\eta = (\sqrt{\frac{(m+1)\ U_e}{2\nu_{ref}\ Cx}})Y \tag{2.17}$$

$$\tau = \frac{U_e t}{x} \tag{2.18}$$

where the free stream velocity must be in the form of a power law

$$U_e = ex^m \quad . \tag{2.19}$$

A dimensionless stream function, $f(\eta,\tau)$, becomes the new dependent variable in the momentum equation and is defined by

$$\psi = (\sqrt{\frac{2\nu_{ref}\ Cx\ U_e}{(m+1)}})f(\eta,\tau) \quad . \tag{2.20}$$

The energy equation is transformed by letting

$$h = g(\eta,\tau)\ G(x,t) \tag{2.21}$$

where $g(\eta,\tau)$ becomes the new dimensionless enthalpy function. Upon substitution of the above expressions into equations (2.15) and (2.16) one obtains

$$\dot{f}'\frac{U_e}{x} + f'^2\frac{\partial U_e}{\partial x} - U_e f'\dot{f}'\frac{\tau}{x} + f'\dot{f}'\tau\frac{\partial U_e}{\partial x} - \frac{1}{2x}ff''U_e + \dot{f}U_e f''\frac{\tau}{x}$$

$$- \dot{f}f''\tau\frac{\partial U_e}{\partial x} - \frac{1}{2}ff''\frac{\partial U_e}{\partial x} - \frac{h}{h_e}\frac{\partial U_e}{\partial x} - C\nu_{ref}A^2\frac{U_e}{x}f''' = 0 \tag{2.22}$$

and

$$\dot{g}G\frac{U_e}{x} + g\frac{\partial G}{\partial t} - \tau\dot{G}\frac{U_e}{x}f' + \tau m\frac{U_e}{x}G\dot{g}f' + g\frac{\partial G}{\partial x}U_e f'$$

$$- \frac{1}{2}\frac{U_e}{x}Gfg' - \frac{1}{2}m\frac{U_e}{x}fGg' + \tau\frac{U_e}{x}\dot{f}Gg' - \tau\dot{f}Gg'm\frac{U_e}{x}$$

$$= -\frac{\rho_e}{\rho}U_e{}^2f'm\frac{U_e}{x} + \frac{(m+1)}{2Pr}Gg'' + \frac{(m+1)}{2}\frac{U_e{}^3}{x}f''^2 \qquad (2.23)$$

where

$$A^2 = \frac{m+1}{2\nu_{ref}C} \qquad \dot{g} \equiv \frac{\partial g}{\partial \tau}$$

$$\dot{f} \equiv \frac{\partial f}{\partial \tau} \qquad g' \equiv \frac{\partial g}{\partial \eta}$$

$$f \equiv \frac{\partial f}{\partial \eta} \quad .$$

It is assumed [4] that at hypersonic speeds the free stream adjusts itself instantaneously to the new state resulting after any sudden change in the free stream. Mathematically this means that

$$\frac{\partial U_e}{\partial t} = \frac{\partial h_e}{\partial t} = \frac{\partial p_e}{\partial t} = 0 \quad . \qquad (2.24)$$

Consequently expressions (2.6a) and (2.6b) can be combined to give

$$\frac{\partial h_e}{\partial x} = -U_e\frac{\partial U_e}{\partial x} \qquad (2.25)$$

and using (2.19)

$$\frac{\partial h_e}{\partial x} = - m \frac{U_e^2}{x} \tag{2.26}$$

and letting $G(x,t) = G(x) = h_e(x)$ one obtains finally

$$\frac{\partial G}{\partial x} = - m \frac{U_e^2}{x} \tag{2.27}$$

Substitution of the pertinent expressions into equations (2.22) and (2.23) yields the equations in their final similarity form, namely

$$(2-\beta)\dot{f}' + 2(1-\beta)\tau(\dot{f}f''-\dot{f}'f') - f''' - ff'' - \beta(g-f'^2) = 0 \tag{2.28}$$

and

$$\Pr(2-\beta)\left[1 - 2\frac{(1-\beta)}{(2-\beta)}\tau f'\right]\dot{g} - g'' - \Pr[f - 2(1-\beta)\tau\dot{f}]g'$$

$$- \Pr(\gamma-1) M_e^2 f''^2 = 0 \tag{2.29}$$

where

$$\beta = \frac{2m}{m+1}$$

and

$$\frac{U_e^2}{h_e} = (\gamma-1) M_e^2 \quad .$$

For the case under consideration in this work (zero pressure gradient, $m = \beta = 0$) equations (2.28) and (2.29) become uncoupled and reduce to

$$2\dot{f}' + 2\tau(\dot{f}f''-\dot{f}'f') - f''' - ff'' = 0 \qquad (2.30)$$

$$2Pr(1-\tau f')\,\dot{g} - g'' - Pr(f-2\tau\dot{f})\,g' - Pr(\gamma-1)\,M_e^{\,2}f''^2 = 0 \qquad (2.31)$$

For the final steady state, equation (2.30) becomes the familiar Blasius equation

$$f_2''' + f_2 f_2'' = 0 \qquad (2.32)$$

and equation (2.31) becomes

$$g_2'' + Prf_2g_2' + Pr(\gamma-1)\,M_e^{\,2}f_2''^2 = 0 \quad . \qquad (2.33)$$

2.4 Linearization of the Momentum Equation

Equation (2.30) is a non-linear partial differential equation. The method of small perturbations, often used to linearize such equations, is in general not applicable to equations governing the flows in the hypersonic regime. Since we are considering only a very small velocity-step increase of the plate, i.e. a 1% velocity jump for only low hypersonic Mach numbers (maximum $M_e = 10$), it has been decided to adopt this linearization technique as was done in Reference

[4]. Furthermore, Gupta and Rodkiewicz [21] have solved the non-linear momentum equation (2.28) for the strong interaction region using a numerical procedure developed by Smith and Clutter [2]. Their results show that the maximum discrepancy in the shear stress parameter f'' from a linearized solution to (2.28) is less than 1% for a 1% jump in the free stream velocity. We therefore assume that

$$f(\eta,\tau) = f_2(\eta) + \Delta f(\eta,\tau) \tag{2.34}$$

where $f_2(\eta)$ is the known solution to the Blasius equation (2.32). (See for example Reference [6]).

From (2.34) we have

$$f' = f_2' + (\Delta f)'$$

$$f'' = f_2'' + (\Delta f)''$$

$$f''' = f_2''' + (\Delta f)'''$$

$$\dot{f} = (\Delta \dot{f})$$

$$\dot{f}' = (\Delta \dot{f})'$$

and substitution into (2.30) yields the linear equation

$$2(\dot{\Delta f})'[1-\tau f_2'] + 2\tau f_2''(\dot{\Delta f}) - (\Delta f)''' - f_2(\Delta f)'' - f_2''(\Delta f) = 0 \quad (2.35)$$

where all higher order terms in Δf have been neglected.

2.5 Associated Boundary and Initial Conditions

When a body is impulsively set into motion from rest in a viscous fluid the boundary layer, immediately after the start of motion, is in the form of an infinitely thin vortex sheet which is a consequence of the non-slip condition on the surface of the plate. In the initial stages of growth of this boundary layer, downstream from the leading edge, the effects of convection are negligible compared with those of diffusion so that in the mathematical formulation of the flow, equation (2.2) may be simplified to

$$\rho \frac{\partial u}{\partial t} = - \frac{\partial p}{\partial x} + \frac{\partial}{\partial y} \left(\mu \frac{\partial u}{\partial y}\right) \quad (2.36)$$

which is linear and indicates a balance of pressure, inertia and viscous forces.

The physical problem we are considering in this work is closely related to boundary - layer flow from rest. The free stream velocity U_e is suddenly changed from one value U_{e0} to another U_{e1} by a small increment of 1% defined by

$$\frac{U_{e1} - U_{e0}}{U_{e2}} = \frac{U_{e2} - U_{e0}}{U_{e2}} = \varepsilon = .01 \quad (2.37)$$

Sears [5] has shown that in this case the initial motion, since the equation governing the initial motion is linear, can be represented by the superposition of the initial flow pattern described above on the established flow pattern existing just before the change. That is, except at the plate surface, the initial boundary layer reacts as if it were inviscid since the sudden change has not allowed sufficient time for viscosity to counteract the increase in velocity so that the governing equation in the major portion of the original boundary layer is

$$\frac{\partial u}{\partial t} = -\frac{1}{\rho}\frac{\partial p}{\partial x} \tag{2.38}$$

(See also Reference [6]). The situation may perhaps be easier visualized with reference to Fig. 2.1.

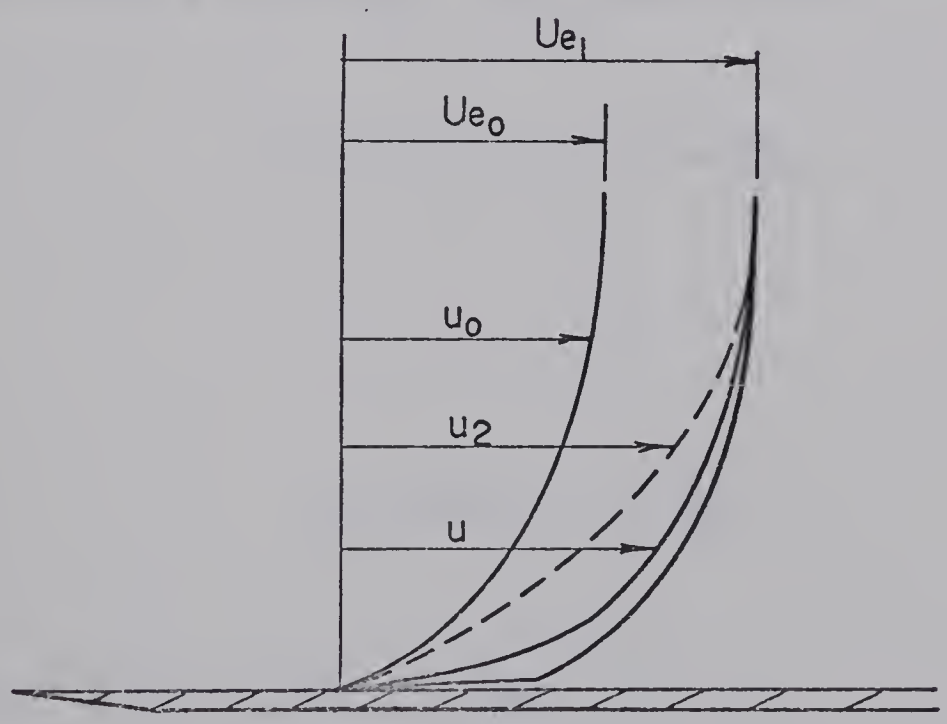

Fig. 2.1 Laminar Velocity Profiles

The associated boundary and initial conditions pertinent to equations (2.35) and (2.31) are therefore as follows:

When $y = y_e$, $Y = Y_e$, $\eta = \eta_e$, $u = U_{e2}$, $f'(\eta_e,\tau) = f_2'(\eta_e,\tau) = 1$,

and
$$\Delta f'(\eta_e,\tau) = 0 \tag{2.39}$$

When $y = 0$, $Y = 0$, $\eta = 0$, $u = 0$, $f'(0,\tau) = f_2'(0,\tau) = 0$,

and
$$\Delta f'(0,\tau) = 0 \tag{2.40}$$

When $y = 0$, $Y = 0$, $\eta = 0$, $\psi = 0$, $f(0,\tau) = f_2(0,\tau) = 0$

and
$$\Delta f(0,\tau) = 0 \tag{2.41}$$

When $t = 0$, $\tau = 0$, $u = u_0 + U_{e1} - U_{e0}$ and for $\eta > 0$

$$f'(\eta>0,0) = f_0' + \varepsilon(1- f_0')$$

so that

$$\Delta f'(\eta>0,0) = \varepsilon(1-f_0') \tag{2.42}$$

When $y = y_e$, $Y = Y_e$, $\eta = \eta_e$, $h = h_{e2}$

and
$$g(\eta_e,\tau) = 1 \tag{2.43}$$

When $y = 0$, $Y = 0$, $\eta = 0$, $h = h_w$ and

$$g(0,\tau) = g_w \tag{2.44}$$

whereas for the case of no heat transfer at the wall

$$g'(0,\tau) = 0 \tag{2.45}$$

When $t = 0$, $\tau = 0$, $h = h_1$ and

$$g(\eta,0) = \frac{h_1}{h_{e2}} \quad . \tag{2.46}$$

An observation made by Rodkiewicz and Reshotko [4] concerns the relationship between variables referenced to the initial and final steady states. Recalling expression (2.17) we have

$$\eta_0 = \left(\sqrt{\frac{(m+1)\,U_{e0}}{2\nu_{ref}\,Cx}}\right) Y \tag{2.47a}$$

and

$$\eta_2 = \left(\sqrt{\frac{(m+1)\,U_{e2}}{2\nu_{ref}\,Cx}}\right) Y \tag{2.47b}$$

so that

$$\frac{\eta_0}{\eta_2} = \sqrt{\frac{U_{e0}}{U_{e2}}} \, .$$

Since f_0 is a function of η_0 and f_2 a function of η_2 , boundary condition (2.42) should strictly speaking be written as

$$\Delta f'(\eta_2>0,0) = \varepsilon[1-f_0'(\sqrt{\frac{U_{e0}}{U_{e2}}}\,\eta_2)] + f_0'(\sqrt{\frac{U_{e0}}{U_{e2}}}\,\eta_2) - f_2'(\eta_2) \, .$$

Considering equation (2.37), however, we have

$$\sqrt{\frac{U_{e0}}{U_{e2}}} = \sqrt{(1 - \varepsilon)} = .995$$

so that $\eta_0 = .995\ \eta_2$ for a 1% velocity jump. This small discrepancy would appear to be insignificant in the numerical solution of the equations and has therefore been ignored. Even for a 10% jump where then $\eta_0 = .95\ \eta_2$, it would seem that the difference is not likely to affect the results a great deal.

CHAPTER III

SOLUTIONS TO THE GOVERNING EQUATIONS

3.1 Numerical Solution of the Momentum Equation

The linearized momentum equation (2.35) subject to the boundary and initial conditions described in Section 2.5 has been solved by Rodkiewicz and Reshotko [4] using the technique of finite differences and a recurrence relationship which is essentially a modification to the method of Gaussian elimination [22]. The range of integration of (2.35) in the direction of τ extends from zero to infinity, however, it turns out that the numerical solution could be generated for values of τ ranging from zero to only slightly greater than 1. The discontinuity, although abrupt mathematically, is a manifestation of a gradual transition from a Rayleigh type of flow to a Blasius flow [6]. Tokuda [23] has considered a suggestion made by Van Dyke who postulated that the mathematical singularity might be avoidable by a simple change of coordinate system such as Euler's transformation given by

$$\xi = \frac{\tau}{1+\tau} \quad . \tag{3.1}$$

Incorporating (3.1) in equation (2.35) yields the transformed momentum equation

$$2(1-\xi)^2 \frac{\partial^2 \Delta f}{\partial \eta \partial \xi} + 2\xi(1-\xi)\{f_2'' \frac{\partial \Delta f}{\partial \xi} - f_2' \frac{\partial^2 \Delta f}{\partial \eta \partial \xi}\}$$

$$- \Delta f''' - f_2 \Delta f'' - f_2'' \Delta f = 0 \ . \qquad (3.2)$$

Unfortunately the author has found that the numerical solution of (3.2) could also not be extended very far beyond a value of $\tau = 1 (\xi = 1/2)$. Now since the range of integration of the differential equations in the τ direction extends from zero to infinity, it was decided to use the Euler transformation (3.1) for the purpose of economizing in computer time and storage since the corresponding range for ξ is 0 to 1. Furthermore, an improved accuracy in the numerical results could be realized since it would be possible to reduce the step-size T in the time direction. The energy equation (2.31) in terms of the new time variable ξ then becomes

$$2\{1-\xi(1+f')\}(1-\xi) \frac{\partial g}{\partial \xi} - \frac{1}{Pr} \frac{\partial^2 g}{\partial \eta^2} - \{f-2\xi(1-\xi)\dot{f}\} \frac{\partial g}{\partial \eta}$$

$$- (\gamma-1) M_e^2 f''^2 = 0 \qquad (3.3)$$

where the dot over any variable is now interpreted as differentiation with respect to ξ.

The computational molecule used in conjunction with a finite difference representation of derivatives is shown schematically in Fig. 3.1. It was employed both in Reference [4] and [8] and utilizes

seven nodal values in a rectangular grid.

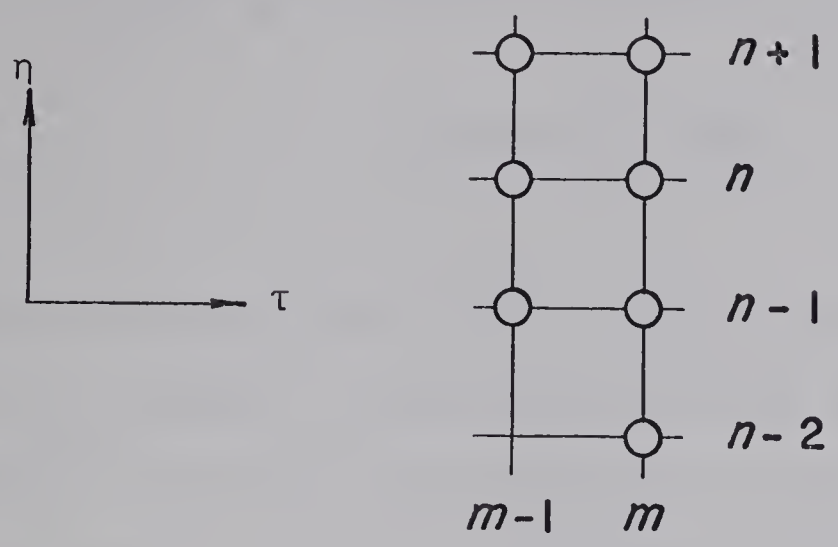

Fig. 3.1 7-Point Computational Molecule

In conjunction with this molecule the finite difference representation of the derivatives of equation (3.2) are as follows:

$$\frac{\partial \Delta f}{\partial \xi} = \frac{1}{T} \{\Delta f(m,n) - \Delta f(m-1,n)\} + O(T) \tag{3.4}$$

$$\frac{\partial \Delta f}{\partial \eta} = \frac{1}{2H} \{\Delta f(m,n+1) - \Delta f(m,n-1)\} + O(H^2) \tag{3.5}$$

$$\frac{\partial^2 \Delta f}{\partial \eta \partial \xi} = \frac{1}{2HT} \{\Delta f(m,n+1) - \Delta f(m,n-1) - \Delta f(m-1,n+1) + \Delta f(m-1,n-1)\} + O(T) + O(H^2) \tag{3.6}$$

$$\frac{\partial^2 \Delta f}{\partial \eta^2} = \frac{1}{H^2} \{\Delta f(m,n+1) - 2\Delta f(m,n) + \Delta f(m,n-1)\} + O(H^2) \tag{3.7}$$

$$\frac{\partial^3 \Delta f}{\partial \eta^3} = \frac{1}{H^3} \{\Delta f(m,n+1) - 3\Delta f(m,n) + 3\Delta f(m,n-1)$$

$$- \Delta f(m,n-2)\} + O(H) \ . \qquad (3.8)$$

It should be mentioned that a Taylor series expansion has been employed in order to eliminate the nodal point (m,n+2) for the difference representation of the third order derivative, equation (3.8). If now the expressions (3.4) to (3.8) are substituted into (3.2) the resulting difference equation is of the form

$$a_{m,n}\, s_{m,n+1} + b_{m,n}\, s_{m,n} + c_{m,n}\, s_{m,n-1} + d_{m,n}\, s_{m,n-2} = e_{m,n} \qquad (3.9)$$

where $s_{m,n} \equiv \Delta f(m,n)$ and

$$a_{m,n} = T + HTf_2(m,n) - H^2(1-\xi_m)[1-\xi_m(1+f_2'(m,n))] \qquad (3.10a)$$

$$b_{m,n} = -3T - 2HTf_2(m,n) + H^3 T f_2''(m,n) - 2\xi_m(1-\xi_m)\, H^3 f_2''(m,n) \qquad (3.10b)$$

$$c_{m,n} = 3T + HTf_2(m,n) + H^2(1-\xi_m)[1-\xi_m(1+f_2'(m,n))] \qquad (3.10c)$$

$$d_{m,n} = -T \qquad (3.10d)$$

$$e_{m,n} = H^2(1-\xi_m)[1-\xi_m(1+f_2'(m,n))][s(m-1,n-1) - s(m-1,n+1)]$$

$$- 2H^3\, \xi_m(1-\xi_m) f_2''(m,n)\, s(m-1,n) \qquad (3.10e)$$

The numerical solution consists of a step by step procedure of finding 's' completely along one time line before proceeding to the next beginning with the known (or assumed) initial conditions. That is, the finite difference representation in the time direction is a backward difference as is evident in (3.4). The nodal values on each time line are evaluated from the recurrence relationship

$$s_{m,n} = R_{m,n}\, s_{m,n+1} + C_{m,n} \tag{3.11}$$

which follows from expression (3.9) with

$$R_{m,n} = \frac{-a_{m,n}}{(b_{m,n} + c_{m,n}\, R_{m,n-1} + d_{m,n}\, R_{m,n-1}\, R_{m,n-2})} \tag{3.12}$$

and

$$C_{m,n} = \frac{e_{m,n} - (c_{m,n} C_{m,n-1} + d_{m,n} R_{m,n-2} C_{m,n-1} + d_{m,n} C_{m,n-2})}{(b_{m,n} + c_{m,n} R_{m,n-1} + d_{m,n} R_{m,n-1} R_{m,n-2})} \tag{3.13}$$

Beginning with the known boundary conditions at the outer edge of the boundary layer and at the plate surface, the values of $R_{m,n}$ and $C_{m,n}$ are calculated by marching up from the plate surface to the free stream. From the boundary conditions at the wall and using a three point forward difference approximation to $\partial s/\partial \eta$ it can be shown that

$$R_{m,1} = C_{m,1} = C_{m,2} = 0 \ , \ R_{m,2} = \frac{1}{4} \tag{3.14}$$

At the free stream where n = N say, the values of $s_{m,n}$ are obtained recursively marching downward using (3.11) with the starting value obtained from the boundary condition at the outer edge of the boundary layer, namely

$$s_{m,N} = \frac{C_{m,N-1} - \dfrac{C_{m,N-2}}{4-R_{m,N-2}}}{\dfrac{3}{4-R_{m,N-2}} - R_{m,N-1}} \quad . \tag{3.15}$$

It will be noticed that the backward difference approximations (3.4) and (3.6) have a truncation error in the time direction of order T whereas the error in the other approximations are of order H^2. Since the maximum numerical value of Δf is only of order 10^{-2} it is imperative that the error in the numerical solution be made as small as possible. Rodkiewicz and Reshotko [4] have tried a symmetrical 11-point computational molecule but with little success. The author, however, has successfully used a 10-point molecule shown in Fig. 3.2.

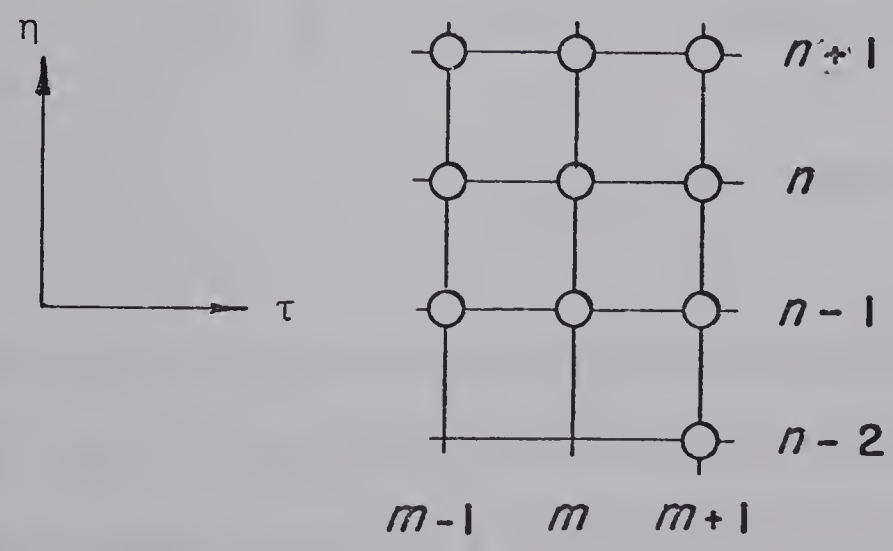

Fig. 3.2 10-Point Computational Molecule

The procedure employed was that only the first time line was calculated using expressions (3.4) to (3.8) relating to the 7-point molecule in Fig. 3.1. All subsequent time lines were then evaluated using the 10-point molecule of Fig. 3.2 with the following finite difference approximations.

$$\frac{\partial \Delta f}{\partial \xi} = \frac{1}{2T}\{3\Delta f(m+1,n) - 4\Delta f(m,n) + \Delta f(m-1,n)\} + O(T^2) \qquad (3.16)$$

$$\frac{\partial \Delta f}{\partial \eta} = \frac{1}{2H}\{\Delta f(m+1,n+1) - \Delta f(m+1,n-1)\} + O(H^2) \qquad (3.17)$$

$$\frac{\partial^2 \Delta f}{\partial \eta \partial \xi} = \frac{1}{4HT}\{3\Delta f(m+1,n+1) - 4\Delta f(m,n+1) + \Delta f(m-1,n+1)$$

$$- 3\Delta f(m+1,n-1) + 4\Delta f(m,n-1) - \Delta f(m-1,n-1)\} + O(T^2) + O(H^2) \qquad (3.18)$$

$$\frac{\partial^2 \Delta f}{\partial \eta^2} = \frac{1}{H^2}\{\Delta f(m+1,n+1) - 2\Delta f(m+1,n) + \Delta f(m+1,n-1)\} + O(H^2) \qquad (3.19)$$

$$\frac{\partial^3 \Delta f}{\partial \eta^3} = \frac{1}{H^3}\{\Delta f(m+1,n+1) - 3\Delta f(m+1,n) + 3\Delta f(m+1,n-1)$$

$$- \Delta f(m+1,n-2)\} + O(H) \qquad (3.20)$$

A three-point Newton backward-difference [2,24] has been used in (3.16) and (3.18) to approximate the derivative with respect to ξ resulting in a balanced system for a square grid with truncation errors of $O(T^2)$

and $O(H^2)$ in the time and space directions respectively. With appropriate revisions to quantities (3.10a) to (3.10e) the numerical solution proceeds in an analogous manner as described previously except that now the recurrence relation (3.11) is applied to each (m+1)st time line in succession. A further refinement, described in Section 3.2, was introduced before the numerical solution was carried out and this involved the reduction of the step sizes H and T to one-tenth of the size used in References [4] and [8]. Furthermore, all calculations were done in double precision on the IBM 360. The solution curves to the unsteady state momentum equation (3.2) are plotted in Figs. 3.4 and 3.5. For easier comparison with previous works all time variations are shown plotted as a function of τ by using the inverse of the transformation (3.1).

A discontinuity in the solution was also encountered in the same neighbourhood of τ as in the results of Reference [4] and [8]. An attempt has been made in these works to discover the cause of the blow up condition and it appears that the discontinuity occurs along a curve defined by $1 - \tau f_2' = 0$ (shown in Figs. 3.4 and 3.5) which is the coefficient of $2(\dot{\Delta f})'$ in equation (2.35). When τ becomes greater than $1/f_2'$, this coefficient changes sign from positive to negative thereby changing the partial differential equation to a type which, evidently, is no longer compatible with the numerical method employed for its solution. At points where $\tau = 1/f'$ in equation (2.30) it can be readily shown that the mixed derivative $\partial^2 f/\partial\eta\partial\tau$ becomes singular. The very fact that it was not possible to obtain a continuous solution

of the momentum equation to its final steady state value has a major influence on the prime objective of this work, namely, to obtain a numerical solution to the unsteady state energy equation for Prandtl numbers different from unity.

3.2 Numerical Solution of the Energy Equation

The case of a zero pressure gradient, applicable in the weak interaction region, allows the solution of the momentum equation to be obtained independently from the energy equation. For the special case of Pr = 1 a closed form solution to the energy equation is possible and has been given in Reference [4] namely,

$$g(\eta,\tau) = 1 + \frac{\gamma-1}{2} M_e^2 [1 - f'^2(\eta,\tau)] \tag{3.21}$$

for zero heat transfer at the wall and

$$g(\eta,\tau) = 1 + \frac{\gamma-1}{2} M_e^2 f'(\eta,\tau)[1-f'(\eta,\tau)] + [g_w-1][1-f'(\eta,\tau)] \tag{3.22}$$

for non-zero heat transfer at the wall. Equation (3.21) satisfies the differential equation (2.31) and also the boundary conditions (2.43) and (2.45). Similarly, the solution (3.22) satisfies (2.31) and the boundary conditions (2.43) and (2.44). It is implied in [4] that the initial condition corresponding to (2.46) is given by

$$g(\eta,0) \equiv \frac{h_1}{h_{e2}} = 1 + \frac{\gamma-1}{2} M_{e2}^2 [1-f'(\eta,0)^2] \tag{3.23}$$

for zero wall heat transfer, or

$$g(\eta,0) \equiv \frac{h_1}{h_{e2}} = 1 + \frac{\gamma-1}{2} M_{e2}^2 f'(\eta,0)[1-f'(\eta,0)]$$

$$+ [g_w-1][1-f'(\eta,0)] \qquad (3.24)$$

for the case of heat transfer at the wall. That is to say that the enthalpy jump corresponding to the 1% velocity jump at zero time can be obtained by substituting the initial condition to the momentum equation (2.42) into the solutions to the energy equation given by (3.21) and (3.22).

The Prandtl number for air has a value nearer to .72 than to 1 and it is attempted to determine what effect this change would have on the solutions (3.21) and (3.22). The steady state solution of equation (2.33) for arbitrary Prandtl numbers is discussed in Section 3.3 and it is well known that reducing Pr from 1.0 to .72 has a significant effect on the enthalpy distribution in the boundary layer. Figure 3.6 illustrates this for a free stream Mach number of 10. For the unsteady energy equation, however, a closed form solution is no longer possible so the numerical method of Section 3.1 has been employed to solve the energy equation (3.3). As mentioned previously, the magnitudes of the incremental stream function Δf are necessarily quite small and also small in relation to the final steady state distribution $f_2(\eta)$. Similarly, the deviation of $g(\eta,\xi)$ from the steady

state distribution $g_2(\eta)$ was also expected to be small in magnitude. For this reason the author has further rewritten equations (3.3) in terms of $\Delta g(\eta,\xi)$ where

$$\Delta g(\eta,\xi) = g_2(\eta) - g(\eta,\xi) \tag{3.25}$$

and $g_2(\eta)$ is the solution to equation (2.33) with $M_e = M_{e2}$. We note that the motivation behind (3.25) is not the same as it was for (2.34) since (3.3) is already a linear partial differential equation. Thus in terms of Δg the energy equation becomes

$$\frac{1}{Pr}\frac{\partial^2 \Delta g}{\partial \eta^2} + \{f-2\xi(1-\xi)\dot{f}\}\frac{\partial \Delta g}{\partial \eta} - 2\{1-\xi(1+f')\}(1-\xi)\frac{\partial \Delta g}{\partial \xi}$$

$$- \frac{1}{Pr} g_2'' - \{f-2\xi(1-\xi)\dot{f}\}g_2' - (\gamma-1)\, M_e{}^2 f''^2 = 0 \,. \tag{3.26}$$

The finite difference approximations used are

$$\frac{\partial \Delta g}{\partial \xi} = \frac{1}{2T}\{3\Delta g(m+1,n) - 4\Delta g(m,n) + \Delta g(m-1,n) + O(T^2) \tag{3.27}$$

$$\frac{\partial \Delta g}{\partial \eta} = \frac{1}{2H}\{\Delta g(m+1,n+1) - \Delta g(m+1,n-1)\} + O(H^2) \tag{3.28}$$

$$\frac{\partial^2 \Delta g}{\partial \eta^2} = \frac{1}{H^2}\{\Delta g(m+1,n+1) - 2\Delta g(m+1,n) + \Delta g(m+1,n-1)\} + O(H^2) \tag{3.29}$$

and the computational molecule appears as sketched in Fig. 3.3

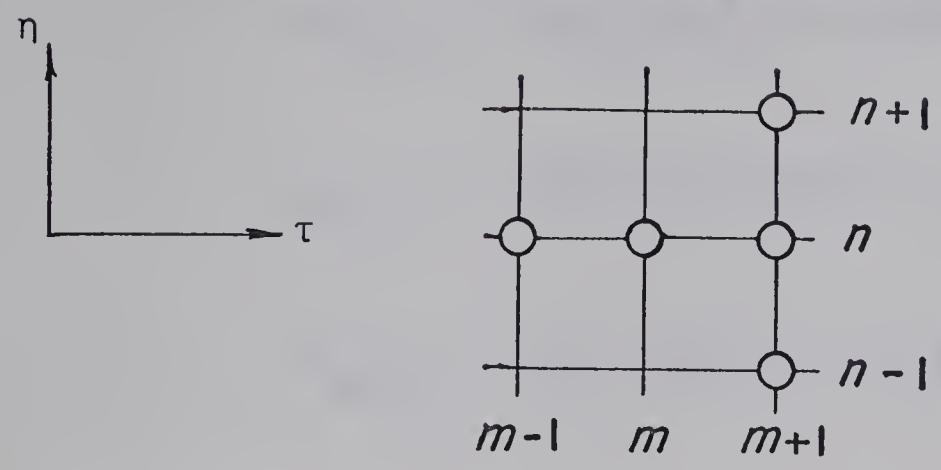

Fig. 3.3 5-Point Computational Molecule

Substituting expressions (3.27) to (3.29) into equation (3.26) and collecting terms one obtains with $U_{m,n} \equiv \Delta g(m,n)$

$$\{\frac{T}{Pr} + \frac{HT}{2}[f-2\xi(1-\xi)\dot{f}]\}U_{m+1,n+1} - \{3H^2[1-\xi(1+f')][1-\xi] + \frac{2T}{Pr}\}U_{m+1,n}$$

$$+ \{\frac{T}{Pr} - \frac{HT}{2}[f-2\xi(1-\xi)\dot{f}]\}U_{m+1,n-1} = -4H^2[1-\xi(1+f')][1-\xi]U_{m,n}$$

$$+ H^2[1-\xi(1+f')][1-\xi]U_{m-1,n} + \frac{H^2T}{Pr}g_2'' + H^2T[f-2\xi(1-\xi)\dot{f}]g_2'$$

$$+ H^2T(\gamma-1)M_e{}^2f''^2 \quad . \qquad (3.30)$$

This can be written in the form of a recursion

$$a_{m+1,n}\, U_{m+1,n+1} + b_{m+1,n}\, U_{m+1,n} + c_{m+1,n}\, U_{m+1,n-1} = d_{m+1,n} \qquad (3.31)$$

with

$$a_{m+1,n} = T\,\{\frac{1}{Pr} + H[\frac{f}{2} - \xi(1-\xi)\dot{f}]\} \qquad (3.32)$$

$$b_{m+1,n} = -\,\{3H^2[1-\xi(1+f')][1-\xi] - \frac{2T}{Pr}\} \qquad (3.33)$$

$$c_{m+1,n} = T\,\{\frac{1}{Pr} - H[\frac{f}{2} - \xi(1-\xi)\dot{f}]\} \qquad (3.34)$$

$$d_{m+1,n} = H^2[1-\xi(1+f')][1-\xi][U_{m-1,n} - 4U_{m,n}]$$

$$+ H^2T\,\{\frac{g_2''}{Pr} + [f-2\xi(1-\xi)\dot{f}]g_2' + (\gamma-1)\,M_e{}^2 f''^2\}. \qquad (3.35)$$

In an analogous manner as for the solution to the momentum equation each (m+1)st time line is evaluated according to the recursion formula

$$U_{m+1,n} = R_{m+1,n}\, U_{m+1,n+1} + C_{m+1,n}\,. \qquad (3.36)$$

Now from (3.31)

$$U_{m+1,n} = \frac{d_{m+1,n} - c_{m+1,n}\, U_{m+1,n-1} - a_{m+1,n}\, U_{m+1,n+1}}{b_{m+1,n}}$$

and from (3.36)

$$U_{m+1,n-1} = R_{m+1,n-1}\, U_{m+1,n} + C_{m+1,n-1}$$

so that

$$U_{m+1,n} = \frac{d_{m+1,n} - c_{m+1,n} R_{m+1,n-1} U_{m+1,n} - c_{m+1,n} C_{m+1,n-1} - a_{m+1,n} U_{m+1,n+1}}{b_{m+1,n}}$$

or

$$U_{m+1,n} = \left[\frac{-a_{m+1,n}}{b_{m+1,n} + c_{m+1,n} R_{m+1,n-1}}\right] U_{m+1,n+1} + \frac{d_{m+1,n} - c_{m+1,n} C_{m+1,n-1}}{b_{m+1,n} + c_{m+1,n} R_{m+1,n-1}} .$$

Upon comparing this with (3.36) we have

$$R_{m+1,n} = \frac{-a_{m+1,n}}{b_{m+1,n} + c_{m+1,n} R_{m+1,n-1}} \tag{3.37}$$

$$C_{m+1,n} = \frac{d_{m+1,n} - c_{m+1,n} C_{m+1,n-1}}{b_{m+1,n} + c_{m+1,n} R_{m+1,n-1}} . \tag{3.38}$$

The values $R_{m+1,n}$ and $C_{m+1,n}$ are then obtained from (3.37) and (3.38) by marching upwards from the plate towards the outer edge of the boundary layer beginning with the known values of $R_{m+1,1}$ and $C_{m+1,1}$.

In terms of Δg boundary condition (2.44) becomes

$$\Delta g(0,\xi) = g_2(0) - g_w = 0 \tag{3.39}$$

and from (3.36)

$$U_{m+1,1} = R_{m+1,1} U_{m+1,2} + C_{m+1,1} \tag{3.40}$$

so that $R_{m+1,1} = C_{m+1,1} = 0$ for the case of non-zero heat transfer at

the wall. Boundary condition (2.45) together with (3.25) gives

$$\Delta g'(0,\xi) = g_2'(0) - g'(0,\xi) = 0 \qquad (3.41)$$

and using a three-point Newton forward difference

$$\Delta g'_{m+1,1} = \frac{1}{2H}\{-3\Delta g_{m+1,1} + 4\Delta g_{m+1,2} - \Delta g_{m+1,3}\}$$

we take $\Delta g_{m+1,1} = \Delta g_{m+1,2} = \Delta g_{m+1,3}$ so that from (3.40) we must have $R_{m+1,1} = 1$ and $C_{m+1,1} = 0$ for the case of zero heat transfer at the wall. Having obtained all $R_{m+1,n}$ and $C_{m+1,n}$ we apply boundary condition (2.43) where we have

$$\Delta g(\eta_e,\xi) = 0 \ . \qquad (3.42)$$

The values of $U_{m+1,n}$ are then obtained by marching down towards the plate using (3.36) beginning with $U_{m+1,N} = 0$.

3.3 Determination of Stepsizes H and T

The stepsizes used in References [4] and [8] were H = 0.10 and T = 0.05. Rodkiewicz and Gupta [8] have studied the effect of varying the grid size in the solution to the momentum equation and found that the values of Δf changed by approximately 2.5% when T and H were chosen such that H = T = 0.05. A similar comparison with H = 0.10 and T = 0.005 resulted in a 5.8% change in the Δf values i.e. when compared with the Δf values obtained with the original grid size of H = 0.10 and T = 0.05.

It was decided in Reference [8] to keep H and T at 0.10 and 0.05 respectively, in order to preclude large round-off errors and to avoid large computer time and storage requirements. In the present work, however, it was found that the total error produced by a grid size with H = 0.10 and T = 0.05 could not be tolerated and furthermore that no large round-off errors were encountered by reducing H to one-tenth its original value. These conclusions are based on the following calculations:

Solutions to the steady state energy equation (2.33) are well known for arbitrary Prandtl numbers. Chapman and Rubesin [20], for example, give the solution first advanced by Pohlhausen. It is

$$g_2(\eta) = 1 + \frac{\gamma-1}{2} M_{e2}^2 \, r(\eta) - (\gamma-1) \, C_1 \, s(\eta) \tag{3.43}$$

where

$$r(\eta) = 2Pr \int_{\zeta=\eta}^{\infty} [f_2'(\zeta)]^{Pr} \int_{0}^{\zeta} [f_2'(\theta)]^{2-Pr} \, d\theta d\zeta \tag{3.44}$$

and

$$s(\eta) = \int_{\zeta=\eta}^{\infty} [f_2'(\zeta)]^{Pr} \, d\zeta. \tag{3.45}$$

For the case of zero wall heat transfer we take $C_1 = 0$ since then $\frac{dg_2}{d\eta}\Big|_{\eta=0} = 0$ so that for the insulated plate we have the solution

$$g_2(\eta) = 1 + \left(\frac{\gamma-1}{2}\right) M_{e2}^2 \, r(\eta) \, . \tag{3.46}$$

For the case of non-zero wall heat transfer

$$g_2(0) = g_w = 1 + \left(\frac{\gamma-1}{2}\right) M_{e2}^2\, r(0) - (\gamma-1) C_1\, s(0)$$

so that

$$C_1 = \frac{1 + \left(\frac{\gamma-1}{2}\right) M_{e2}^2\, r(0) - g_w}{(\gamma-1)\, s(0)} . \qquad (3.47)$$

Substituting (3.47) into the general solution (3.43) we obtain for the case of non-zero wall heat transfer

$$g_2(\eta) = 1 + \left(\frac{\gamma-1}{2}\right) M_{e2}^2\, r(\eta) - \left\{1 + \left(\frac{\gamma-1}{2}\right) M_{e2}^2\, r(0) - g_w\right\} \frac{s(\eta)}{s(0)} \qquad (3.48)$$

For Pr = 1 expression (3.44) reduces to

$$r(\eta) = 1 - [f_2'(\eta)]^2 \qquad (3.49a)$$

and

$$s(\eta) = 1 - f_2'(\eta) \qquad (3.49b)$$

so that

$$r(0) = s(0) = 1 \quad .$$

Substitution into (3.46) yields for zero wall heat transfer and Pr = 1

$$g_2(\eta) = 1 + \left(\frac{\gamma-1}{2}\right) M_{e2}^2 \left[1 - f_2'^2(\eta)\right] . \qquad (3.50)$$

Similarly, for non-zero wall heat transfer and Pr = 1 equation (3.48)

becomes

$$g_2(\eta) = 1 + (\frac{\gamma-1}{2})M_{e2}^2 f_2'(\eta)[1 - f_2'(\eta)] + [g_w-1][1-f_2'(\eta)] \quad . \quad (3.51)$$

We note immediately that for Pr = 1 the solutions (3.21) and (3.22) to the unsteady energy equations are exactly of the same form as the corresponding solutions (3.50) and (3.51) to the steady state energy equation. This observation has been further investigated and leads to a plausible alternative solution of the unsteady energy equation for Prandtl numbers which are only slightly different from one. Such a solution will be discussed in Section 3.5.

Returning to the problem of obtaining an optimum stepsize it was decided to solve the steady state energy equation by a similar recurrence relation as used in the solution to the unsteady momentum and energy equations. Varying the stepsize H and comparing the resulting numerical solution with the published solution (3.43) would be an indication of the magnitude of the error to be expected in the numerical solution of equations (3.2) and (3.26). Figure 3.7 shows the error curves obtained in the numerical solution of the non-dimensional surface equilibrium-enthalpy for a free stream Mach number of 10, γ = 1.4 and for Prandtl numbers 1 and 0.72. For Pr = 0.72 the "recovery factor" r(0) from equation (3.44) is equal to 0.845 [20] so that equation (3.46) yields $g_2(0)$ = 17.900. Figure 3.7 shows that for H = 0.1 the recurrence relation method resulted in an error of approximately 4.0% representing

an absolute error of 0.700. For Pr = 1.0, r(0) = 1 so that $g_2(0)$ = 21.000 whereas the recurrence relationship gave $g_2(0)$ = 20.069 with H = 0.1 which is an error of about 4.5%. Since the absolute error in these cases was of the same order of magnitude as Δg, it is clear that H = 0.10 could not be accepted. Reducing the stepsize H to one-tenth of this value, however, resulted in an error of less than 0.5% in both cases. Hence it was decided to take H = T = .01 for the numerical solution of the unsteady momentum and energy equations (3.2) and (3.26) respectively. Figure 3.7 shows, furthermore, that the effects of round-off errors have not yet significantly come into play for H = .01.

Finally, it should be pointed out that the actual solutions to the steady state energy equation (3.43) used in conjunction with the numerical solution of equations (3.26) were obtained with the application of Simpson's rule to expressions (3.44) and (3.45) as supplied by a scientific-subroutine-package library program with the IBM 360. The maximum error thus introduced was at most 0.20% and in the majority of cases, comparison with known solutions showed a discrepancy of less than 0.1%.

3.4 The Assumption $\dot{g}(\eta,0) = 0$ as Initial Condition for the Unsteady Energy Equation

Examining the unsteady energy equation (2.31) it is seen that we require two boundary conditions in space and one in time. The space boundary conditions (2.43) and (2.44) or (2.45) apply to the solu-

tion of (2.31) for any arbitrary Prandtl number, however, this is not true for the initial condition (2.46). For the special case of Pr = 1, the solution given by (3.21) or (3.22) was obtained in Reference [4] in closed form without any specific regard to the initial condition given symbolically by (2.46). In fact, the initial condition is implied from the solution and is given by either (3.23) or (3.24). For Pr different from unity, a closed form solution to the unsteady energy equation cannot be found and hence it becomes necessary to resort to numerical techniques. The numerical method has already been described in Section 3.2 and we recall that the step by step procedure, as with any numerical technique, requires a given initial time line before it is able to commence.

It is evident that the solution $g(\eta,\tau)$ obtained from (2.31) must eventually coincide with some final steady state solution $g_2(\eta)$ in the limit as $\tau \to \infty$ ($\xi \to 1$) and this would satisfy the requirement of one boundary condition in time. Intuition indicates that the approach to the final steady state would be asymptotical so that a method similar to Reference [25] might be applied where an original guess at the initial $g(\eta,0)$ distribution is successively modified until the boundary condition at infinity is satisfied to within a predetermined tolerance and sufficiently large enough value of τ. Unfortunately any thought in this direction is already ruled out since, as was pointed out before, the solution to the unsteady momentum equation is not available for large values of τ. Thus, lacking any experimental evidence, it becomes necessary to fall back on physical and mathematical

reasoning to arrive at a reasonable approximation to the initial enthalpy distribution $g(\eta,0)$ corresponding to a sudden increase in velocity in the boundary layer.

Now any solution $g(\eta,\tau)$ to equation (2.31) must necessarily satisfy this equation for all times and in particular

$$2Pr \frac{\partial g}{\partial \tau} - \{g'' + Prfg' + Pr(\gamma-1) M_e^2 f''^2\} = 0 \qquad (3.52)$$

which is the unsteady energy equation (2.31) specialized to $\tau = 0$. Before any jump in velocity takes place, the enthalpy distribution in the boundary layer is given by the solution of the initial steady state, namely, the solution of

$$g_0'' + Pr\, f_0 g_0' + Pr(\gamma-1) M_{e0}^2 f_0''^2 = 0 \qquad (3.53)$$

where subscript "0" means symbolically $\tau < 0$. Intuitively one might think that the enthalpy jump corresponding to a sudden increase in velocity would simply be given by the solution of (3.53) with the initial values of the momentum equation substituted in place of the Blasius values. If this were indeed so, it would imply that $\partial g/\partial\tau(\eta,0) \equiv \dot{g}(\eta,0) = 0$ in expression (3.52). In view of definition (3.25) for Δg we have $\partial\Delta g/\partial\tau = \partial\Delta g/\partial\xi = -\partial g/\partial\tau$ at $\tau = 0$. When the solutions (3.21) and (3.22) for $Pr = 1$ are plotted in terms of Δg as a function of τ as in Fig. 3.8 for the insulated wall and also for non-zero wall heat transfer (case $g_w = 0$), it is observed that in both cases $\partial\Delta g/\partial\tau(\eta,0)$

is virtually zero even for very small values of η. We recall that one of the basic hypersonic assumptions (2.24) already made states that $\partial h_e/\partial t = 0$ so that in the free stream $\partial g/\partial \tau = 0$ is satisfied exactly. We have also seen that for the case of Pr = 1 the g-distribution is obtained at $\tau = 0$ simply by specializing the solution to the energy equation to zero time, that is, the initial values of the momentum equation are substituted in the solution to obtain the initial conditions (3.23) and (3.24). Figure 3.9 shows the results obtained when the initial condition (3.24) with $g_w = 21$ is used in the numerical solution of the energy equation with Pr = 1 up to $\tau = 1$. This is compared with the closed form solution (3.22), in terms of Δg, and it is clear that the two solutions agree almost exactly.

For an arbitrary Prandtl number there is, of course, no closed form solution and an initial $g(\eta,0)$ distribution must be found in a different way. Rewriting the exact equation (3.52) at zero time in the form

$$g'' + Prfg' = Pr[2\dot{g} - (\gamma-1)(M_e f'')^2] \qquad (3.54)$$

and assuming for the moment that the correct $\dot{g}(\eta,0)$ was known from some other source, the entire right-hand side of (3.54) could then be viewed as the inhomogeneous part of a second order ordinary differential equation for g. Now for Pr = 1 it is formally possible to obtain the range of magnitude for $\dot{g}(\eta,0)$; we have already shown an example, by

plotting the solutions in Fig. 3.8, where $\dot{g}(\eta,0) = -\Delta\dot{g}(\eta,0)$ is small for all η. An exact calculation for a particular case of $g_w = 21$, $Pr = 1$, $\gamma = 1.4$, and $M_e = 10$, shows that $\dot{g}(\eta,0)$ reaches its maximum value of only 0.9 very close to the wall ($\eta = .04$), diminishes rapidly to zero between $\eta = .43$ and .44 and attains a magnitude no greater than .056 as it approaches zero at $\eta = \eta_e$. Thus, for $Pr = 1$, the largest magnitude of $2\dot{g}(\eta,0)$ is 1.8. On the other hand, $f''(\eta,0) = f_2''(\eta) + \Delta f''(\eta,0)$ is also larger in magnitude near the plate and also tending to zero at $\eta = \eta_e$. In particular, at $\eta = .04$ $f'' = .4649$ so that the term $(\gamma-1)(M_e f'')^2$ is of magnitude 8.64 or approximately five times as great. In an order of magnitude analysis this would not quite justify neglect of the term $2\dot{g}$ relative to $(\gamma-1)(M_e f'')^2$. However, only slightly further up from the wall and out to the boundary layer edge the two terms compare more like 45 to 1 which clearly justifies neglect of $2\dot{g}(\eta,0)$ in equation (3.54) for the major portion of the boundary layer excluding only the region very close to the plate surface.

Considering the observations made above for the case of $Pr = 1$, it is speculated that for arbitrary Prandtl numbers different from unity, the required g-distribution at zero time might be obtained from the solution of

$$g_1''(\eta,0) + Pr\, f_1(\eta,0)\, g_1'(\eta,0) + Pr(\gamma-1)\, M_{e1}^2\, f_1'^2(\eta,0) = 0 \quad (3.55)$$

where subscript "1" means symbolically $\tau = 0$. Thus we are substituting

the initial values of the momentum equation into equation (3.52) and make the assumption that $\dot{g}(\eta,0) = 0$ for arbitrary values of Pr.

From physical considerations, the assumption that $\dot{g}(\eta,0) = 0$ is further reinforced when we recall Section 2.5 where, for the momentum equation, it was argued that at the instant of change of the free stream velocity the governing equation in the major portion of the boundary layer was

$$\frac{\partial u}{\partial t} = -\frac{1}{\rho}\frac{\partial p}{\partial x} \quad . \tag{3.56}$$

Since we are dealing with the region of zero pressure gradient we have, for the momentum equation, $\partial u/\partial t = 0$ at zero time. If we apply the same reasoning to the energy equation (2.4) we would neglect all viscous and convective terms and again for constant pressure the governing energy equation at zero time would then be

$$\frac{\partial h}{\partial t} = 0 \tag{3.57}$$

which is equivalent to saying $\partial g/\partial \tau(\eta,0) = 0$ in equation (2.31).

3.5 Alternative Solution of the Unsteady Energy Equation

It was observed in Section 3.3 that the form of the solutions for the steady state enthalpy distributions (3.50) and (3.51) are identical with the corresponding unsteady distributions (3.21) and (3.22) when the Prandtl number equals unity. That is, the time vari-

able τ in the solutions appears only as an independent variable in the function $f'(\eta,\tau)$. When the Prandtl number does not differ greatly from unity as in the case of gases, N. Curle [26] published an empirical steady state enthalpy distribution (due partly to R.J. Monaghan) which satisfies the boundary conditions both at the plate surface and at the edge of the boundary layer. Thus for $0.725 \leq Pr \leq 1.25$ and with the notation used here the empirical distributions become

$$g = 1 + [Pr^{1/2} \frac{\gamma-1}{2} M_e^2][1-(f')^3] - \frac{\gamma-1}{2} M_e^2 Pr[(f')^2-(f')^3] \quad (3.58)$$

for the adiabatic wall, and

$$g = 1+[g_w-1][1-(f')^3] + Pr^{1/3}[1+Pr^{1/2} \frac{\gamma-1}{2} M_e^2-g_w][f'-(f')^3] \quad (3.59)$$
$$- \frac{\gamma-1}{2} M_e^2 Pr[(f')^2 - (f')^3]$$

for the isothermal wall.

Figure 3.10 shows a comparison of the enthalpy distributions obtained from the empirical formulae and from the exact solution given by equation (3.43) for the case of $Pr = 0.72$ and $M_e = 10$. Agreement is seen to be fairly good throughout the entire boundary layer and almost exact agreement is obtained in the more important region close to the plate surface.

To justify the use of expressions (3.58) and (3.59) as approximate solutions of the unsteady energy equation (3.3) it is

necessary to show that the degree of satisfaction of (3.3), even though not exact, is at least constant throughout the time domain of integration. That equation (3.3) would not be satisfied exactly by such an empirical distribution is evident from Fig. 3.10 although better satisfaction would be expected nearer the plate. If we take for example the case of zero wall heat transfer with Pr = 0.72, M_e = 10, and τ = 0.25, evaluate from (3.58) the partial derivatives $\partial g/\partial \eta$, $\partial^2 g/\partial \eta^2$, $\partial g/\partial \xi$, substitute these into equation (3.3), denote by D the degree of satisfaction (i.e. the deviation from zero) of (3.3) and compare this quantity with the highest order partial derivative, we obtain the results shown in Fig. 3.11. It is seen that satisfaction is not exact (D = 0) as expected but the degree of satisfaction is about the same for the unsteady energy equation as for the initial steady state. Figure 3.12 shows the quantity D plotted against τ and it is observed to be practically constant in the range of τ from 0 to 1 for each η with the degree of satisfaction improving as we approach the wall. A similar result was observed for the isothermal wall using expression (3.59) for $g(\eta,\xi)$.

In concluding this Chapter, it is worth pointing out that aside from verifying that (3.24) is the correct $g(\eta,0)$ distribution for the solution (3.22) Fig. 3.9 also serves to show that the error in the numerical procedure used to solve the unsteady equations is quite small, as was expected from the results of Section 3.3.

CHAPTER IV

TRANSIENT HEAT TRANSFER, SKIN FRICTION AND INDUCED PRESSURE

4.1 Unsteady Heat Transfer Coefficient

The heat transfer at the plate is given by

$$q_w = - k \left.\frac{\partial T}{\partial y}\right|_{y=0} \tag{4.1}$$

or using (2.7) and (2.17)

$$q_w = - \frac{k_w h_e}{c_p} \frac{\rho_w}{\rho_{ref}} \left(\sqrt{\frac{U_e}{2\nu_{ref} Cx}}\right) \frac{\partial g}{\partial \eta} (0,\tau) \quad . \tag{4.2}$$

In high speed flow it has been found experimentally that the direction of heat flow at the wall does not depend on the difference between the wall temperature and the free stream temperature as in sub-sonic flow but rather on the difference between the wall temperature and the adiabatic wall temperature. Thus the surface convective conductance is defined by

$$\alpha = \frac{q_w}{(T_w - T_{raw})} \tag{4.3}$$

where α is time dependent for the unsteady problem, or in other words,

α represents the instantaneous local heat-transfer coefficient [27]. T_{raw} is the reference adiabatic wall temperature which, for consistency with the steady state, is taken as the final steady state adiabatic wall temperature. Using (4.2) and the definitions of the Prandtl number and local Reynolds number

$$Pr = \frac{\mu c_p}{k} \tag{4.4a}$$

and

$$Re_x = \frac{U_e x}{\nu} \tag{4.4b}$$

we obtain

$$(\sqrt{\frac{C}{2}})\, g'(0,\tau) = (\sqrt{Re_x})\, Pr\, St(g_{raw}-g_w)$$

where the Stanton number has also been employed with the definition

$$St = \frac{\alpha}{\rho c_p U_e} \quad . \tag{4.5}$$

In terms of the Nusselt number Nu = St Re Pr the local, non-dimensional, unsteady heat transfer coefficient may then be written as

$$\frac{Nu_x}{\sqrt{\frac{C}{2}}\, Re_x} = \frac{g'(0,\tau)}{(g_{raw}-g_w)} \tag{4.6}$$

4.2 Unsteady Skin Friction Coefficient

The skin friction coefficient C_f is defined as

$$C_f = \frac{\tau_w}{\frac{1}{2}\rho_{ref} U_e^2} \tag{4.7}$$

where the wall shear stress τ_w is given by

$$\tau_w = (\mu \frac{\partial u}{\partial y})\Big|_{y=0} \quad . \tag{4.8}$$

Again using (2.7) and (2.17) we obtain

$$\tau_w = \frac{\mu_w \rho_w}{\rho_{ref}} \frac{U_e^{3/2}}{\sqrt{2\nu_{ref} Cx}} f''(0,\tau) \tag{4.9}$$

so that (4.7) becomes

$$C_f \sqrt{\frac{Re_x}{2C}} = f''(0,\tau) \quad . \tag{4.10}$$

4.3 The Weak-Interaction Unsteady Induced Pressure

For the acoustic approximation to the induced pressure we have from [12]

$$\Delta p_v = \rho_e a_e v_e \, . \tag{4.11}$$

From [15] the expression for v_e with U_e a constant is

$$v_e = \frac{D\Delta}{Dt} = \frac{\partial \Delta}{\partial t} + U_e \frac{\partial \Delta}{\partial x} \quad . \tag{4.12}$$

Also from [15] the expression for the displacement thickness of the unsteady boundary layer is

$$\nabla \cdot \{\rho_e \vec{U}_e \Delta - \int_0^\infty (\rho_e \vec{U}_e - \rho \vec{u})\, dy\} + \frac{\partial}{\partial t} \{\rho_e \Delta - \int_0^\infty (\rho_e - \rho) dy\} = 0 \quad . \tag{4.13}$$

For our case U_e and ρ_e are constants so that (4.13) becomes

$$\frac{\partial}{\partial t} (\Delta - \delta_\rho) + U_e \frac{\partial}{\partial x} (\Delta - \delta^*) = 0 \tag{4.14}$$

where

$$\delta^* = \int_0^{y_e} (1 - \frac{\rho u}{\rho_e U_e})\, dy \tag{4.15}$$

and

$$\delta_\rho = \int_0^{y_e} (1 - \frac{\rho}{\rho_e})\, dy \quad . \tag{4.16}$$

In terms of the transformed variables used these expressions become in turn

$$\delta^* = \int_0^{Y_e} (\frac{T}{T_e} - \frac{u}{U_e}) dY = (\sqrt{\frac{2\nu_e Cx}{U_e}}) \int_0^{\eta_e} (g - f')\, d\eta \tag{4.17}$$

and

$$\delta_\rho = \int_0^{Y_e} \left(\frac{T}{T_e} - 1\right) dY = \left(\sqrt{\frac{2\nu_e Cx}{U_e}}\right) \int_0^{\eta_e} (g-1)d\eta \ . \qquad (4.18)$$

Combining (4.11), (4.12) and (4.14) we obtain

$$\frac{\Delta p_v}{p_e} = \frac{\rho_e a_e}{p_e} \left\{\frac{\partial \delta_\rho}{\partial t} + U_e \frac{\partial \delta^*}{\partial x}\right\} \qquad (4.19)$$

or

$$\frac{\Delta p_v}{p_e} = \gamma\left\{\frac{1}{a_e} \frac{\partial \delta_\rho}{\partial t} + M_e \frac{\partial \delta^*}{\partial x}\right\} \ . \qquad (4.20)$$

Differentiating (4.17) with respect to x and (4.18) with respect to t

$$\frac{\partial \delta^*}{\partial x} = \left(\sqrt{\frac{2\nu_e C}{U_e}}\right)\left\{\frac{I}{2\sqrt{x}} + (\sqrt{x})\frac{\partial I}{\partial x}\right\} \qquad (4.21)$$

and

$$\frac{\partial \delta_\rho}{\partial t} = \left(\sqrt{\frac{2\nu_e Cx}{U_e}}\right) \frac{\partial J}{\partial t} \qquad (4.22)$$

where

$$I = I(\tau) = \int_0^{\eta_e} (g-f')d\eta \qquad (4.23)$$

and

$$J = J(\tau) = \int_0^{\eta_e} (g-1)\,d\eta \quad . \tag{4.24}$$

Introducing the fundamental hypersonic interaction parameter χ [1,3] defined as

$$\chi = M_e^{\,3} \sqrt{\frac{C}{Re_x}} = M_e^{\,3} \sqrt{\frac{\nu_e C}{U_e x}} \tag{4.25}$$

then

$$M_e \frac{\partial \delta^*}{\partial x} = \frac{1}{\sqrt{2}\, M_e^{\,2}} \chi \{I - 2\tau \frac{\partial I}{\partial \tau}\} \tag{4.26}$$

and

$$\frac{1}{a_e} \frac{\partial \delta_\rho}{\partial t} = \frac{\sqrt{2}}{M_e^{\,2}} \chi \frac{\partial J}{\partial \tau} \quad . \tag{4.27}$$

Substituting (4.26) and (4.27) into expression (4.20) we obtain

$$\frac{\Delta p_v}{p_e} = \frac{\gamma \chi}{M_e^{\,2}} \{\sqrt{2} \frac{\partial J}{\partial \tau} + \frac{1}{\sqrt{2}} (I - 2\tau \frac{\partial I}{\partial \tau})\} \tag{4.28}$$

which for the final steady state reduces to

$$\frac{\Delta p_{v2}}{p_e} = \frac{\gamma\, I_2}{\sqrt{2}\, M_e^{\,2}} \chi \quad . \tag{4.29}$$

CHAPTER V

DISCUSSION AND CONCLUSIONS

5.1 Discussion of Results

Keeping in mind the small magnitudes of our Δg function defined by (3.25), it had to be ensured that the errors involved in the numerical solutions to both $g_2(\eta)$ and $g_1(\eta,0)$ as well as those in the solution of the unsteady energy equation (3.26) are by far below the scale of Δg. We have already seen from Fig. 3.9 that, using the closed form initial condition, the error in the solution of (3.26) for Pr = 1 is virtually negligible. In Section 3.3 it was shown that the errors in $g_2(\eta)$ were, relatively speaking, insignificant as well. Although equation (3.55) is of the same form as equation (2.33) the solution given by (3.43) does not apply since $f_1(\eta,0)$ does not satisfy $f_1''' + f_1 f_1'' = 0$. However, the recurrence relationship used to determine the stepsize H in Section 3.3 was used as a means of calculating the $g_1(\eta,0)$ distribution from equation (3.55) with a stepsize H = 0.01. In addition the $g_1(\eta,0)$ distribution associated with (3.55) was also obtained from a general subroutine called DLBVP, which is supplied with the Scientific Subroutine Package for the IBM 360 [28], and solves a general linear boundary value problem. The results obtained with the recurrence method checked almost perfectly with those using this subroutine. The added advantage of subroutine DLBVP is that it

permits the subdivision of the initial stepsize H = 0.01 as much as ten times in order to attain an almost arbitrary accuracy specified by the user. Thus we can be reasonably confident that any discrepancies observed in subsequent results are most likely to be due to our assumptions or approximations and not due to the numerical methods.

Recalling that the underlying concern of this work was to obtain an enthalpy "jump" in the boundary layer corresponding to a certain jump in the free stream velocity, the assumption $\dot{g}(\eta,0) = 0$ should really be scrutinized in the following light: One of the fundamental characteristics of hypersonic flow is that relatively small perturbations in the velocity are accompanied by relatively large perturbations in the density, pressure, temperature, and speed of sound [29]. Hence in hypersonic flow the Mach number changed primarily as a result of the change in the speed of sound. Let us consider as an example a flow for which the final free stream Mach number M_{e2} has a value of 10. Then it may be shown that before the 1% jump in velocity occurred, the initial free stream Mach number M_{e0} was approximately 8.45 for a gas with $\gamma = 1.4$. For the case of Pr = 1 and $g_w = 0$ say, we can calculate from equation (3.53) the initial steady state enthalpy distribution $g_0(\eta)$ corresponding to a Mach number of 8.45 by using solution (3.22). From the closed form solution, equation (3.24), we can also calculate the $g_1(\eta,0)$ distribution corresponding to $M_{e1} = M_{e2} = 10$. Subtracting $g_0(\eta)$ from $g_1(\eta,0)$ will yield the corresponding jump in enthalpy for the case of Pr = 1. The solid curve in Fig. 5.1 shows the resulting enthalpy jump. If

we now apply our assumption of $\dot{g}(\eta,0) = 0$ and hence calculate the $g_1(\eta,0)$ distribution from equation (3.55) we obtain an enthalpy jump shown plotted by the broken curve in Fig. 5.1. The corresponding enthalpy jumps for the adiabatic wall is shown in Fig. 5.2. The first thing to notice is that the enthalpy jump is certainly not a constant as might perhaps be speculated from the discussion in Section 3.4. The second observation is, of course, that our assumption results in an enthalpy jump which closely resembles that predicted by the closed form solution, at least within errors that could be tolerated. From Fig. 5.1 we determine a maximum discrepancy of about 7.5% and from Fig. 5.2 about 9.5%. It is most likely that any experimental determination of the unsteady enthalpy profiles would contain errors of magnitude at least of the same order as depicted in Figs. 5.1 and 5.2.

In order to discuss the effect of the deviation of the Prandtl number from unity, solutions for Pr = 1 should be obtained by the application of the same assumptions or approximations as for the solutions of Pr different from one. That is, in Section 3.4 all comparison should be made on the basis that $\dot{g}(\eta,0) = 0$ and in Section 3.5 comparison should be made with the closed form solutions of Reference [4] since (3.58) and (3.59) reduce to (3.21) and (3.22) respectively when Pr = 1.

Figures 5.3 and 5.4 illustrate the effect of reducing the Prandtl number from 1 to 0.72 upon the assumption that $\dot{g}(\eta,0) = 0$.

The solutions of (3.26) here for the adiabatic wall and the cold wall ($g_w = 0$) have been plotted in the form $\Delta g(\eta,\tau) = g(\eta,\tau) - g_1(\eta,0)$ since it is not entirely obvious that the solution $g_2(\eta)$ of (2.33) is the corresponding final steady state when the initial condition $g_1(\eta,0)$ is given by the solution of (3.55). The initial steady state $g_0(\eta)$ is a natural reference state for this solution but presentation of the results in the form $\Delta g(\eta,\tau) = g(\eta,\tau) - g_0(\eta)$ did not lend itself very well in displaying the transient behaviour of the solution. The instantaneous local Nusselt number given by expression (4.6) is represented in Fig. 5.5 with $M_e = 10$ and for Pr = 1.0 and 0.72. That the enthalpy gradient at the wall $g_2'(0)$ is less for Pr = .72 than for Pr = 1.0 is evident from inspection of Fig. 3.6, however, the reference enthalpies g_{raw} differ also for Pr = .72 ($g_{raw} = 17.9$, $M_e = 10$) and for Pr = 1.0 ($g_{raw} = 21$, $M_e = 10$). Thus it might have been anticipated that (4.6) is independent of Prandtl number. A net reduction of the Nusselt number, however, makes physical sense since the dynamic viscosity μ is smaller for a gas with a lower Prandtl number which in turn results in a lower frictional heating of the gas and hence a lower rate of heat transfer to the wall when the wall enthalpy g_w is less than the adiabatic wall enthalpy. We note also in Fig. 5.5 that the curves differ slightly with different values of g_w and that the coefficient rises rapidly to a more or less constant value. In view of Fig. 3.4 the point $\tau = \eta = 0$ must be excluded for which reason the curves on Fig. 5.5 have not been extended to $\tau = 0$.

The transient weak-interaction induced pressure given by

expression (4.28) is shown plotted in Fig. 5.6 for Pr = 1 and .72 with $\chi = 4.5$ and $M_e = 10$. The value of $\chi = 4.5$ has been chosen merely for comparison of results given in Reference [4]; for the weak interaction region the interaction parameter χ assumes a magnitude not much greater than one [1,3]. Again it appears as if the transient portions of the curves may, for all practical purposes, be neglected, at least in the event of only a small velocity impulse of 1%. Strickly speaking the points $\tau = 0$ should again be disregarded and it has, furthermore, been pointed out [12] that the acoustic approximation (4.11) becomes invalid at $\tau = 0$.

The results from the empirical distributions of Section 3.5 are shown on Figures 5.7 and 5.8. They are plotted in the form $\Delta g(\eta,\tau) = g_2(\eta) - g(\eta,\tau)$ this time since the solutions are made to satisfy the necessary time boundary condition at infinity. The solid curves for Pr = 1 have also been obtained from (3.58) and (3.59) but they are in fact coincident with the closed form solutions given in Reference [4]. An interesting outcome of the numerical solutions for $g(\eta,\tau)$ pertains to the case of an insulated wall. The boundary condition to be satisfied at the wall is $\partial g/\partial\eta(0,\tau)\big|_{\eta=0} = 0$ i.e. (2.45), but also, because there is no heat transfer to the wall and no slip velocity, the wall enthalpy must remain constant. The velocity of the layer of fluid immediately adjacent to the wall, however, is varying as the boundary layer adjusts itself to the new steady state so that the temperature in this layer is also expected to vary during this period of readjustment. The result is a temperature jump at the wall which is brought out by the computer program because the finite difference

representation of the derivative at the wall relates the wall temperature to the temperature in the first layer of fluid. Figure 5.3 depicts such a jump whereas Fig. 5.7 does not. We also note that the associated boundary condition, namely $\partial\Delta g/\partial\eta(0,\tau) = 0$ is satisfied for all time curves in our solution assuming $\dot{g}(\eta,0) = 0$ whereas this boundary condition is not satisfied in Fig. 5.7 for $\tau = 0$. Thus, some doubt is cast on the validity of the closed form solution and it must be emphasized that without experimental evidence it is difficult to pass judgement as to which of the two solutions predicts more closely the actual state of affairs.

The heat transfer expression (4.6) from the empirical solution is shown in Fig. 5.9. Here also a rapid advance to a constant value is observed although high values are predicted for small τ in contrast with Fig. 5.5. Also the two curves in Fig. 5.9 represent all values of M_e and g_w which was not the case of Fig. 5.5. That the heat transfer data is obtainable from a single curve for Pr = 1 is the result of Reynolds analogy and it can be shown that the solid curve in Fig. 5.9 may be obtained from the shear stress parameter in Fig. 5.13. For Pr = 0.72, Reynolds analogy is no longer valid but the fact that we have based the Nusselt number on the difference $T_w - T_{raw}$ renders the Nusselt number as some function $f(Pr,Re_x)$ i.e. explicit dependence only on the Reynolds and Prandtl numbers. Conversely, basing the Nusselt number on the difference $T_w - T_e$ would lead to some function $\bar{f}(Pr,Re_x,E)$ i.e. explicit dependence on the Eckert number $E = \frac{(\gamma-1)}{(g_w-1)} M_e^2$ [2].

The weak-interaction induced pressure is shown in Fig. 5.10 again with $M_e = 10$ and $\chi = 4.5$. These curves are very similar to those in Fig. 5.6 except that for smaller g_w the transition to a constant value is slightly more gradual. One major difference, however, is that for $g_w \geq 10$ the induced pressure with the assumption $\dot{g}(\eta,0) = 0$ for Pr = .72 is larger than for Pr = 1.0 whereas in Fig. 5.10, using the empirical distribution, the induced pressure is smaller for Pr = .72 for all values of g_w up to its equivalent adiabatic value. If we calculate a steady state induced pressure from equation (4.29) using the solution $g_2(\eta)$ of equation (2.33) as the final steady state enthalpy distribution and plot the results as a function of g_w for both Pr = 1 and Pr = 0.72 the curves shown in Fig. 5.11 are obtained. We observe that the induced pressure for the steady state case and for Pr = .72 does indeed exceed that for Pr = 1 for values of g_w greater than approximately 10. We note also that the solution of (2.33) given by (3.43) is exact and is free from the kind of assumptions and approximations made for the unsteady case. Thus Fig. 5.6 appears to give to more correct results although it is possible in Fig. 5.10 that the Pr = .72 curves for $g_w > 10$ might eventually overtake the Pr = 1.0 curves since they have not yet exactly leveled off at $\tau = 1$. Experimental evidence would again be helpful here.

Figure 5.12 shows the transient induced pressure as a function of the interaction parameter χ for $g_w = 0$ and for different free stream Mach numbers as obtained from the empirical distribution. The Mach number is seen to have only a very small effect when increased from

5 to 10, which is a rather surprising result. Finally Fig. 5.13 shows the wall shear stress parameter of Section 4.2 which differs only slightly from the curve given in Reference [4] since it was calculated here using the 10-point computational molecule.

5.2 Conclusions

In the steady state case, a reduction of Prandtl number from 1 to 0.72 has the effect, according to Fig. 3.6, of reducing the maximum dimensionless enthalpy by approximately 19.5% for the cold wall ($g_w = 0$) and approximately 15% for the adiabatic wall. According to the assumption $\dot{g}(\eta,0) = 0$, the corresponding reduction in the transient Δg distributions is on the average approximately 8% for the adiabatic wall and 15% for the cold wall. With the empirical distributions we observe an approximate average reduction of 16% for the adiabatic wall (Fig. 5.7) and 22% for the cold wall (Fig. 5.8). When viewed in this manner the Prandtl number effect is about the same for the unsteady solutions as for the steady state case except perhaps for the results of Fig. 5.3.

The effect on the local heat transfer expression (4.6) in accordance with the assumption $\dot{g}(\eta,0) = 0$ (Fig. 5.5) is a reduction by about 11% for $g_w = 0$, 11.3% for $g_w = 10$ and 12.2% for $g_w = 15$ at $\tau = 1$. Similarly from Fig. 5.9 using the empirical distribution, the reduction due to a change in Pr from 1 to .72 is 10.3% at $\tau = 1$ which applies for all M_e and g_w below the equivalent adiabatic value. The assumption $\dot{g}(\eta,0) = 0$ predicts a fairly sudden increase in heat transfer from some lower value at $\tau = 0$ to a larger, more or less

constant value. The empirical distribution results of Fig. 5.9 for Pr = .72 on the other hand follows the form of the closed form solution for Pr = 1 which predicts a slightly more gradual reduction in heat transfer from some larger value at $\tau = 0$ to a more or less constant value at later times.

The induced pressures from Figs. 5.6 and 5.10 behave quite similar and it appears that the transient behaviour may be neglected since a fairly constant value is reached almost instantaneously. The results with $\dot{g}(\eta,0) = 0$ predict a behaviour with g_w which is more consistent with that observed in the final steady state, Fig. 5.11, namely, that a larger induced pressure is observed with a smaller Prandtl number for wall enthalpy ratios g_w greater than about 10 but less than their equivalent adiabatic wall values. With the assumption of $\dot{g}(\eta,0) = 0$ a reduction in the induced pressure according to Fig. 5.6 is observed as follows: 8.4% for the adiabatic wall and about 15% for the cold wall. From Fig. 5.10 we observe a reduction of 12.9% for the adiabatic wall and 22.6% for the cold wall.

Finally we conclude that the Mach number effect on the induced pressure as seen from Fig. 5.12 is virtually negligible compared with the effect of a small change in Prandtl number and that the transient shear stress parameter $\Delta f''$ Fig. 5.13 is larger than that given in Ref. [4] when the 10-point computational molecule with H = T = .01 is used in the solution of the unsteady momentum equation.

REFERENCES

[1] Dorrance, W.H., "Viscous Hypersonic Flow", McGraw-Hill Series in Missile and Space Technology, 1962.

[2] Schlichting, H., "Boundary-Layer Theory", McGraw-Hill, 6th ed., translated by Dr. J. Kestin.

[3] Hayes, W.D. and Probstein, R.F., "Hypersonic Flow Theory", Academic Press, 1959.

[4] Rodkiewicz, C.M. and Reshotko, E., "Time Dependent Hypersonic Viscous Interactions", AFOSR Scientific Report, AFOSR 67-2451, FTAS/TR-67-28, 1967.

[5] Sears, W.R., "Theory of Time-Dependent Laminar Flows", in "Theory of Laminar Flows, High Speed Aerodynamics and Jet Propulsion", F.K. Moore, ed. Vol. IV, Princeton University Press, 1964.

[6] Rosenhead, L., "Laminar Boundary Layers", Oxford University Press, 1963.

[7] Stewartson, K., "On the Impulsive Motion of a Flat Plate in a Viscous Fluid", Quart. Appl. Math. and Mech., Vol. 4, pp. 182-98.

[8] Rodkiewicz, C.M. and Gupta, R.N., "Time-Dependent Shear Stress and Temperature Distribution Over an Insulated Flat Plate Moving at Hypersonic Speed", Transactions of the Canadian Aeronautics and Space Institute, 1971.

[9] Flügge-Lotz, A.F. and Johnson, A.F., "Laminar Compressible Boundary Layer Along a Curved Insulated Surface", J.A.S. Vol. 22, July, 1955.

[10] Ostrach, S., "Compressible Laminar Boundary Layer and Heat Transfer for Unsteady Motions of a Flat Plate", NACA TN 3569, November, 1955.

[11] Dorrance, W.H., "Two-Dimensional Airfoils at Moderate Hypersonic Velocities" J.A.S. Vol. 19, Feb. 1952, pp. 593-600.

[12] Moore, F.K., "Hypersonic Boundary Layer Theory", F.K. Moore, ed. "Theory of Laminar Flows, High Speed Aerodynamics and Jet Propulsion", Vol. IV, Princeton University Press, 1964.

[13] Lighthill, M.J., "Oscillating Airfoils at High Mach Number", J.A.S. Vol. 20, June, 1953.

[14] Miles, J.W., "Unsteady Flow at Hypersonic Speeds" in Hypersonic Flow, Proceedings of the Eleventh Symposium of the Colston Research Society held in the University of Bristol, 1959, Edited by A.R. Collar and J. Tinkler.

[15] Moore, F.K. and Ostrach, S., "Displacement Thickness of the Unsteady Boundary Layer", J.A.S., January, 1957.

[16] Shen, S.F., "On the Boundary Layer Equations in Hypersonic Flow", J.A.S., Vol. 19, July, 1952.

[17] Butler, T.D., "Numerical Solutions of Hypersonic Sharp-Leading-Edge Flows", The Physics of Fluids, Vol. 10, No. 6, June, 1967.

[18] Stewartson, K., "The Theory of Laminar Boundary Layers in Compressible Fluids", Oxford Mathematical Monographs, 1964.

[19] Miles, J.W., "The Potential Theory of Unsteady Supersonic Flow", Cambridge Monographs on Mechanics and Applied Mathematics, 1959.

[20] Chapman, D.R. and Rubesin, M.W., "Temperature and Velocity Profiles in the Compressible Laminar Boundary Layer with Arbitrary Distribution of Surface Temperature", J.A.S., Vol. 16 , No. 9, 1949, pp. 547-565.

[21] Gupta, R.N. and Rodkiewicz, C.M., "Unsteady Boundary-Layer Induced Pressure at Hypersonic Speed", The Physics of Fluids, 1971.

[22] Richtmyer, R.D. and Morton, K.W., "Difference Methods for Initial-Value Problems", Interscience Publishers, 1967.

[23] Tokuda, N., "On the Impulsive Motion of a Flat Plate in a Viscous Fluid", J. Fluid Mech., Vol. 33, 1968, pp. 657-672.

[24] Conte, S.D., "Elementary Numerical Analysis", McGraw-Hill Book Co., 1965.

[25] Nachtsheim, P.R. and Swigert, P., "Satisfaction of Asymptotic Boundary Conditions in Numerical Solution of Systems of Nonlinear Equations of Boundary-Layer Type", NASA TN D-3004.

[26] Curle, N., "The Effects of Heat Transfer on Laminar-Boundary-Layer Separation in Supersonic Flow", Aeronautical Quarterly, Vol. XII, Nov. 1961.

[27] Sparrow, E.M. and Gregg, J.L., "Nonsteady Surface Temperature Effects on Forced Convection Heat Transfer", J.A.S. Vol. 24, October, 1957, pp. 776-777.

[28] System/360 Scientific Subroutine Package (360 A-CM-03X) Version III Programmer's Manual, IBM Publication H20-0205-3.

[29] Chernyi, G.G., "Introduction to Hypersonic Flow" translated by Probstein, R.F., Academic Press, 1961.

APPENDIX A

CURVES FOR CHAPTERS III AND IV

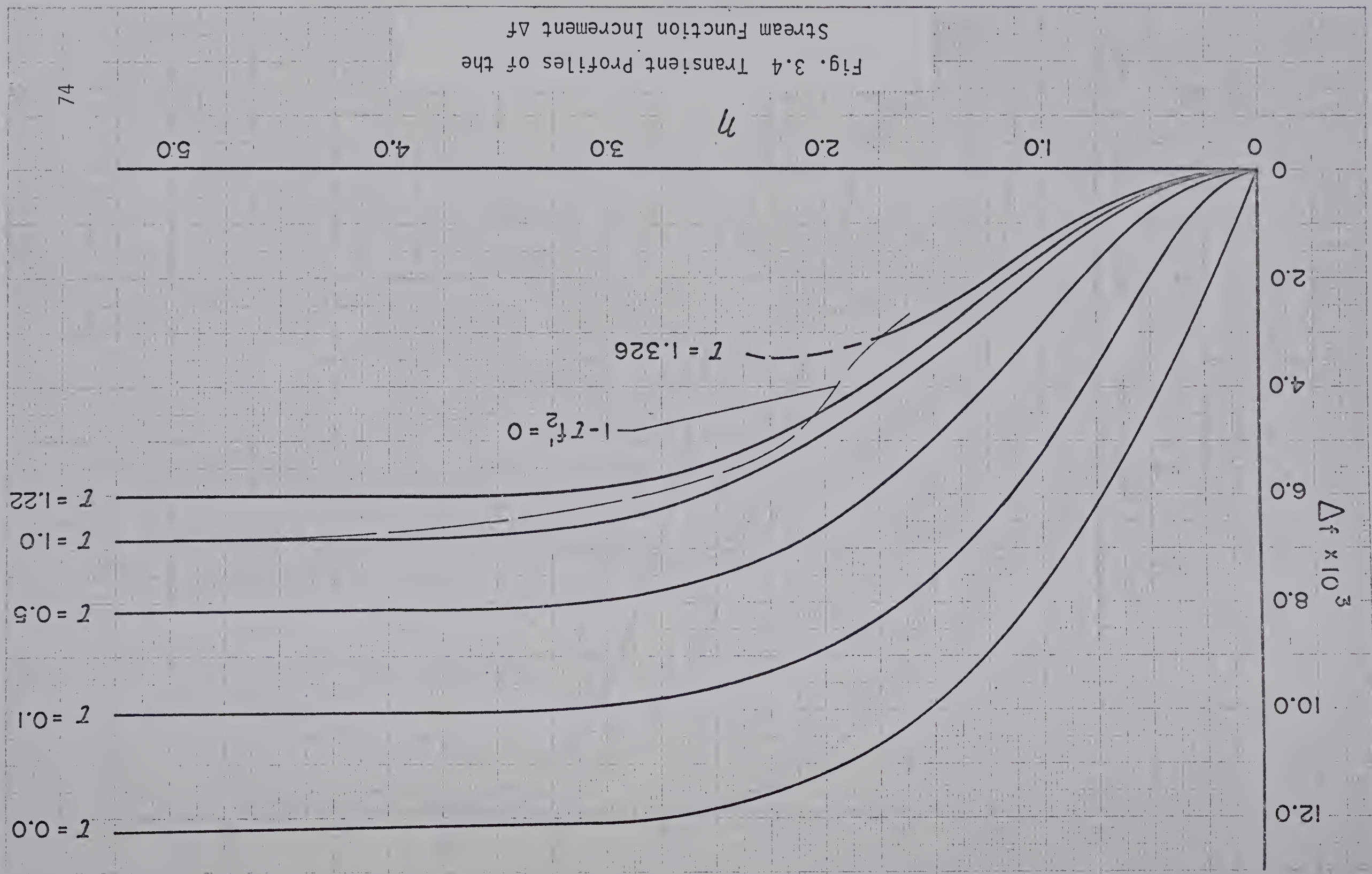

Fig. 3.4 Transient Profiles of the Stream Function Increment Δf

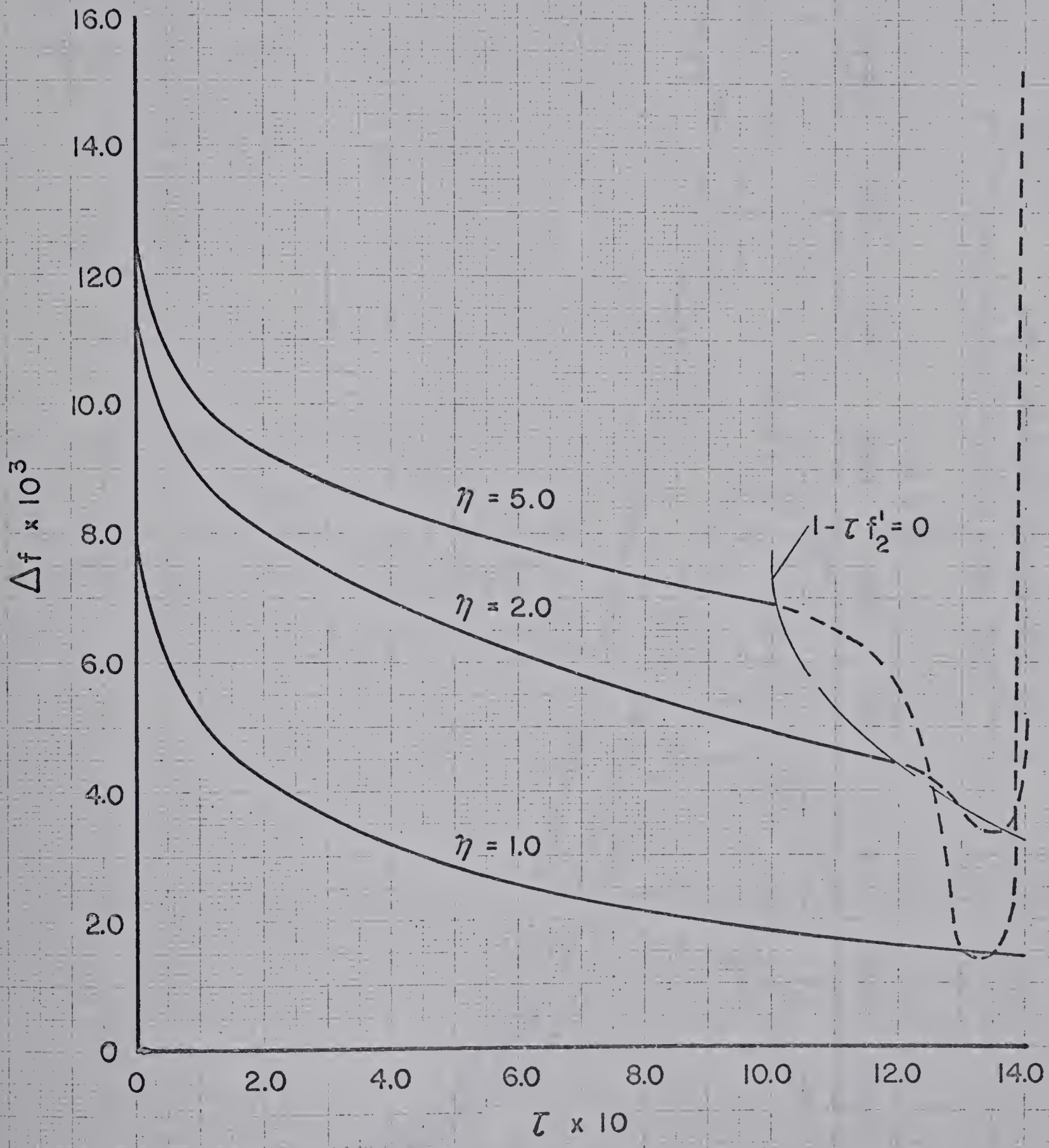

Fig. 3.5 Dimensionless-time Dependence of the Stream Function Increment Δf

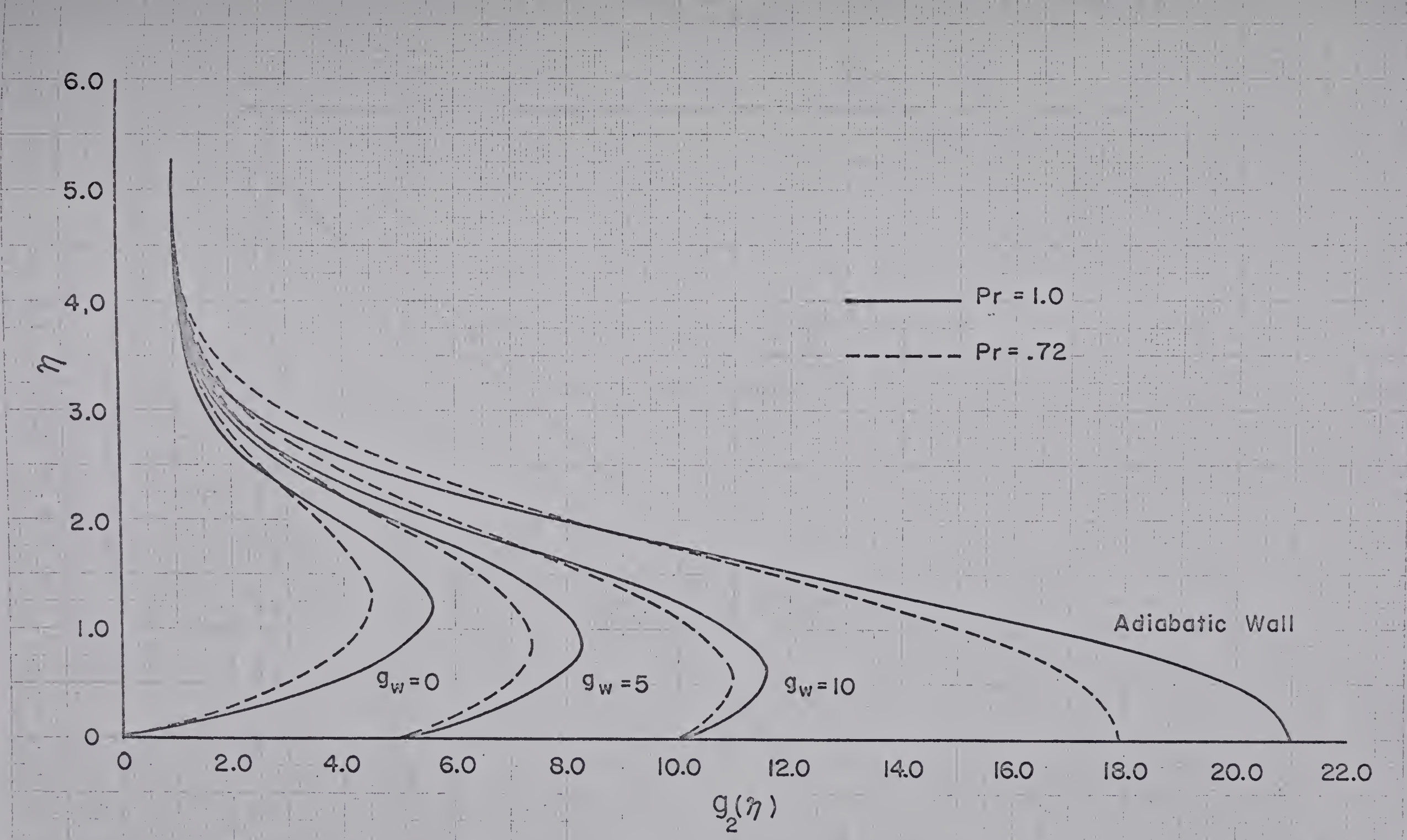

Fig. 3.6 Steady State Enthalpy Distributions in the Compressible Boundary Layer for $M_e = 10$

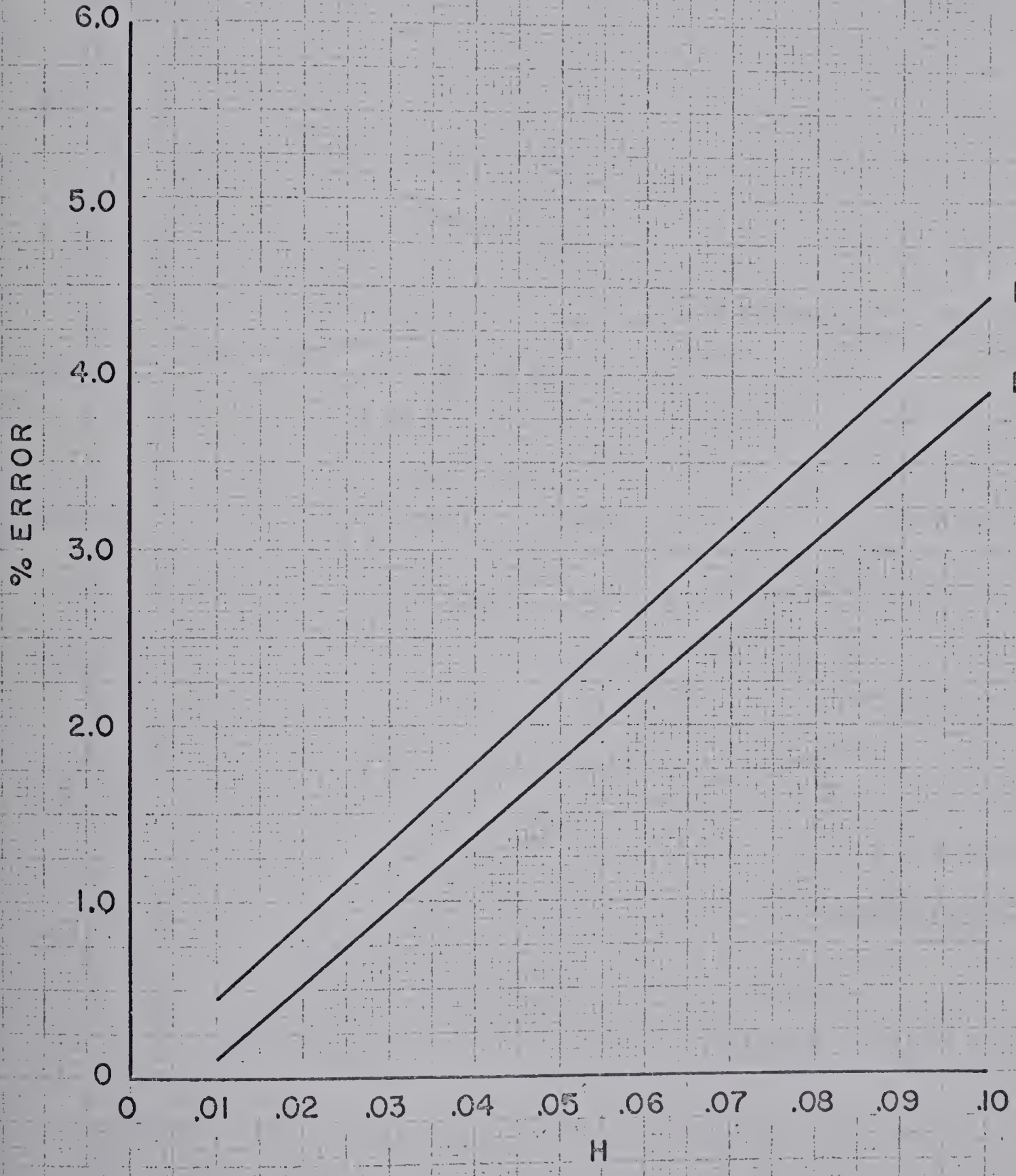

Fig. 3.7 Error Curves in the Recurrence Solution of the Dimensionless Adiabatic-Wall Enthalpy for $M_e = 10$

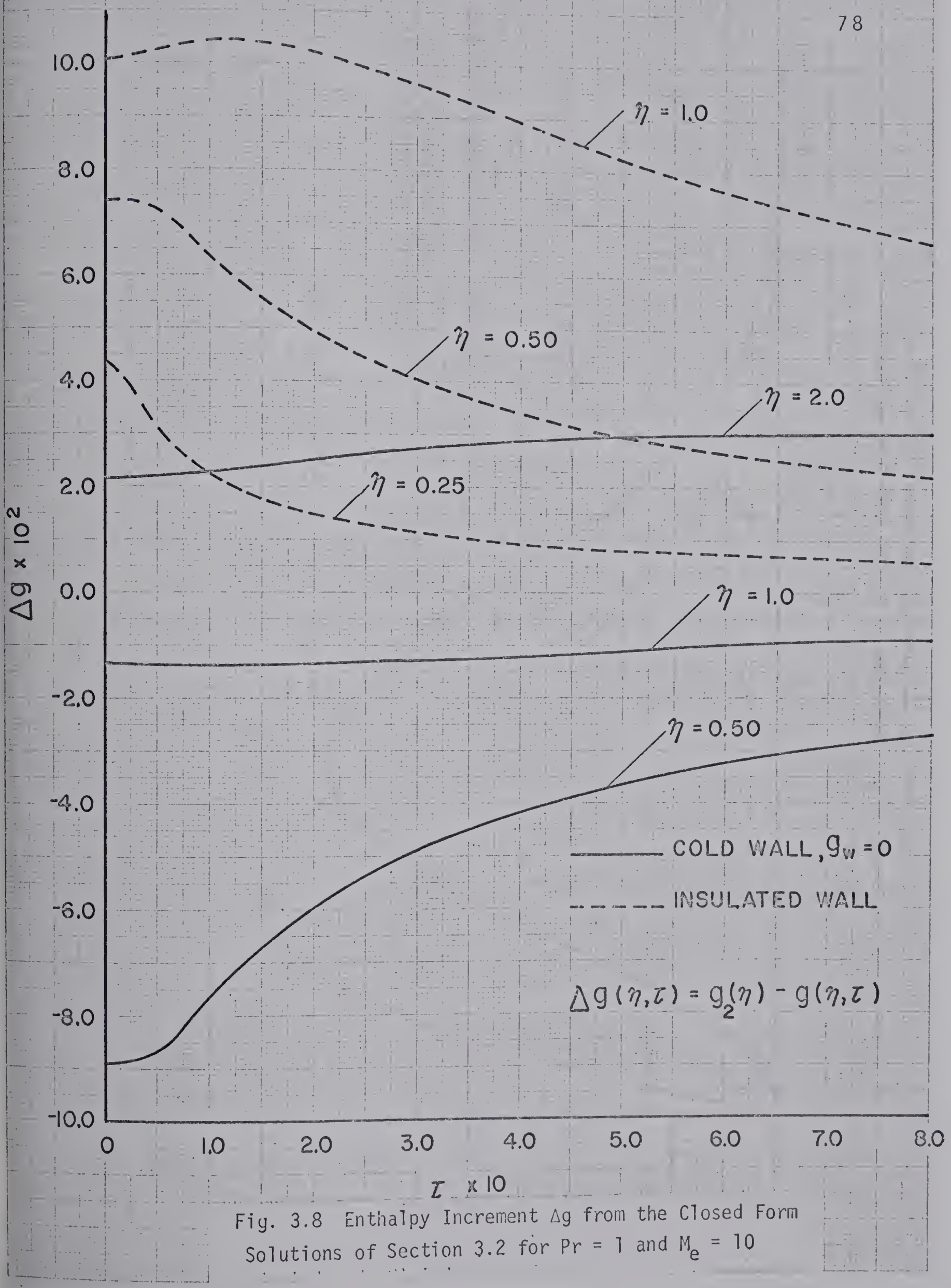

Fig. 3.8 Enthalpy Increment Δg from the Closed Form Solutions of Section 3.2 for Pr = 1 and M_e = 10

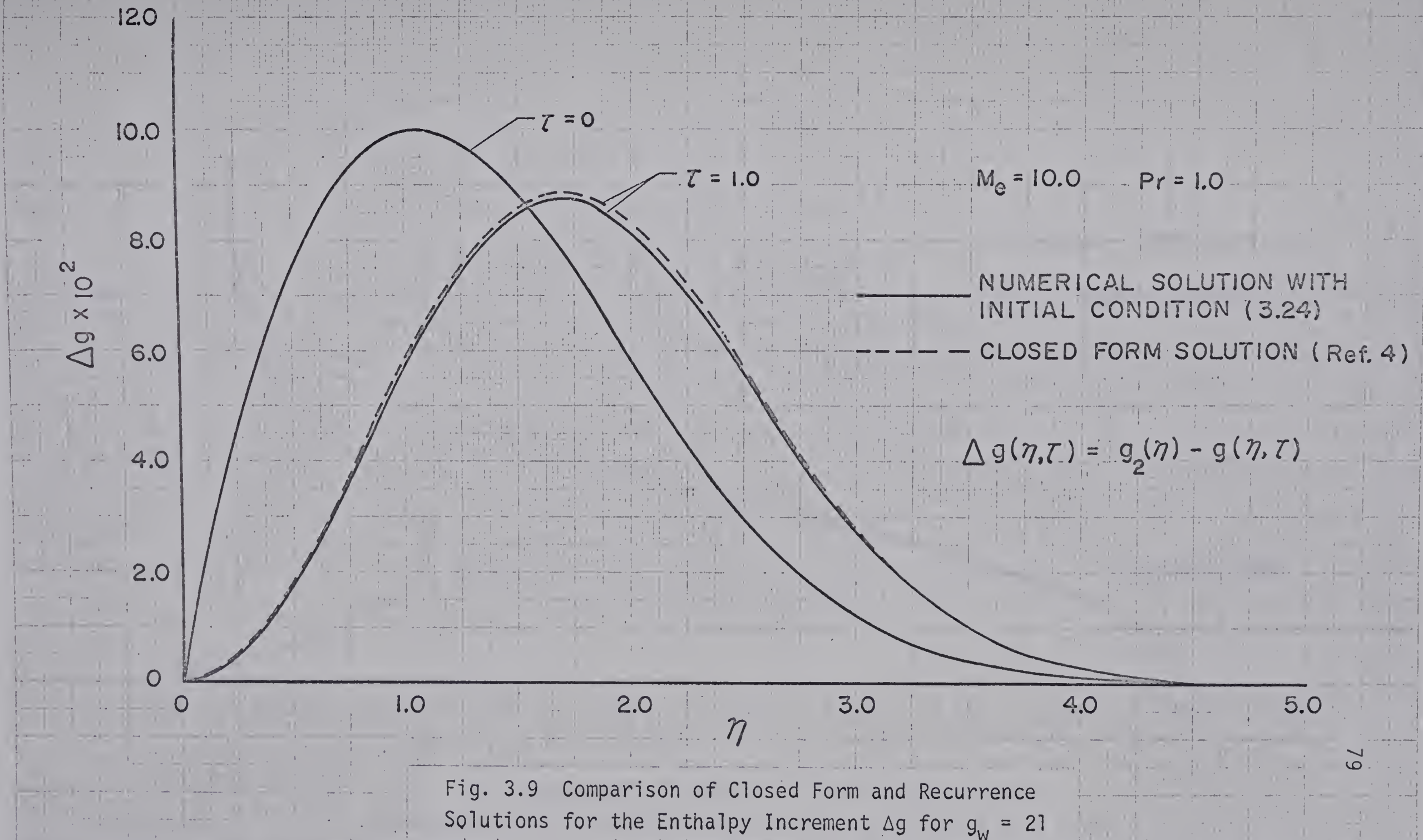

Fig. 3.9 Comparison of Closed Form and Recurrence Solutions for the Enthalpy Increment Δg for $g_w = 21$

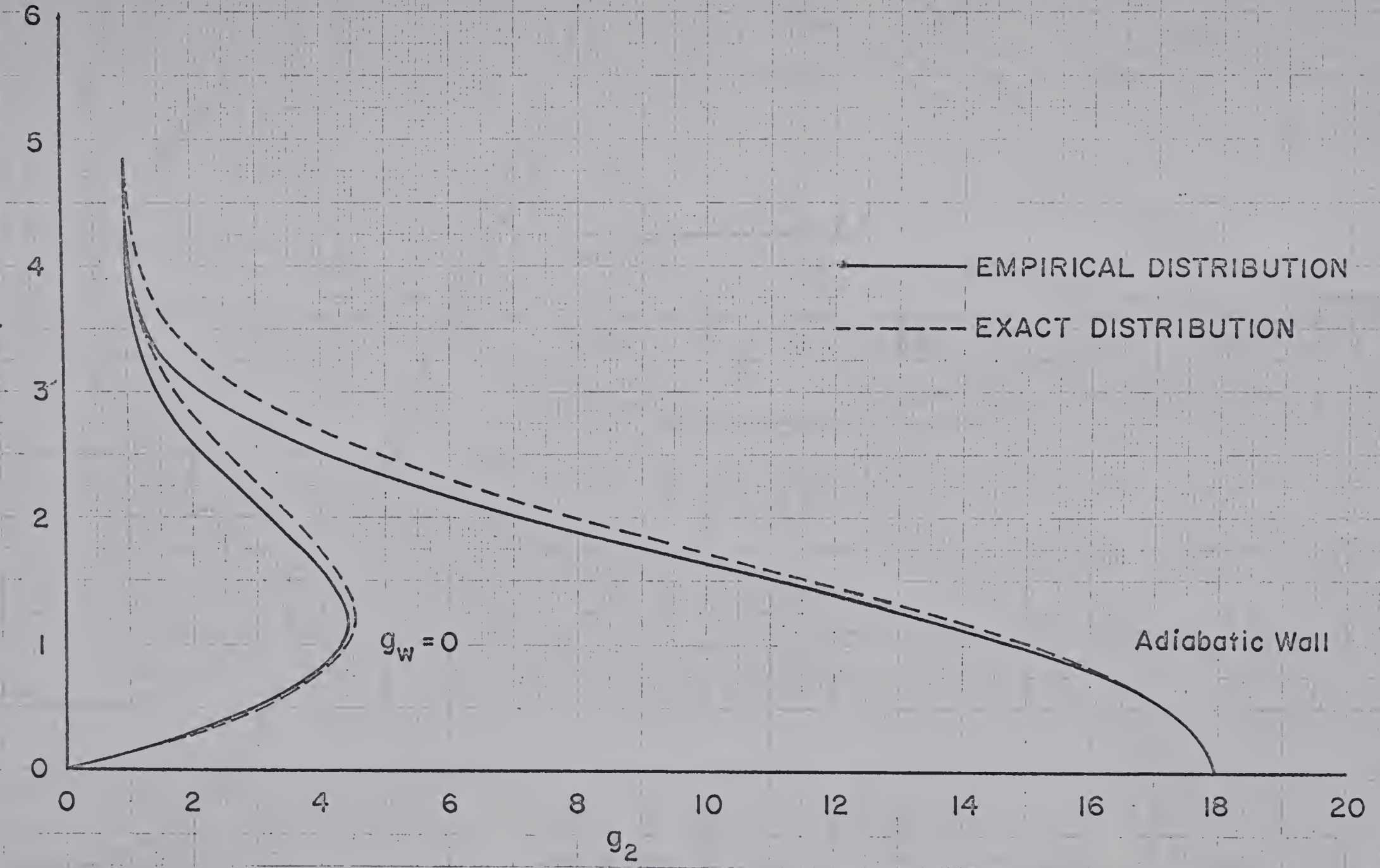

Fig. 3.10 Comparison of Empirical Steady State Enthalpy Distribution with the Exact Solution for M_e = 10 and Pr = 0.72

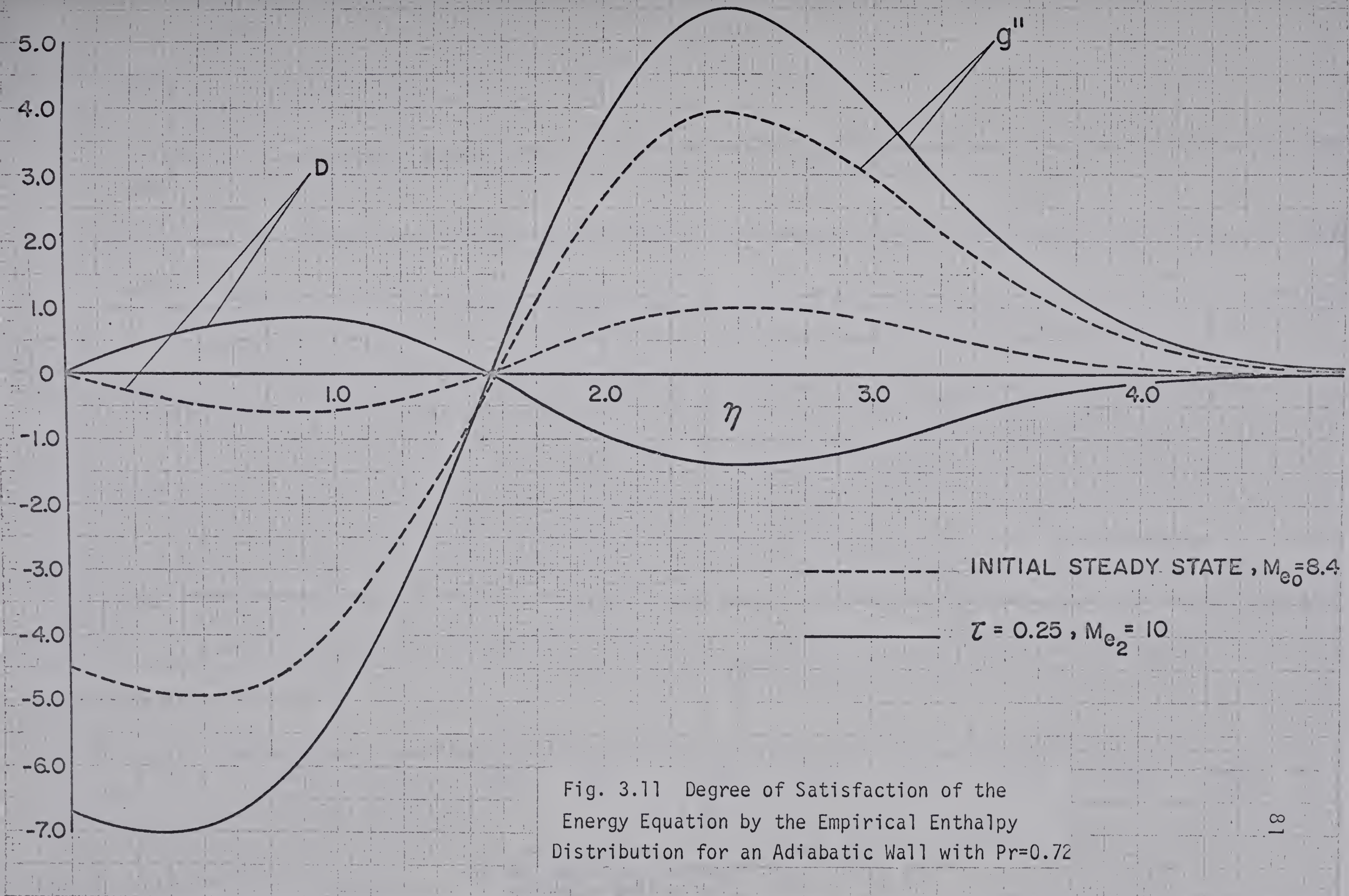

Fig. 3.11 Degree of Satisfaction of the Energy Equation by the Empirical Enthalpy Distribution for an Adiabatic Wall with Pr=0.72

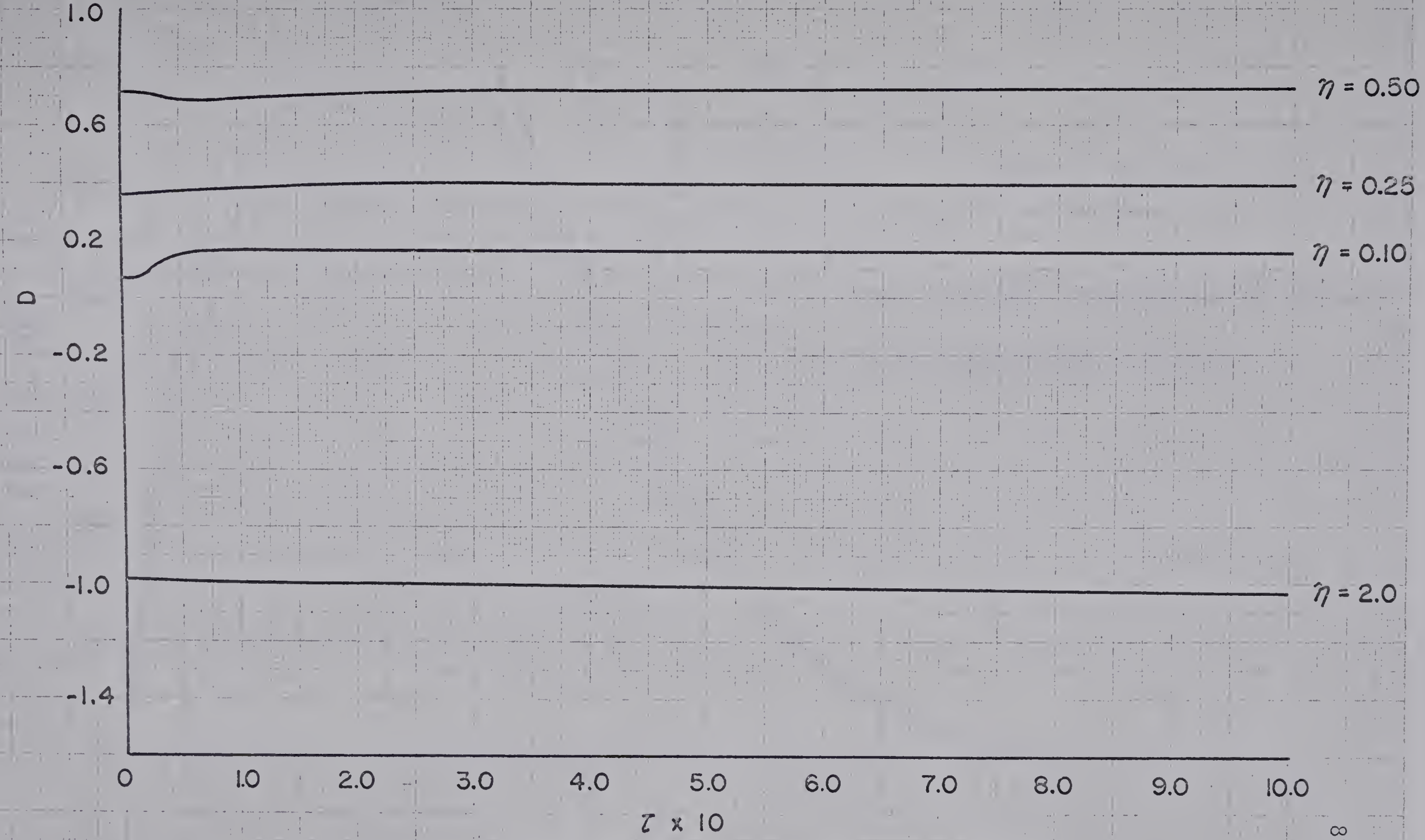

Fig. 3.12 Satisfaction of the Unsteady Energy Equation by the Empirical Enthalpy Distribution for an Adiabatic Wall with $M_e = 10$, $Pr = 0.72$

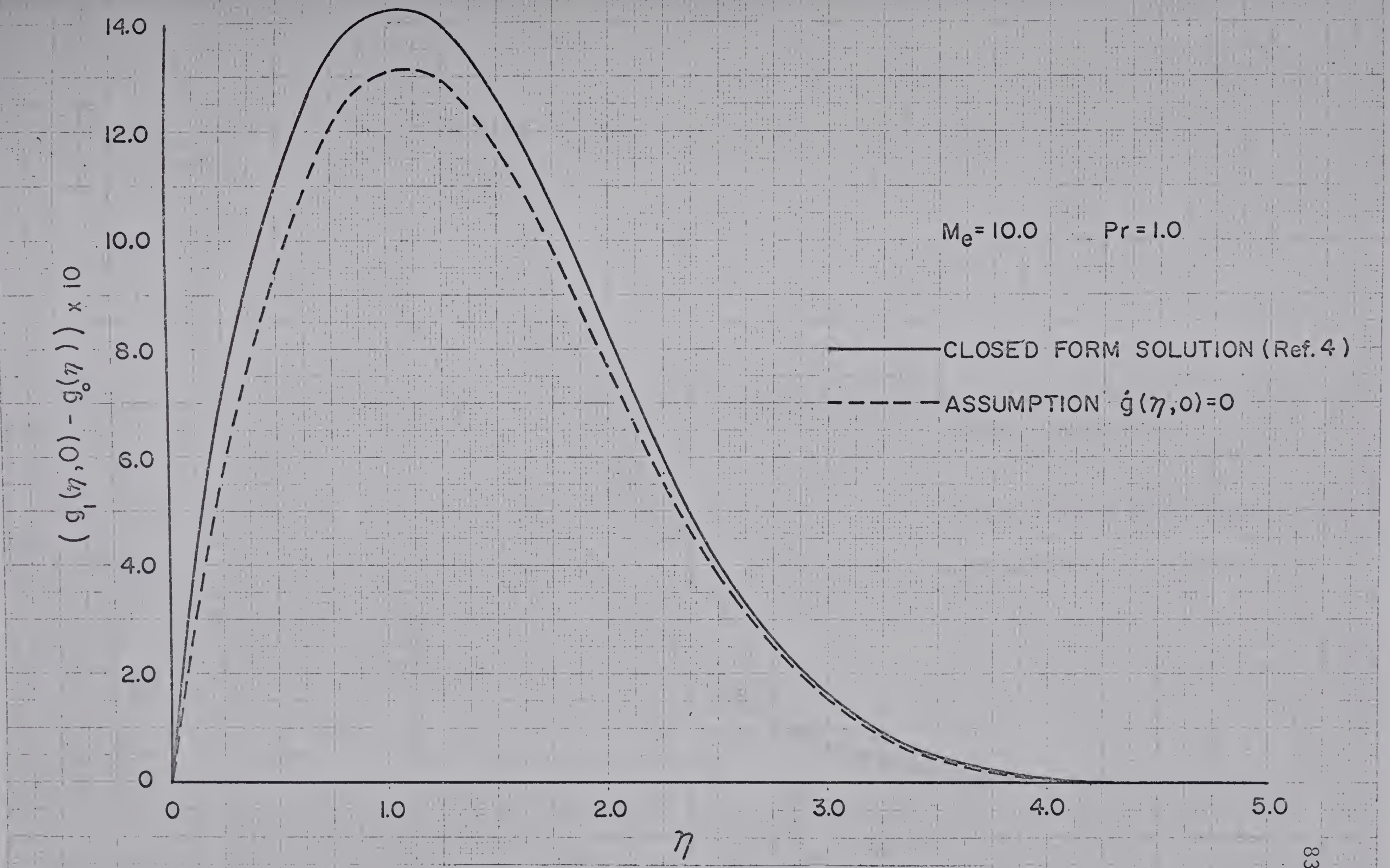

Fig. 5.1 Enthalpy Jump for a Cold Wall, $g_w = 0$

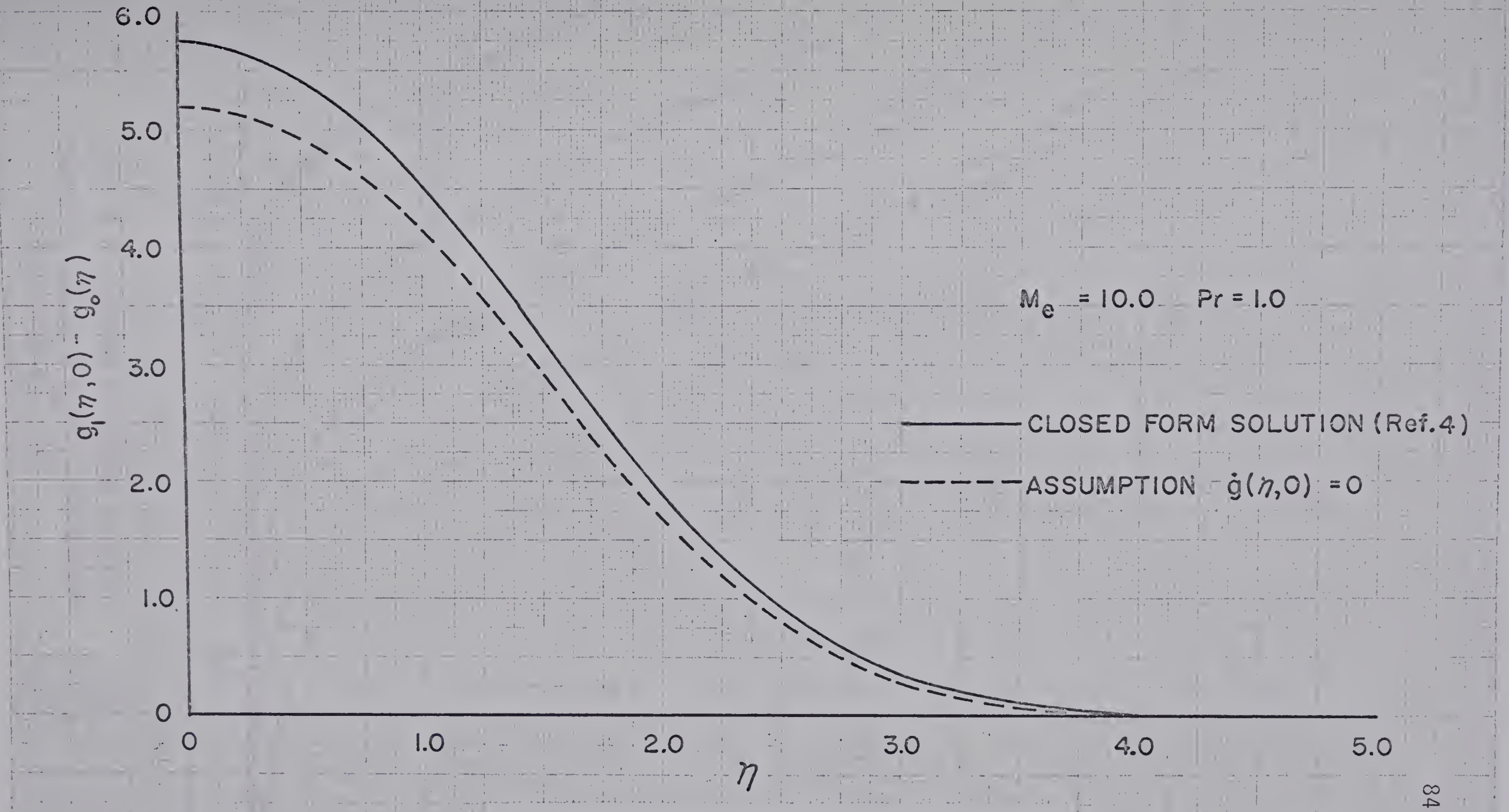

Fig. 5.2 Enthalpy Jump for an Adiabatic Wall

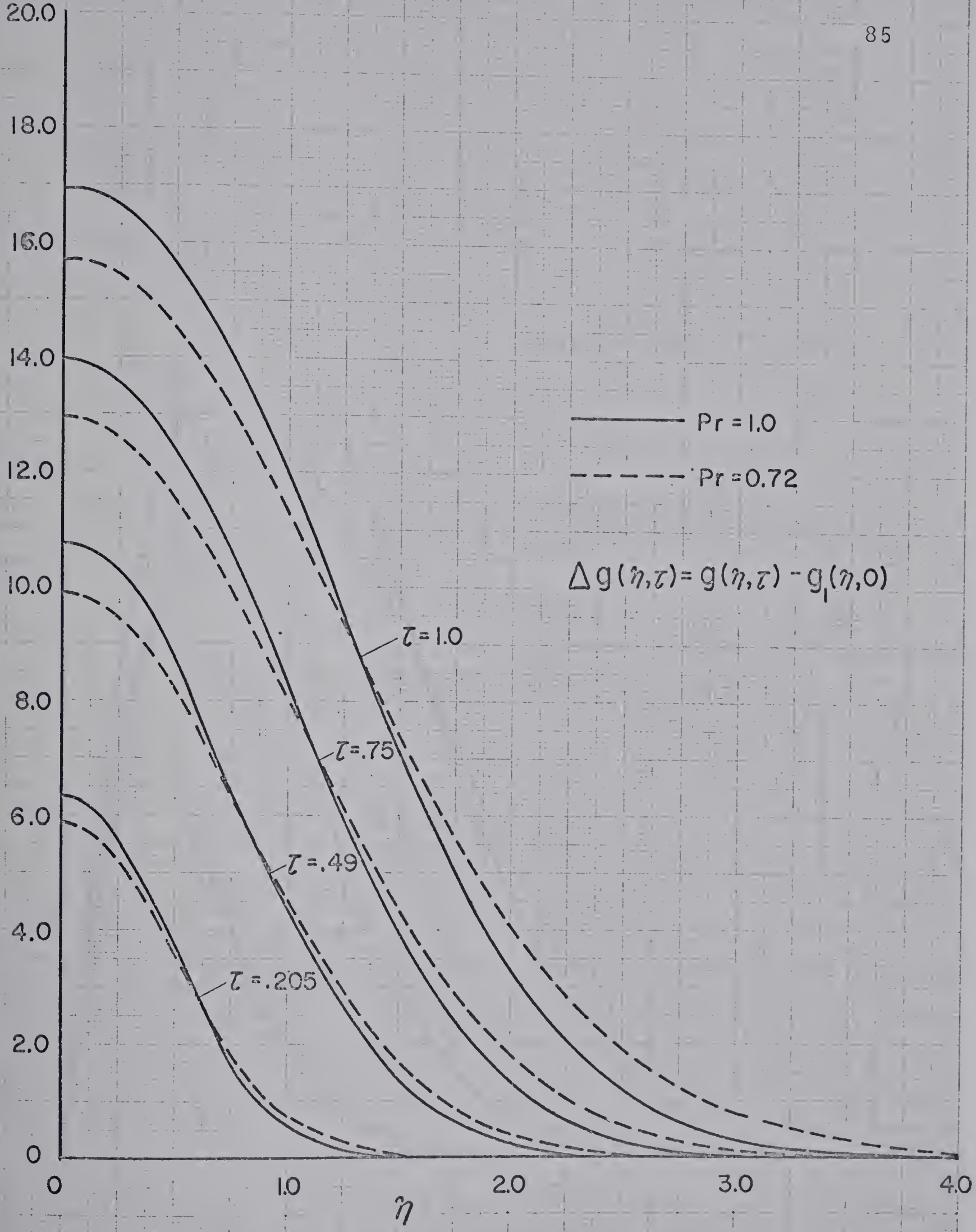

Fig. 5.3 Enthalpy Increment Δg from Assumption $g(\eta,0) = 0$ for an Adiabatic Wall with $M_e = 10$

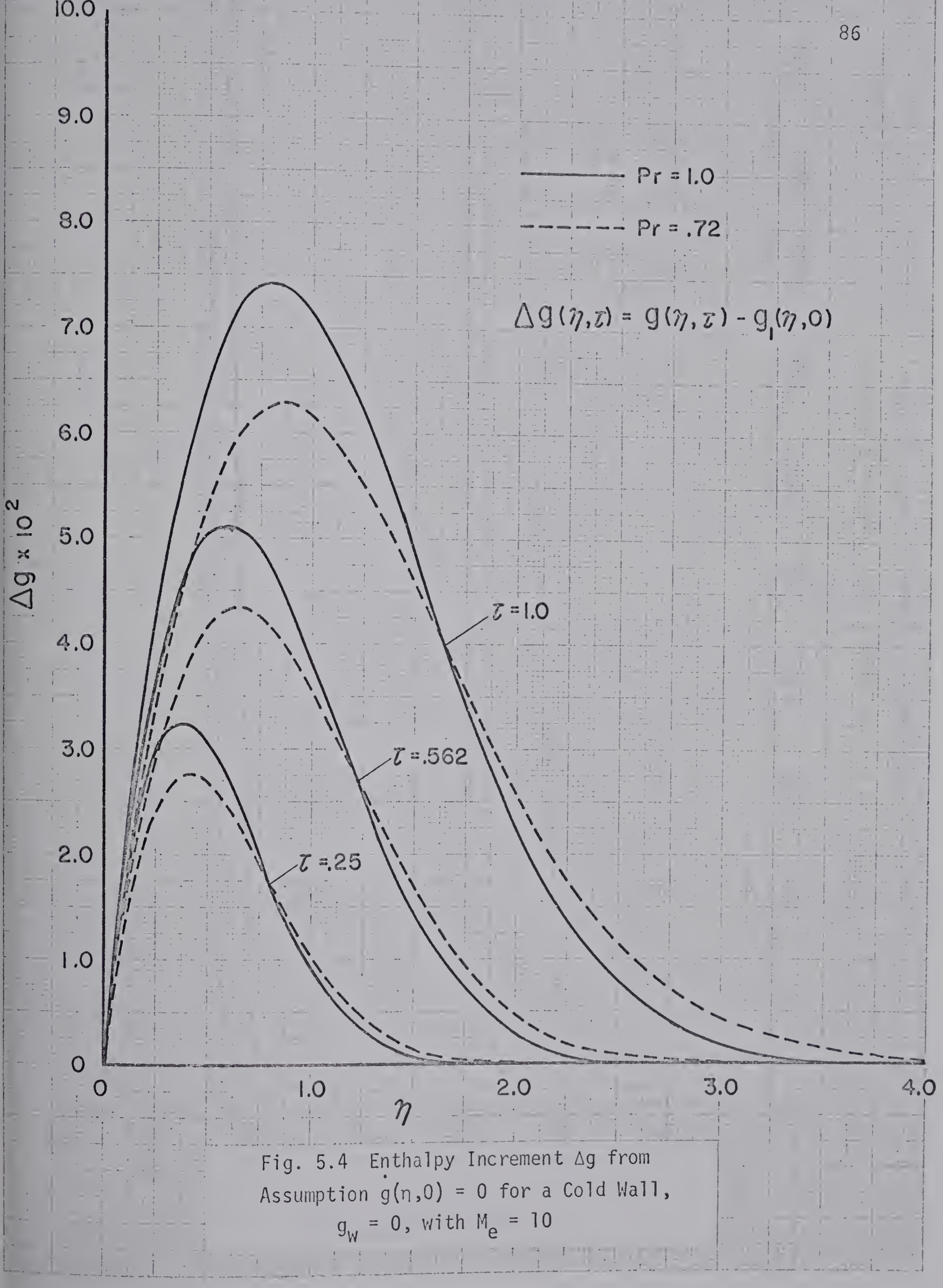

Fig. 5.4 Enthalpy Increment Δg from Assumption $g(\eta,0) = 0$ for a Cold Wall, $g_w = 0$, with $M_e = 10$

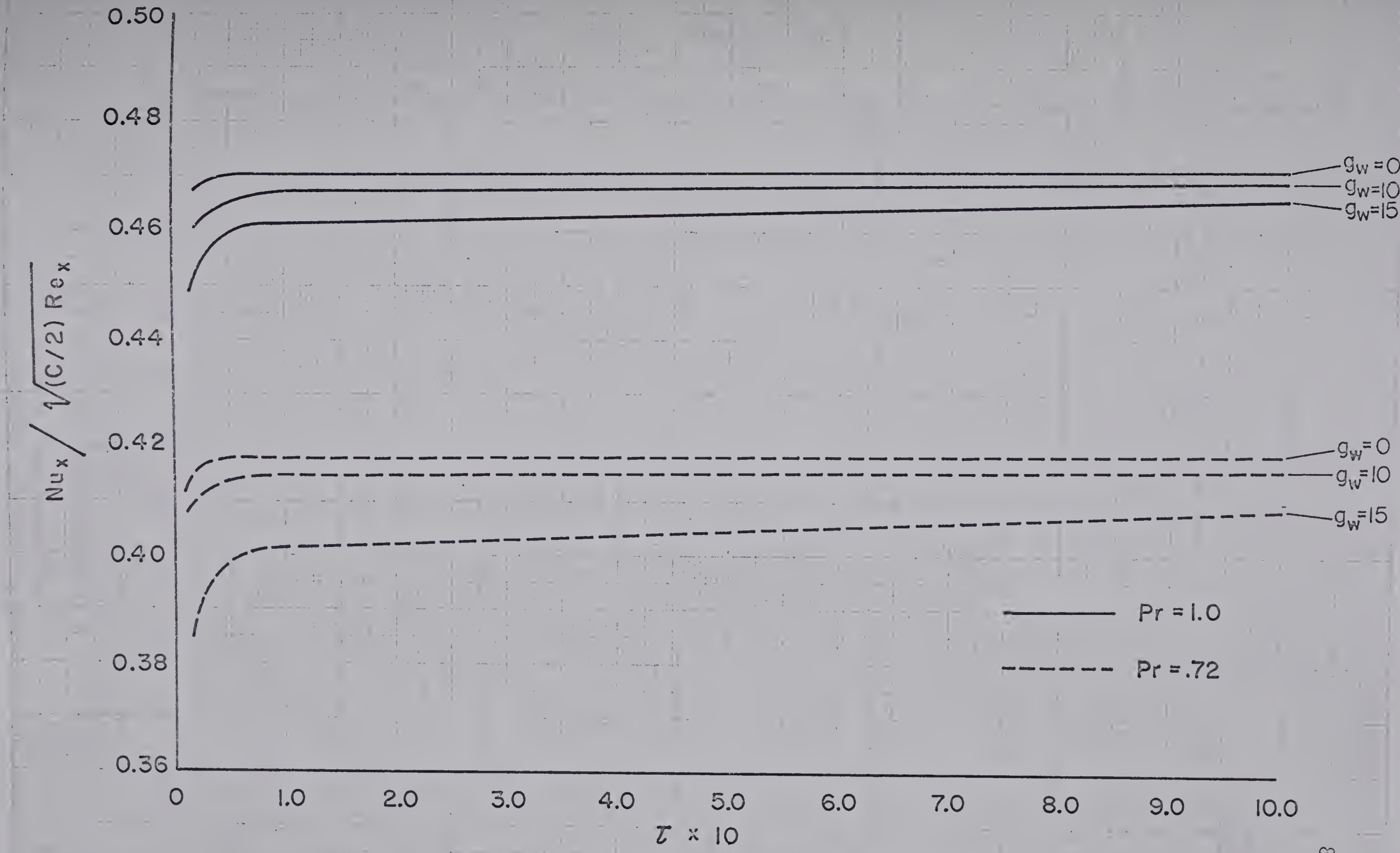

Fig. 5.5 Transient Heat Transfer Parameter from Assumption $g(\eta,0) = 0$ with $M_e = 10$

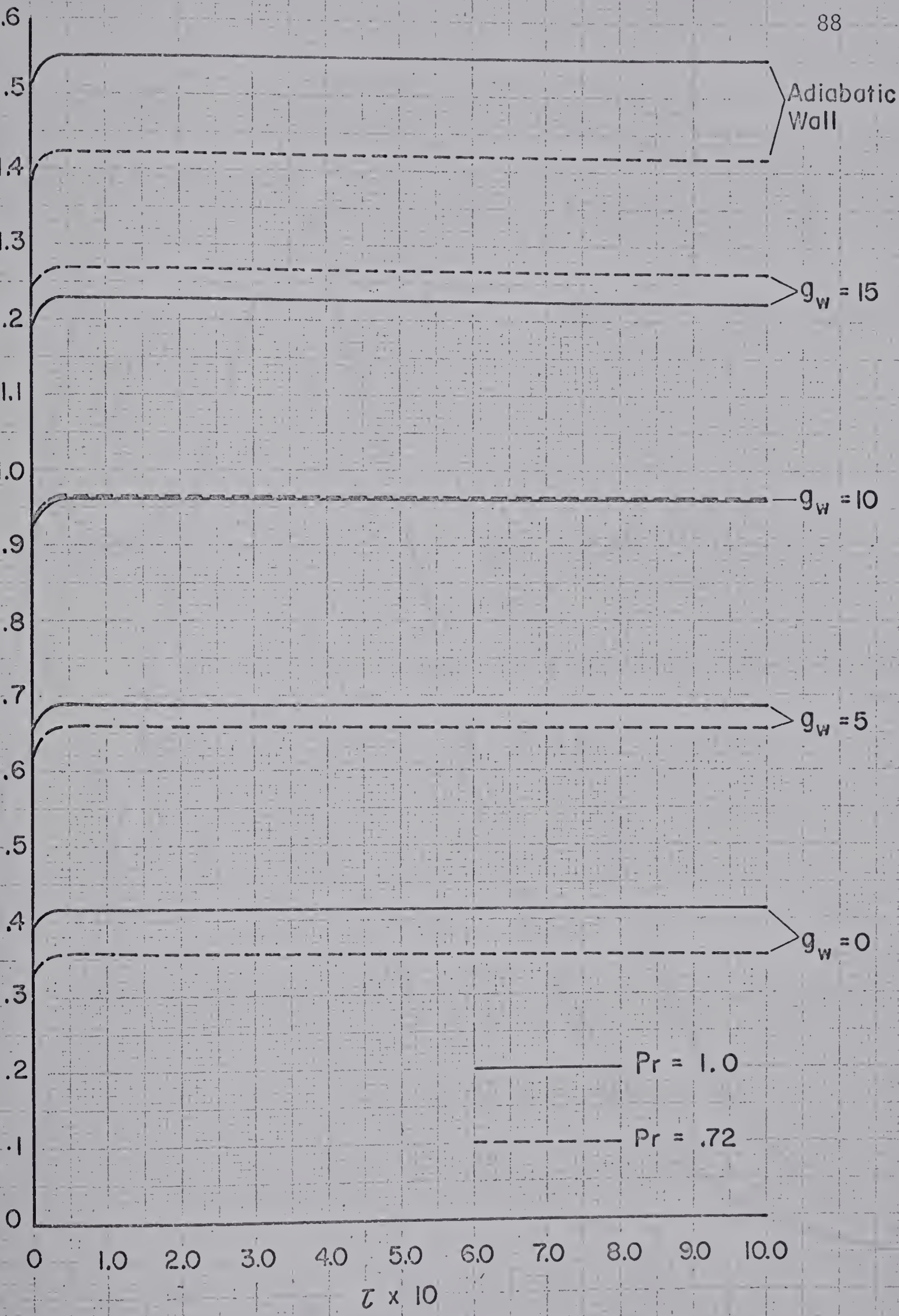

Fig. 5.6 Transient Weak-Interaction Induced Pressure from Assumption $\dot{g}(\eta,0) = 0$ with $M_e = 10$, $\chi = 4.5$

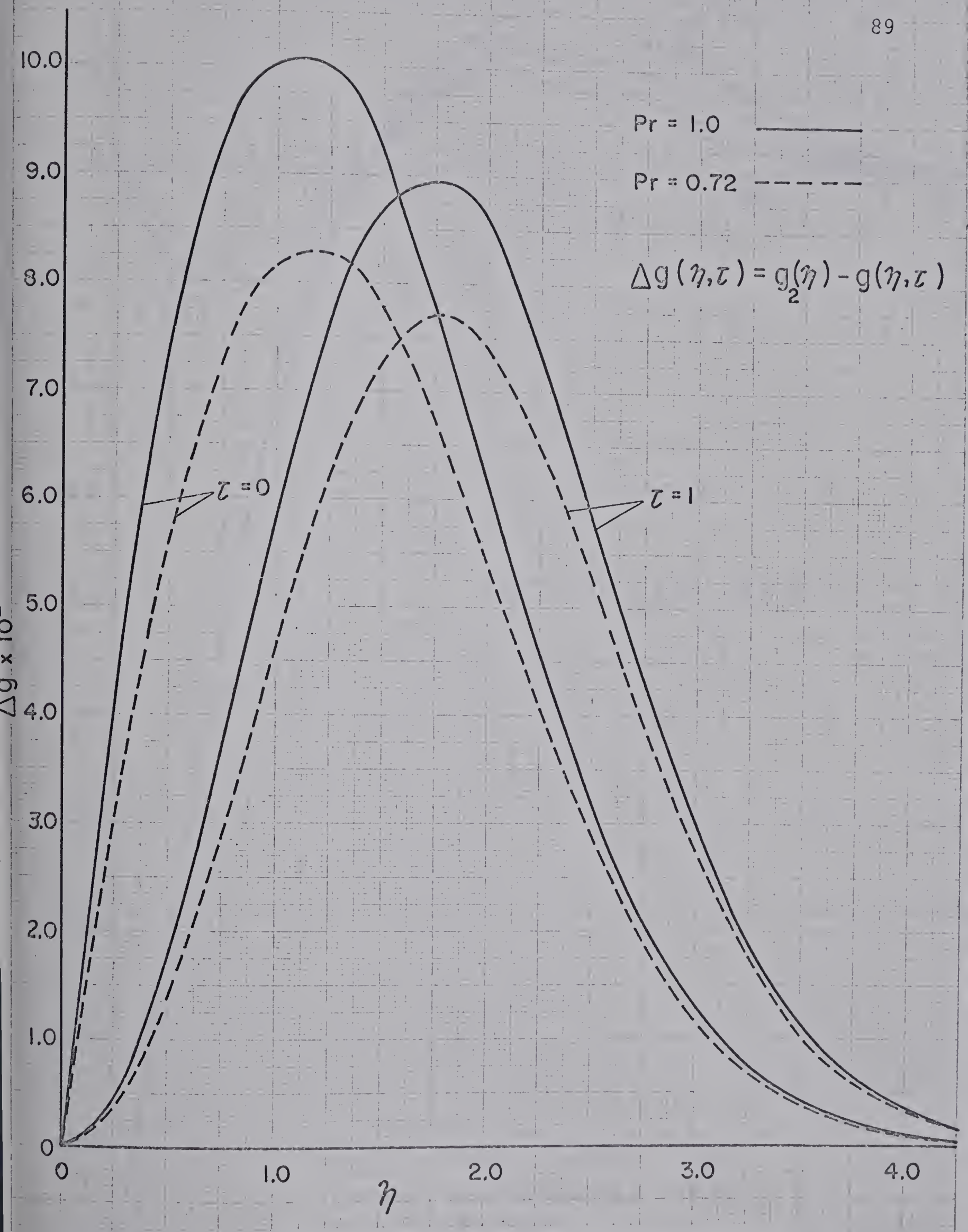

Fig. 5.7 Enthalpy Increment Δg from Empirical Distribution for an Adiabatic Wall with $M_e = 10$

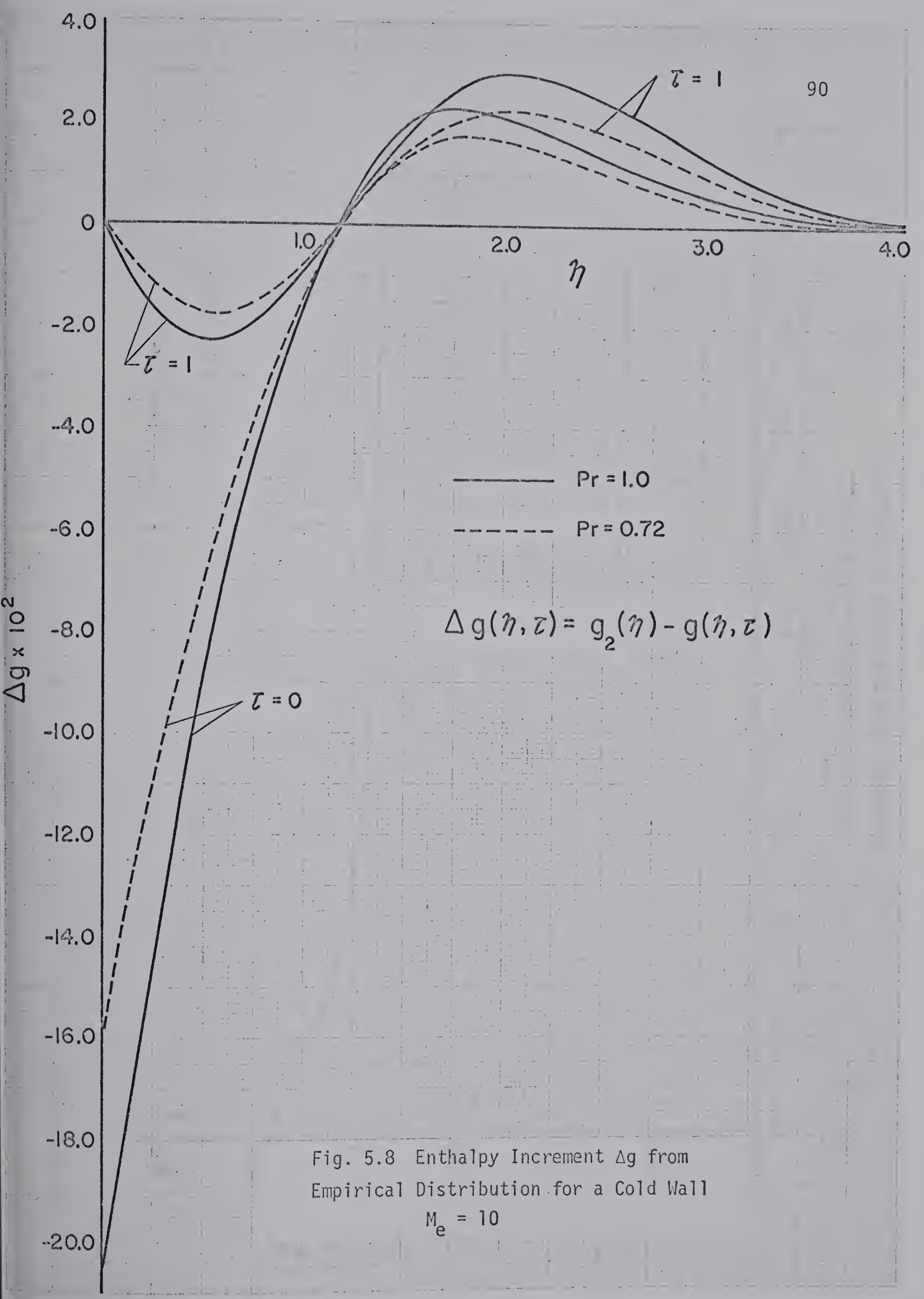

Fig. 5.8 Enthalpy Increment Δg from Empirical Distribution for a Cold Wall

$M_e = 10$

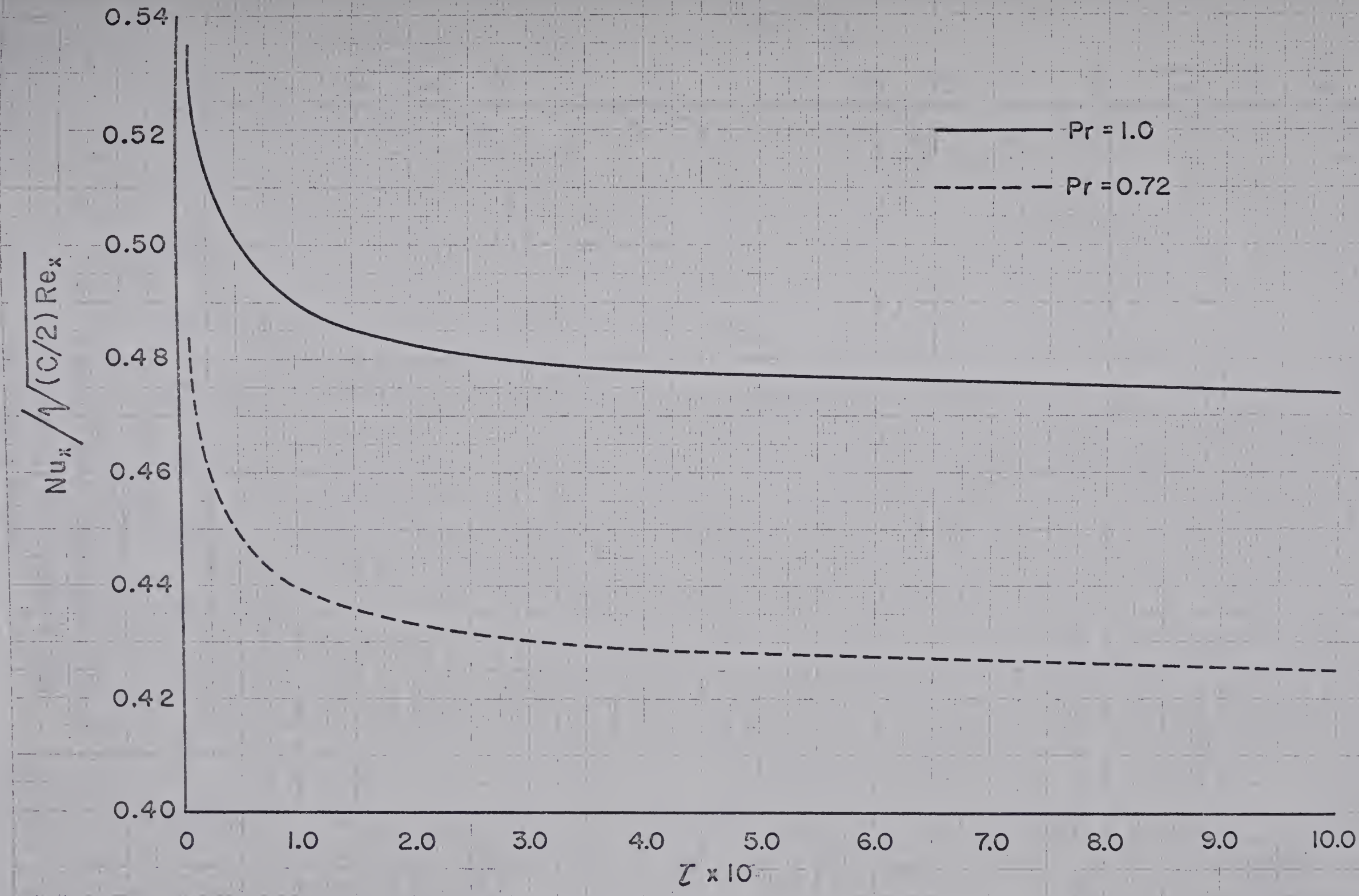

Fig. 5.9 Transient Heat Transfer Parameter from Empirical Distribution

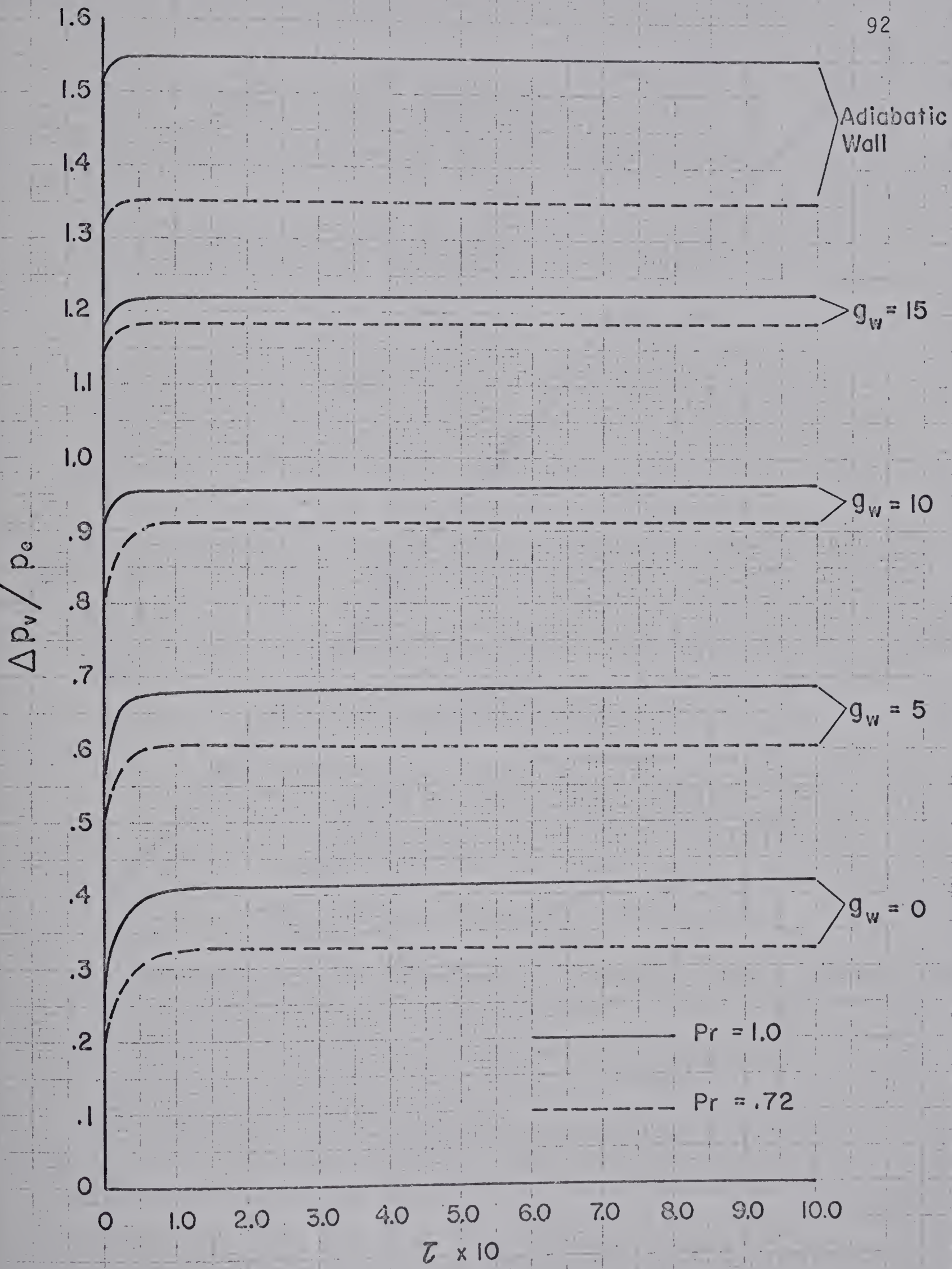

Fig. 5.10 Transient Weak-Interaction Induced Pressure from Empirical Distribution with $M_e = 10$, $\chi = 4.5$

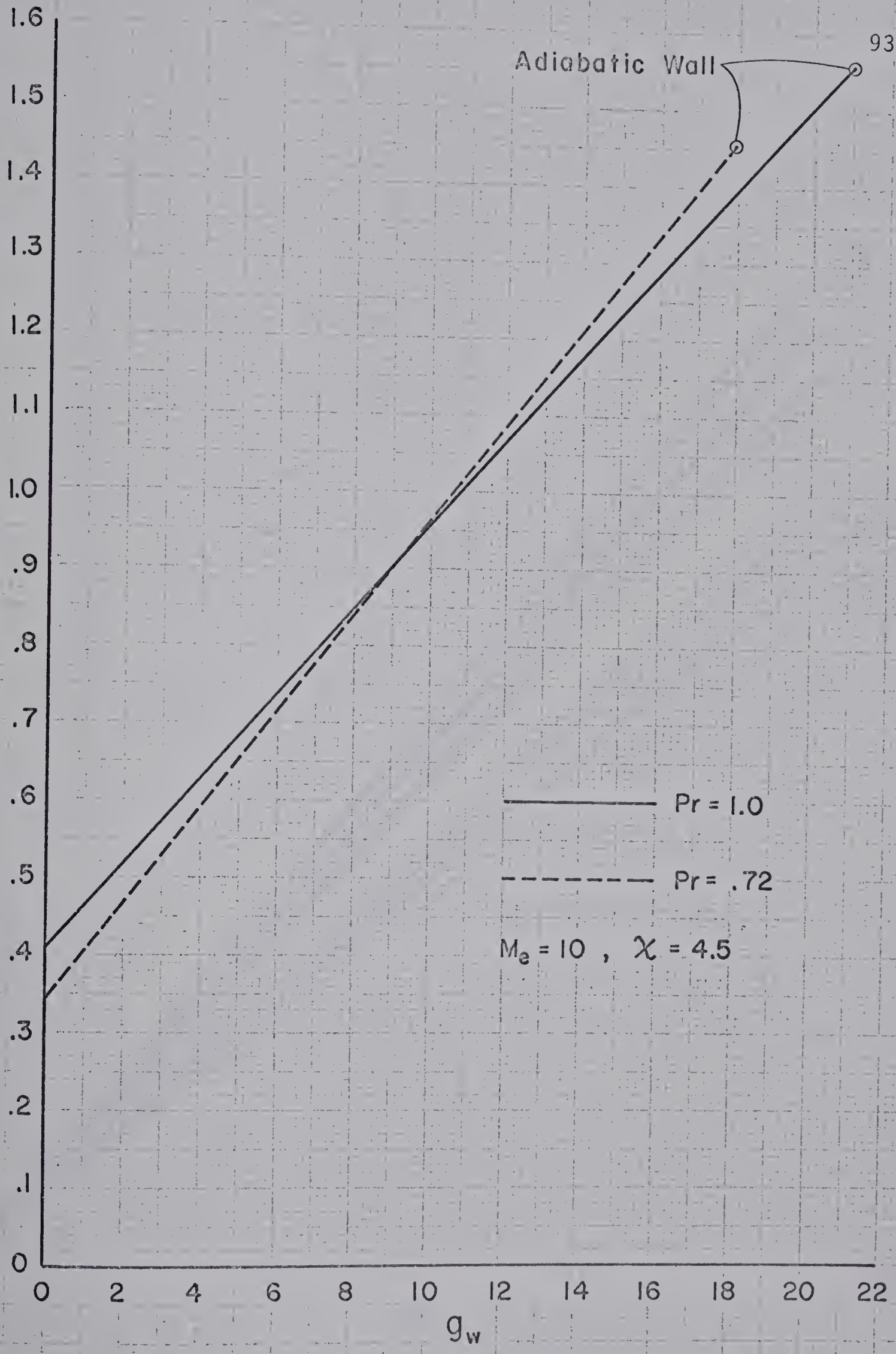

Fig. 5.11 Steady State Weak-Interaction Induced Pressure for $M_e = 10$, $\chi = 4.5$

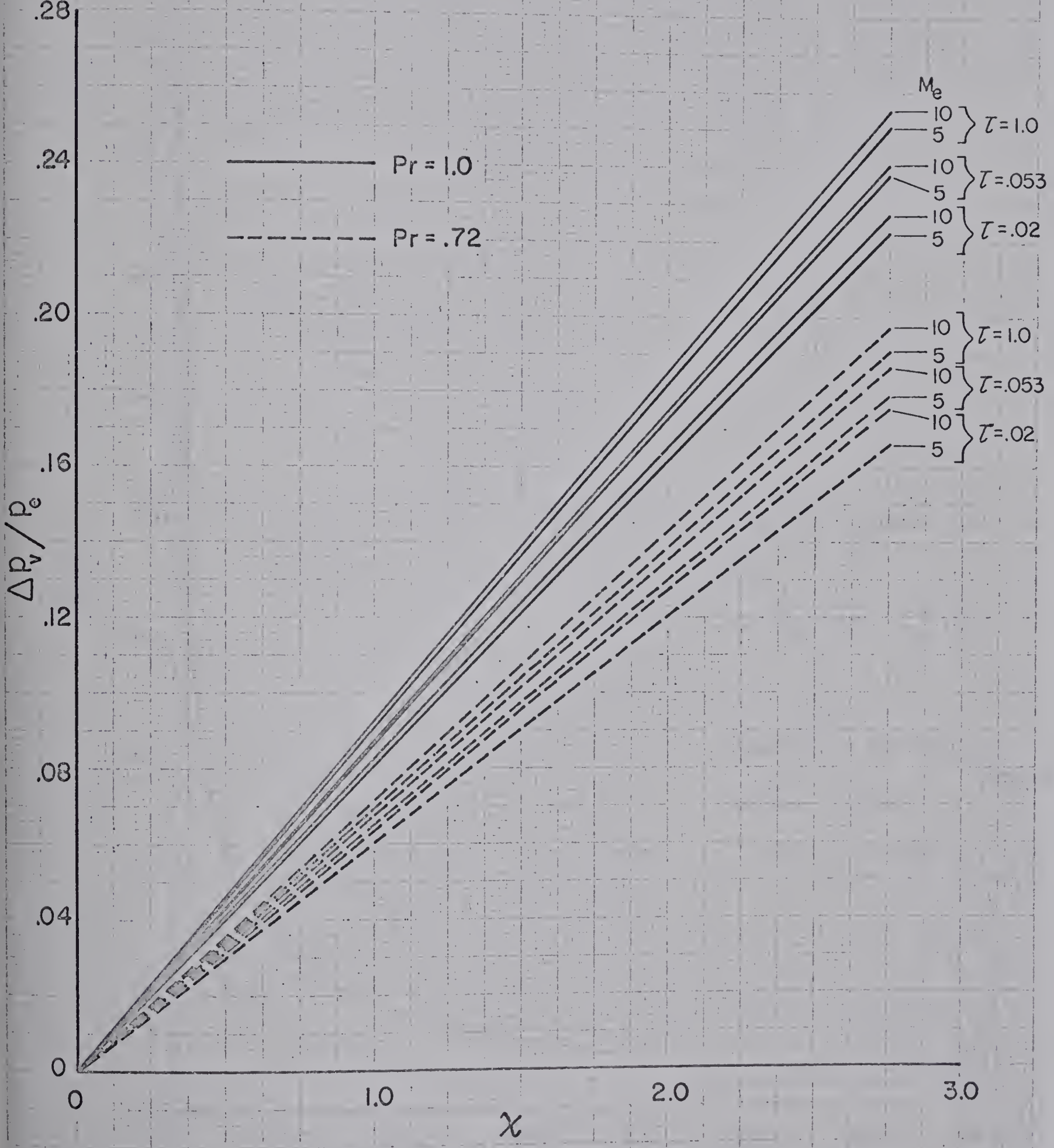

Fig. 5.12 Transient Weak-Interaction Induced Pressure from Empirical Distribution as a Function of χ, $g_w = 0$

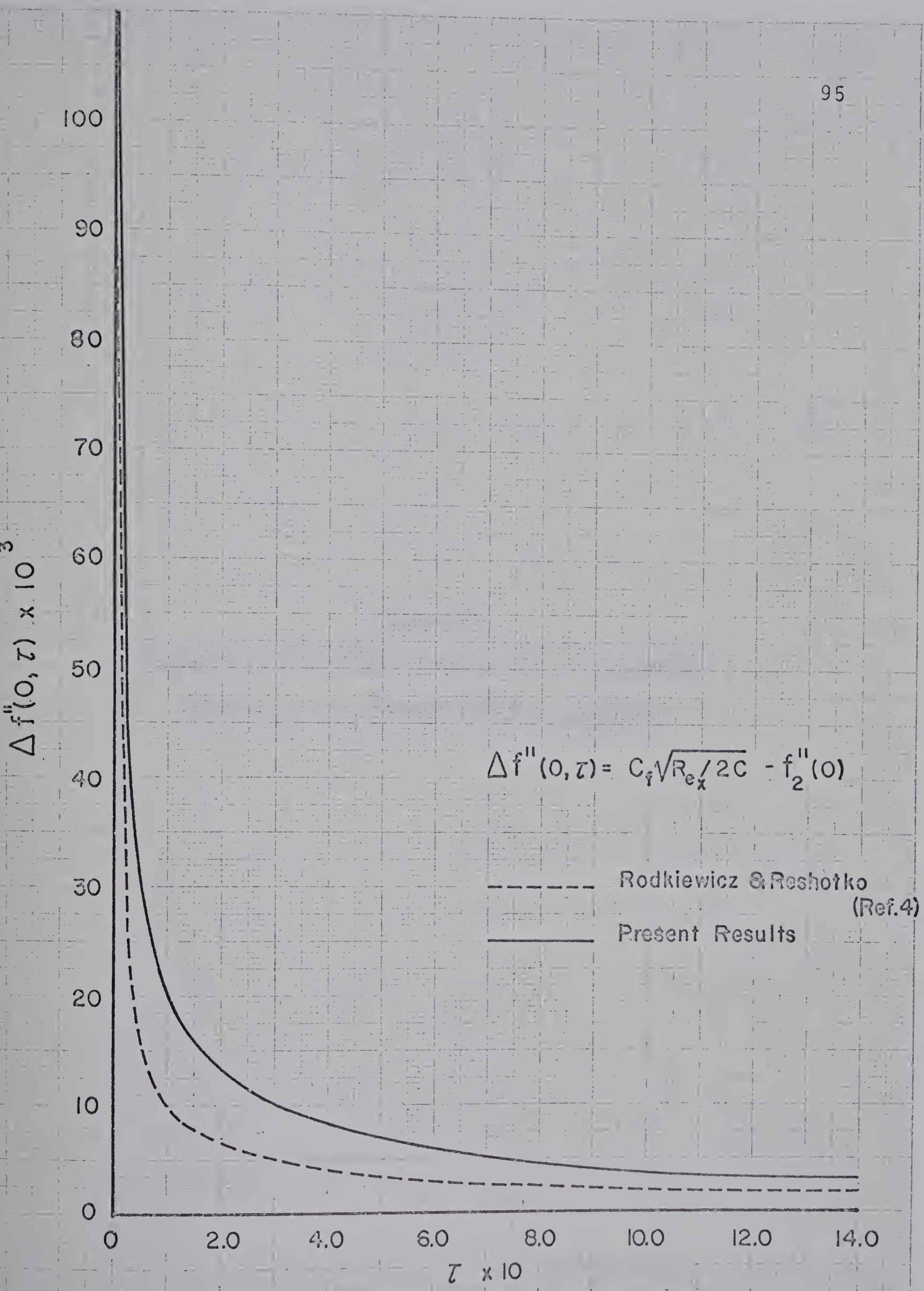

Fig. 5.13 Transient Wall-Shearing Stress Parameter on a Flat Plate

APPENDIX B

COMPUTER PROGRAM SOURCE LISTING FOR THE RECURRENCE SOLUTION OF THE UNSTEADY MOMENTUM EQUATION

APPENDIX B

FORTRAN PROGRAM

```
------------------------------------------------------------------

'*' IN COL. 6: THIS LINE IS A PART OF PREVIOUS STATEMENT

------------------------------------------------------------------


C       CALCULATION OF DELTA F DISTRIBUTION USING DOUBLE PRECI
     *  SION
C       AND USING THE TRANSFORMATION XI=TAU/(1+TAU)
        EXTERNAL FCT,OUTP
        DIMENSION PRMT(5),AUX(16,3),Y(3),DERY(3),F0(501),F0PRI
     *  M(501),
     1F02PRI(501),R(501),CC(501),S1(501),S2(501),S3(501)
        REAL*8 NUM,PRMT,AUX,Y,DERY,F0,F0PRIM,F02PRI,S1,S2,S3,S
     *  ,R,CC,TOP,
     1BOT,EPS,H,T,DENOM,A,B,C,D,E,XI
        COMMON /BLOCK1/F0/BLOCK2/F0PRIM/BLOCK3/F02PRI/BLOCK4/N
     *  N/BLOCK5/H
        EPS=0.01D0
        NN=501
        NNN=NN-1
        MM=51
        MMM=MM-1
        H=0.01D0
        T=0.01D0
C       GENERATION OF BLASIUS SOLUTION USING SSP HAMMINGS PRED
     *  ICTOR
C       CORRECTOR METHOD
        PRMT(1)=0.0D0
        PRMT(2)=5.0D0
        PRMT(3)=H
        PRMT(4)=0.5D-6
        NDIM=3
        DERY(1)=.333D0
        DERY(2)=.333D0
        DERY(3)=.334D0
        Y(1)=0.0D0
        Y(2)=0.0D0
        Y(3)=0.469600D0
        CALL DHPCG(PRMT,Y,DERY,NDIM,IHLF,FCT,OUTP,AUX)
C       NUMERICAL SOLUTION OF THE MOMENTUM EQ (3.2) USING RECU
     *  RRENCE
C       RELATIONSHIP (3.11)
C       APPLYING BOUNDARY CONDITION (2.42)
        S1(1)=0.0D0
```

```
      S2(1)=0.0D0
      S3(1)=0.0D0
C     APPLYING BOUNDARY CONDITION (2.42)
      DO 10 N=1,NNN
      S1(N+1)=S1(N)+H*(EPS*(1.-F0PRIM(N)))
   10 CONTINUE
      WRITE(6,20)
      HH=0.0
      DO 30 N=1,496,5
      WRITE(6,50) HH,S1(N),S1(N+1),S1(N+2),S1(N+3),S1(N+4)
      HH=HH+0.05
   30 CONTINUE
      HH=5.0
      WRITE(6,50) HH,S1(NN)
C     WRITING DELTA F VALUES ON TAPE
      WRITE(4,ERR=40) S1
C     EVALUATION OF FIRST TIME LINE USING 7-POINT COMPUTATIO
     *  NAL MOLECULE
C     OF FIGURE 3.1
      R(1)=0.0D0
      R(2)=0.25D0
      CC(1)=0.0D0
      CC(2)=0.0D0
      R1=R(1)
      R2=R(2)
      C1=CC(1)
      C2=CC(2)
      CALL FIRST(NN,H,T,R1,R2,C1,C2,F0,F0PRIM,F02PRI,S1,S2)
      XI=T
      TAU=SNGL(XI/(1.-XI))
      WRITE(6,60) XI,TAU
      HH=0.0
      DO 70 N=1,496,5
      WRITE(6,50) HH,S2(N),S2(N+1),S2(N+2),S2(N+3),S2(N+4)
      HH=HH+0.05
   70 CONTINUE
      HH=5.0
      WRITE(6,50) HH,S2(NN)
C     WRITING DELTA F VALUES ON TAPE
      WRITE(4,ERR=40) S2
      DO 80 M=3,MM
      XI=XI+T
      TAU=SNGL(XI/(1.-XI))
      DO 90 N=3,NNN
      A=4.0*T+4.0*H*T*F0(N)+6.0*H*H*(1.0-XI)*(XI*F0PRIM(N)-1
     *  .0+XI)
      B=-12.0*T-8.0*H*T*F0(N)+4.0*H*H*H*F02PRI(N)*(T-3.0*XI*
     *  (1.0-XI))
      C=12.0*T+4.0*H*T*F0(N)+6.0*(1.0-XI)*H*H*(1.0-XI*(1.0+F
     *  0PRIM(N)))
      D=-4.0*T
      E=8.0*(1.0-XI)*H*H*(1.0-XI*(1.0+F0PRIM(N)))*(S2(N-1)-S
     *  2(N+1))
```

```
     1+(4.0*XI*(1.0-XI)*H*H*H*F02PRI(N))*(S1(N)-4.0*S2(N))+(
     *  2.0*(
     21.0-XI)*(1.0-XI)*H*H)*(S1(N+1)-S1(N-1))+(2.0*XI*(1.0-X
     *  I)
     3*H*H*F0PRIM(N))*(S1(N-1)-S1(N+1))
      R(N)=-A/(B+C*R(N-1)+D*R(N-1)*R(N-2))
      NUM=E-(C*CC(N-1)+D*R(N-2)*CC(N-1)+D*CC(N-2))
      DENOM=B+C*R(N-1)+D*R(N-1)*R(N-2)
   90 CC(N)=NUM/DENOM
C     USING THE STARTING POINT (3.15)
      TOP=CC(NN-1)-CC(NN-2)/(4.0-R(NN-2))
      BOT=3.0/(4.0-R(NN-2))-R(NN-1)
      S3(NN)=TOP/BOT
      II=NN-2
      DO 100 I=1,II
      N=NN-I
      S3(N)=R(N)*S3(N+1)+CC(N)
  100 CONTINUE
      WRITE(6,60) XI,TAU
      HH=0.0
      DO 110 N=1,496,5
      WRITE(6,50) HH,S3(N),S3(N+1),S3(N+2),S3(N+3),S3(N+4)
      HH=HH+0.05
  110 CONTINUE
      HH=5.0
      WRITE(6,50) HH,S3(NN)
C     WRITING DELTA F VALUES ON TAPE
      WRITE(4,ERR=40) S3
      DO 120 N=2,NN
      S1(N)=S2(N)
      S2(N)=S3(N)
  120 CONTINUE
   80 CONTINUE
   20 FORMAT(1H1,'DELTA F DISTRIBUTION FOR  XI=0.00 IE FOR T
     *  AU=0.00'//)
   50 FORMAT(1H ,F10.2,5F22.8)
   60 FORMAT(1H1,'DELTA F DISTRIBUTION FOR  XI='F6.3,' IE FO
     *  R TAU ='F6.3
     1//)
      STOP
   40 WRITE(6,130)
  130 FORMAT(' ERROR WHILE WRITING ON TAPE')
      STOP
      END
```

```
SUBROUTINE FCT(X,Y,DERY)
DOUBLE PRECISION DERY(3),Y(3)
DERY(1)=Y(2)
DERY(2)=Y(3)
DERY(3)=-Y(1)*Y(3)
RETURN
END
```

```
      SUBROUTINE OUTP(X,Y,DERY,IHLF,NDIM,PRMT)
      REAL*8 Y(3),F0(501),F0PRIM(501),F02PRI(501),H
      COMMON /BLOCK1/F0/BLOCK2/F0PRIM/BLOCK3/F02PRI/BLOCK4/N
     *  N/BLOCK5/H
      C=0.0
      X0=0.0
      AH=SNGL(H)
      DO 10 J=1,NN
      I=J
      XJ=X0+C*AH
      IF(ABS(XJ-X).LT.1.E-3) GO TO 20
   10 C=C+1.0
      RETURN
   20 F0(I)=Y(1)
      F0PRIM(I)=Y(2)
      F02PRI(I)=Y(3)
      RETURN
      END
```

```
      SUBROUTINE FIRST(NN,H,T,R1,R2,C1,C2,F0,F0PRIM,F02PRI,S
     *   1,S2)
C     CALCULATION OF FIRST TIME LINE USING RECURRENCE SOLUTI
     *   ON WITH
C     7-POINT MOLECULE OF FIGURE 3.1
      DIMENSION F0(501),F0PRIM(501),F02PRI(501),R(501),CC(50
     *   1),S1(501),
     1S2(501)
      REAL*8 NUM,DENOM,F0,F0PRIM,F02PRI,R,CC,S1,S2,A,B,C,D,E
     *   ,XI,H,T,R1,
     1R2,C1,C2,TOP,BOT
      NNN=NN-1
      R(1)=R1
      R(2)=R2
      CC(1)=C1
      CC(2)=C2
      XI=T
      DO 10 N=3,NNN
      A=T+H*T*F0(N)-H*H*(1.0-XI)*(1.0-XI*(1.0+F0PRIM(N)))
      B=-3.0*T-2.0*H*T*F0(N)+H*H*H*T*F02PRI(N)-2.0*XI*(1.0-X
     *   I)*H*H*H*
     1F02PRI(N)
      C=3.0*T+H*T*F0(N)+H*H*(1.0-XI)*(1.0-XI*(1.0+F0PRIM(N))
     *   )
      D=-T
      E=H*H*(1.0-XI)*(1.0-XI*(1.0+F0PRIM(N)))*(S1(N-1)-S1(N+
     *   1))-
     12.0*XI*(1.0-XI)*F02PRI(N)*H*H*H*S1(N)
      R(N)=-A/(B+C*R(N-1)+D*R(N-1)*R(N-2))
      NUM=E-(C*CC(N-1)+D*R(N-2)*CC(N-1)+D*CC(N-2))
      DENOM=B+C*R(N-1)+D*R(N-1)*R(N-2)
      CC(N)=NUM/DENOM
10    CONTINUE
      TOP=CC(NN-1)-CC(NN-2)/(4.0-R(NN-2))
      BOT=3.0/(4.0-R(NN-2))-R(NN-1)
      S2(NN)=TOP/BOT
      II=NN-2
      DO 20 I=1,II
      N=NN-I
      S2(N)=R(N)*S2(N+1)+CC(N)
20    CONTINUE
      RETURN
      END
```

APPENDIX C

COMPUTER PROGRAM SOURCE LISTING FOR THE RECURRENCE SOLUTION OF THE UNSTEADY ENERGY EQUATION

APPENDIX C

FORTRAN PROGRAM

```
------------------------------------------------------------------

'*' IN COL. 6: THIS LINE IS A PART OF PREVIOUS STATEMENT

------------------------------------------------------------------


C       SOLUTION OF UNSTEADY STATE ENERGY EQUATION ASSUMING GD
     *  OT=0 AT TAU=
C       CASE OF MACH NUMBER = 10,PRANDTL NUMBER = 0.72 AND ISO
     *  THERMAL WALL
        EXTERNAL AFCT,FCT,DFCT,OUTP
        REAL*8 MACH,GAMMA,PR,H,T,NUM,DENOM,U,GS,GSPRIM,GS2PRI,
     *  F,FPRIM,
     1F2PRIM,FDOT, XI,A,B,C,D,R,CC,F0,FO2PRI,G0,F0PRIM,F3PRI
     *  M,CCC,BB,RR,
     2Y,AUX,PRMT,AA,DERY,FDPRIM,GW,G0DOT,ME0,EPS,G1
        DIMENSION U(3,501),GS(501),GSPRIM(501),GS2PRI(501),R(5
     *  01),CC(501),
     1F0(501),FO2PRI(501),G0(501),F(501),FPRIM(501),F2PRIM(5
     *  01),FDOT(501
     2),F0PRIM(501),PRMT(5),F3PRIM(501),CCC(2,2),BB(2,2),Y(2
     *  ),AUX(20,2),
     3RR(2),AA(2,2),DERY(2),FDPRIM(501),G0DOT(501),G1(501)
        COMMON/BLOCK1/F
        COMMON/BLOCK2/F2PRIM
        COMMON/BLOCK3/F0PRIM/BLOCK4/F02PRI
        COMMON/BLOCK5/G1
        MACH=10.0D0
        PR=0.72D0
        GAMMA=1.4D0
        GW=0.0D0
        NN=501
        NNN=NN-1
        MM=51
        MMM=MM-1
        H=0.01D0
        T=0.01D0
        EPS=0.01D0
C       EVALUATING MACH NUMBER CORRESPONDING TO INITIAL STEADY
     *    STATE
        ME0=DSQRT(MACH*MACH/(1.+MACH*MACH*EPS*(GAMMA-1.)))
C       READING THE BLASIUS VALUES STORED ON TAPE
        READ(3,ERR=250) F0
        READ(3,ERR=250) F0PRIM
        READ(3,ERR=250,END=10) F02PRI
```

```
   10 CONTINUE
C       EVALUATING STEADY STATE G2 ENTHALPY DISTRIBUTION FROM
     *   SOLUTION (3.
C       USING SSP SIMPSON'S RULE
        CALL FINAL(PR,1,GW,MACH,GAMMA,F02PRI,GS)
        WRITE(6,20) PR,MACH
   20 FORMAT(1H1,'STEADY STATE G DISTRIBUTION FOR PR= 'F6.2,
     *   ' AND MACH
     1NO. 'F6.2,' USING SUBROUTINE FINAL'//)
        HH=0.0
        DO 1 N=1,496,5
        WRITE(6,30) HH,GS(N),GS(N+1),GS(N+2),GS(N+3),GS(N+4)
        HH=HH+0.05
    1 CONTINUE
        HH=5.0
        WRITE(6,30) HH,GS(NN)
C       WRITING STEADY STATE VALUES ON TAPE
        WRITE(4,ERR=40) GS
C       EVALUATION OF FIRST AND SECOND STEADY STATE DERIVATIVE
     *   S USING SSP
        CALL DDET5(H,GS,GSPRIM,NN,IER)
        CALL DDET5(H,GSPRIM,GS2PRI,NN,IER)
C       READING MOMENTUM EQUATION SOLUTION FROM TAPE
        DO 50 N=1,NN
        READ(3,ERR=250) F(N),FPRIM(N),F2PRIM(N),FDOT(N)
   50 CONTINUE
        FDPRIM(1)=(-3.*FDOT(3)+4.*FDOT(2)-FDOT(1))/(2.*H)
        DO 60 N=2,NNN
        FDPRIM(N)=(FDOT(N+1)-FDOT(N-1))/(2.*H)
   60 CONTINUE
        FDPRIM(NN)=(3.*FDOT(NN)-4.*FDOT(NN-1)+FDOT(NN-2))/(2.*
     *   H)
C       USING DIFFERENTIAL EQUATION TO OBTAIN THIRD DERIVATIVE
C       USING VECTOR SPACES F0PRIM AND F02PRI
        DO 70 N=1,NN
        F3PRIM(N)=2.*FDPRIM(N)-F(N)*F2PRIM(N)
        F0PRIM(N)=F2PRIM(N)
        F02PRI(N)=F3PRIM(N)
   70 CONTINUE
C       EVALUATION OF G1 DISTRIBUTION USING SSP DLBVP
        NDIM=2
        BB(1,1)=1.0D0
        BB(1,2)=0.0D0
        BB(2,1)=0.0D0
        BB(2,2)=0.0D0
        CCC(1,1)=0.0D0
        CCC(1,2)=0.0D0
        CCC(2,1)=1.0D0
        CCC(2,2)=0.0D0
        RR(1)=GW
        RR(2)=1.0D0
        DERY(1)=0.5D0
```

```
      DERY(2)=0.5D0
      PRMT(1)=0.0D0
      PRMT(2)=5.0D0
      PRMT(3)=H
      PRMT(4)=0.5D-4
      CALL DLBVP(PRMT,BB,CCC,RR,Y,DERY,NDIM,IHLF,AFCT,FCT,DF
     *  CT,OUTP,AUX,
     1AA)
      WRITE(6,80) IHLF
   80 FORMAT(1H0,'ERROR PARAMETER IHLF IS 'I5//)
      WRITE(6,90)
   90 FORMAT(1H1,'INITIAL G1 DISTRIBUTION USING SUBROUTINE D
     *  LBVP'//)
      HH=0.0
      DO 100 N=1,496,5
      WRITE(6,30) HH,G1(N),G1(N+1),G1(N+2),G1(N+3),G1(N+4)
      HH=HH+0.05
  100 CONTINUE
      HH=5.0
      WRITE(6,30) HH,G1(NN)
C     USING SUBROUTINE FINAL TO CALCULATE INITIAL STEADY STA
     *  TE ENTHALPY
C     DISTRIBUTION
      CALL FINAL(PR,1,GW,MEO,GAMMA,F02PRI,G0)
      WRITE(6,110)
  110 FORMAT(1H1,'ENTHALPY JUMP FROM ASSUMPTION GDOT = 0'//)
      DO 120 N=1,NN
      GODOT(N)=G1(N)-G0(N)
  120 CONTINUE
      HH=0.0
      DO 130 N=1,496,5
      WRITE(6,30)HH,GODOT(N),GODOT(N+1),GODOT(N+2),GODOT(N+3
     *  ),GODOT(N+4)
      HH=HH+0.05
  130 CONTINUE
      HH=5.0
      WRITE(6,30) HH,GODOT(NN)
C     EVALUATING INCREMENTAL ENTHALPY DISTRIBUTION USING GOD
     *  OT VECTOR SP
      XI=0.0
      TAU=0.0
      WRITE(6,140) XI,TAU
  140 FORMAT(1H1,'DELTA G DISTRIBUTION FOR  XI= 'F6.3,' IE F
     *  OR TAU= '
     1F6.3//)
      DO 150 N=1,NN
      U(1,N)=GS(N)-G1(N)
      U(2,N)=U(1,N)
      GODOT(N)=GS(N)-U(1,N)-G1(N)
  150 CONTINUE
      HH=0.0
      DO 160 N=1,496,5
```

```
      WRITE(6,30)HH,GODOT(N),GODOT(N+1),GODOT(N+2),GODOT(N+3
     *   ),GODOT(N+4)
      HH=HH+0.05
  160 CONTINUE
      HH=5.0
      WRITE(6,30) HH,GODOT(NN)
      XI=T
      TAU=SNGL(XI/(1.-XI))
      WRITE(6,140) XI,TAU
      HH=0.0
      DO 170 N=1,496,5
      WRITE(6,30)HH,GODOT(N),GODOT(N+1),GODOT(N+2),GODOT(N+3
     *   ),GODOT(N+4)
      HH=HH+0.05
  170 CONTINUE
      HH=5.0
      WRITE(6,30) HH,GODOT(NN)
   30 FORMAT(1H ,F10.2,5F20.8)
C     WRITING INCREMENTAL ENTHALPY DISTRIBUTION ON TAPE
      WRITE(4,ERR=40) (U(1,N),N=1,NN)
      WRITE(4,ERR=40) (U(2,N),N=1,NN)
C     SOLVING THE UNSTEADY STATE ENERGY EQUATION FOR TAU > 0
      DO 180 N=1,NN
      READ(3,ERR=250) F(N),FPRIM(N),F2PRIM(N),FDOT(N)
  180 CONTINUE
      R(1)=0.0D0
      CC(1)=0.0D0
      DO 190 M=3,MM
      XI=XI+T
      TAU=SNGL(XI/(1.-XI))
      DO 200 N=1,NN
      READ(3,ERR=250) F(N),FPRIM(N),F2PRIM(N),FDOT(N)
  200 CONTINUE
      DO 210 N=2,NNN
      A=T*(1./PR+H*(F(N)/2.-XI*(1.-XI)*FDOT(N)))
      B=-3.*H*H*(1.-XI*(1.+FPRIM(N)))*(1.-XI)-2.*T/PR
      C=T*(1./PR-H*(F(N)/2.-XI*(1.-XI)*FDOT(N)))
      D=-H*H*(1.-XI*(1.+FPRIM(N)))*(1.-XI)*(4.*U(2,N)-U(1,N)
     *   )+H*H*T*(
     1GS2PRI(N)/PR+(F(N)-2.*XI*(1.-XI)*FDOT(N))*GSPRIM(N)+(G
     *   AMMA-1.)*
     2MACH*MACH*F2PRIM(N)*F2PRIM(N))
      DENOM=B+C*R(N-1)
      R(N)=-A/DENOM
      NUM=D-C*CC(N-1)
      CC(N)=NUM/DENOM
  210 CONTINUE
      U(3,NN)=0.0D0
      GODOT(NN)=GS(NN)-U(3,NN)-G1(NN)
C     MARCHING DOWNWARD USING THE RECURRENCE RELATION
      DO 220 I=1,NNN
      N=NN-I
```

```
      U(3,N)=R(N)*U(3,N+1)+CC(N)
      GODOT(N)=GS(N)-U(3,N)-G1(N)
  220 CONTINUE
      WRITE(6,140) XI,TAU
      HH=0.0
      DO 230 N=1,496,5
      WRITE(6,30)HH,GODOT(N),GODOT(N+1),GODOT(N+2),GODOT(N+3
     *   ),GODOT(N+4)
      HH=HH+0.05
  230 CONTINUE
      HH=5.0
      WRITE(6,30) HH,GODOT(NN)
      WRITE(4,ERR=40) (U(3,N),N=1,NN)
      DO 240 N=1,NN
      U(1,N)=U(2,N)
      U(2,N)=U(3,N)
  240 CONTINUE
  190 CONTINUE
      ENDFILE 4
      STOP
  250 WRITE(6,260)
  260 FORMAT(' ERROR WHILE READING FROM TAPE')
      STOP
   40 WRITE(6,270)
  270 FORMAT(' ERROR WHILE WRITING ON TAPE')
      STOP
      END
```

```
      SUBROUTINE AFCT(X,AA)
      REAL*8 AA(2,2),F(501),PR
      COMMON/BLOCK1/F
      PR=0.72D0
      AA(1,1)=0.0D0
      AA(1,2)=1.0D0
      AA(2,1)=0.0D0
      NN=501
      H=.01
      C=0.0
      X0=0.0
      DO 10 I=1,NN
      N=I
      XI=X0+C*H
      IF(ABS(XI-X).LE.0.005) GO TO 20
      C=C+1.
   10 CONTINUE
      WRITE(6,30) XI,X
   30 FORMAT(1H0,'AFCT COULD NOT MATCH XI AND X='2F15.5)
      STOP
   20 AA(2,2)=-PR*F(N)
      RETURN
      END
```

```
      SUBROUTINE FCT(X,FF)
      REAL*8 PR,GAMMA,MACH,F2PRIM(501),FF(2)
      COMMON/BLOCK2/F2PRIM
      PR=0.72D0
      GAMMA=1.4D0
      MACH=10.0D0
      FF(1)=0.0D0
      NN=501
      H=.01
      C=0.0
      X0=0.0
      DO 10 I=1,NN
      N=I
      XI=X0+C*H
      IF(ABS(XI-X).LE.0.005) GO TO 20
      C=C+1.
   10 CONTINUE
      WRITE(6,30) XI,X
   30 FORMAT(1H0,'FCT COULD NOT MATCH XI AND X='2F15.5)
      STOP
   20 FF(2)=-PR*(GAMMA-1.)*MACH*MACH*F2PRIM(N)*F2PRIM(N)
      RETURN
      END
```

```
      SUBROUTINE DFCT(X,DF)
      REAL*8 DF(2),F0PRIM(501),F02PRI(501),PR,GAMMA,MACH
      COMMON/BLOCK3/F0PRIM/BLOCK4/F02PRI
      GAMMA=1.4D0
      PR=0.72D0
      MACH=10.0D0
      DF(1)=0.0D0
      NN=501
      H=.01
      C=0.0
      X0=0.0
      DO 10 I=1,NN
      N=I
      XI=X0+C*H
      IF(ABS(XI-X).LE.0.005) GO TO 20
      C=C+1.
   10 CONTINUE
      WRITE(6,30) XI,X
   30 FORMAT(1H0,'DFCT COULD NOT MATCH XI AND X='2F15.5)
      STOP
   20 DF(2)=-2.*PR*(GAMMA-1.)*MACH*MACH*F0PRIM(N)*F02PRI(N)
      RETURN
      END
```

```
      SUBROUTINE OUTP(X,Y,DERY,IHLF,NDIM,PRMT)
      REAL*8 Y(2),G1(501)
      COMMON/BLOCK5/G1
      NN=501
      H=.01
      C=0.0
      X0=0.0
      DO 10 I=1,NN
      N=I
      XI=X0+C*H
      IF(ABS(XI-X).LT.0.5E-3) GO TO 20
      C=C+1.
   10 CONTINUE
   20 G1(N)=Y(1)
      RETURN
      END
```

```
      SUBROUTINE FINAL(PR,I,GW,MACH,GAMMA,F2PRIM,GS)
C     I=0 FOR ZERO WALL HEAT TRANSFER SOLUTION
C     I=1 FOR NON-ZERO WALL HEAT TRANSFER SOLUTION
      DIMENSION R(501),AF(501),AF1(501),F2PRIM(501),S(501),G
     *  S(501)
      REAL*8 PR,H,MACH,GAMMA,R,AF,AF1,F2PRIM,S,GS,E,GW
      NN=501
      H=0.01D0
C     INTEGRATION BY SSP SIMPSON'S RULE
C     EVALUATION OF AF(N) USING AF1(N) VECTOR SPACE TEMPORAR
     *  ILY
      E=2.-PR
      DO 10 N=1,NN
      IF(F2PRIM(N).LE.0.0) GO TO 20
      AF1(N)=(F2PRIM(N))**E
      GO TO 10
   20 AF1(N)=0.0
   10 CONTINUE
      CALL DQSF(H,AF1,AF,NN)
C     EVALUATION OF AF1(N)
      DO 30 N=1,NN
      IF(F2PRIM(N).LE.0.0) GO TO 40
      AF1(N)=((F2PRIM(N))**PR)*AF(N)
      GO TO 30
   40 AF1(N)=0.0
   30 CONTINUE
C     EVALUATION OF R(N) USING AF(N) VECTOR SPACE TEMPORARIL
     *  Y
      CALL DQSF(H,AF1,AF,NN)
      DO 50 N=1,NN
      R(N)=2.*PR*(AF(NN)-AF(N))
   50 CONTINUE
      IF(I.EQ.1) GO TO 60
C     EVALUATION OF STEADY STATE G DISTRIBUTION FOR ZERO WAL
     *  L HEAT TRANS
      DO 70 N=1,NN
      GS(N)=1.+.5*(GAMMA-1.)*MACH*MACH*R(N)
   70 CONTINUE
      RETURN
   60 CONTINUE
C     EVALUATION OF STEADY STATE G DISTRIBUTION FOR NON-ZERO
     *  WALL HEAT T
C     EVALUATION OF S(N) USING(N) AND AF(N) VECTOR SPACES
      DO 80 N=1,NN
      IF(F2PRIM(N).LE.0.0) GO TO 90
      AF1(N)=(F2PRIM(N))**PR
      GO TO 80
   90 AF1(N)=0.0
   80 CONTINUE
      CALL DQSF(H,AF1,AF,NN)
      DO 100 N=1,NN
      S(N)=AF(NN)-AF(N)
```

```
      GS(N)=1.+.5*(GAMMA-1.)*MACH*MACH*R(N)-(1.+.5*(GAMMA-1.
     *   )*MACH*MACH
     1*R(1)-GW)*S(N)/S(1)
  100 CONTINUE
      RETURN
      END
```

APPENDIX D

COMPUTER PROGRAM SOURCE LISTING FOR THE CALCULATION OF THE TRANSIENT HEAT TRANSFER AND INDUCED PRESSURE

APPENDIX D

FORTRAN PROGRAM

'*' IN COL. 6: THIS LINE IS A PART OF PREVIOUS STATEMENT

```
C      CALCULATION OF UNSTEADY STATE HEAT TRANSFER PARAMETER
C      AND TRANSIENT INDUCED PRESSURE WITH WALL HEAT TRANSFER
C      CASE OF MACH NO.=10,PRANDTL NO.=0.72,CHI=4.5 AND GW=0
     *  (COLD WALL)
       REAL*8 NU,GW,GPRIM,G,GS,U,FOPRIM,FO2PRI,H,GSPRIM,UPRIM
     *  ,NUS,
     1GAWS,MACH,PR,X,GAMMA,DNU,KEI,Y,FPRIM,I,J,I2,DI,DJ,Y1,Z
     *  1,T,P,A,XI,
     2Z,I1,J1,DI1,DJ1,I21,NU1,GPRIM1,DNU1,P1,P2,E,YE,GEPRIM,
     *  NE,DNE,IE,
     3JE,DIE,DJE,REC,GAWS1,NUS1,GSPRI1,IE2,MEO
       DIMENSION NU(51),G(501),GS(501),U(501),FOPRIM(501),GPR
     *  IM(51),
     1FO2PRI(501),NU1(51),   DNU(51),I(51),J(51),DI(51),DJ(5
     *  1),Y(501),
     2FPRIM(501),Y1(501),Z1(501),P(51),Z(501),I1(51),J1(51),
     *  DI1(51),
     3DJ1(51),DNU1(51),P1(51),P2(51),E(501),YE(501),NE(51),D
     *  NE(51),
     4IE(51),JE(51),DIE(51),DJE(51)
       MACH=10.0D0
       PR=0.72D0
       GW=0.0D0
       CHI=4.5D0
       GAMMA=1.4D0
       T=0.01D0
       H=0.01D0
       MM=51
       NN=501
       REC=DSQRT(PR)
C      EVALUATION OF ADIABATIC WALL ENTHALPY RATIO
       GAWS=1.+REC*0.5*(GAMMA-1.)*MACH*MACH
       GAWS1=1.+0.5*(GAMMA-1.)*MACH*MACH
       A=DSQRT(2.D0)
C      READING BLASIUS VALUES FROM TAPE
       READ(3,EPR=10) (X,N=1,NN)
       READ(3,EPR=10) (FOPRIM(N),N=1,NN)
       READ(3,EPR=10,END=20) (FO2PRI(N),N=1,NN)
    20 CONTINUE
```

```
C       READING STEADY STATE GS VALUES WITH WALL HEAT TRANSFER
        READ(4,ERR=10) GS
C       EVALUATION OF STEADY STATE INTEGRAL I2
C       INTEGRATING USING SSP LIBRARY SIMPSON'S RULE
        DO 30 N=1,NN
        Y1(N)=GS(N)-FOPRIM(N)
        Y(N)=1.+0.5*(GAMMA-1.)*MACH*MACH*FOPRIM(N)*(1.-FOPPIM(
       *  N))+(GW-1.)*
       1(1.-FOPRIM(N))-FOPRIM(N)
C       USING VECTOR SPACE E TEMPORARILY  FOR EMPIRICAL ENTHAL
       *  PY DISTRIBUT
        E(N)=1.+(GW-1.)*(1.-FOPRIM(N)**3)+(PR**.333)*(1.+.5*(G
       *  AMMA-1.)*MAC
       1H*MACH*DSQRT(PR)-GW)*FOPRIM(N)*(1.-FOPRIM(N)**2)-.5*(G
       *  AMMA-1.)*PR*
       2(FOPRIM(N)**2)*(1.-FOPRIM(N))*MACH*MACH-FOPRIM(N)
C       USING VECTOR SPACE G TEMPORARILY
        G(N)=Y(N)+FOPRIM(N)
   30 CONTINUE
        CALL DQSF(H,Y1,Z1,NN)
        I2=Z1(NN)
        CALL DQSF(H,Y,Z,NN)
        I21=Z(NN)
        CALL DQSF(H,E,Z,NN)
        IE2=Z(NN)
C       EVALUATING STEADY STATE SLOPE AT PLATE SURFACE USING F
       *  ORWARD DIFFE
        GSPRIM=(-11.*GS(1)+18.*GS(2)-9.*GS(3)+2.*GS(4))/(6.*H)
C       EVALUATION OF STEADY STATE HEAT TRANSFER PARAMETER
        NUS=GSPRIM/(GAWS-GW)
        GSPRI1=(-11.*G(1)+18.*G(2)-9.*G(3)+2.*G(4))/(6.*H)
        NUS1=GSPRI1/(GAWS1-GW)
C       EVALUATION OF INTEGRALS I AND J BY SIMPSON'S RULE
        DO 40 M=1,MM
        DO 50 N=1,NN
        READ(3,ERR=10) X,FPRIM(N),X,X
   50 CONTINUE
C       READING DELTA G (=U) VALUES FROM TAPE(WITH WALL HEAT T
       *  RANSFER)
        READ(4,ERR=10)  (U(N),N=1,NN)
        DO 60 N=1,NN
        G(N)=1.+.5*(GAMMA-1.)*MACH*MACH*FPRIM(N)*(1.-FPRIM(N))
       *  +(GW-1.)*(1.
       1-FPRIM(N))
        Y1(N)=GS(N)-U(N)-FPRIM(N)
        E(N)=1.+(GW-1.)*(1.-FPPIM(N)**3)+(PR**.333)*(1.+.5*(GA
       *  MMA-1.)*MACH
       1*MACH*DSQRT(PR)-GW)*FPRIM(N)*(1.-FPRIM(N)**2)-.5*(GAMM
       *  A-1.)*PR*(FP
       2RIM(N)**2)*(1.-FPRIM(N))*MACH*MACH
C       USING Y VECTOR FOR PR = 1 SOLUTION
        Y(N)=G(N)-FPRIM(N)
```

```
      YE(N) =E(N)-FPPIM(N)
   60 CONTINUE
C     EVALUATING SLOPE AT PLATE SURFACE USING FORWARD DIFFER
     *  ENCE
      UPRIM=(-11.*U(1)+18.*U(2)-9.*U(3)+2.*U(4))/(6.*H)
      GPRIM(M)=GSPRIM-UPRIM
      GPRIM1=(-11.*G(1)+18.*G(2)-9.*G(3)+2.*G(4))/(6.*H)
      GEPRIM=(-11.*E(1)+18.*E(2)-9.*E(3)+2.*E(4))/(6.*H)
C     EVALUATION OF HEAT TRANSFER PARAMETER
      NU1(M)=GPRIM1/(GAWS1-GW)
      DNU1(M)=NU1(M)-NUS1
      NU(M)=GPRIM(M)/(GAWS-GW)
      DNU(M)=NU(M)-NUS
      NE(M)=GEPRIM/(GAWS-GW)
      DNE(M)=NE(M)-NUS
      CALL DGSF(H,Y1,Z ,NN)
      I(M)=Z (NN)
      CALL DGSF(H,Y,Z,NN)
      I1(M)=Z(NN)
      CALL DGSF(H,YE,Z,NN)
      IE(M)=Z(NN)
      DO 70 N=1,NN
      Y1(N)=GS(N)-U(N)-1.
      Y(N)=G(N)-1.
      YE(N)=E(N)-1.
   70 CONTINUE
      CALL DGSF(H,Y1,Z1,NN)
      J(M)=Z1(NN)
      CALL DGSF(H,Y,Z1,NN)
      J1(M)=Z1(NN)
      CALL DGSF(H,YE,Z1,NN)
      JE(M)=Z1(NN)
   40 CONTINUE
      WRITE(6,80) PR,MACH,GW,NUS
   80 FORMAT(1H1,'STEADY STATE HEAT TRANSFER PARAMETER FOR P
     *  R='F6.2,' MA
     1CH NO.'F6.2,' GW 'F6.2,' IS 'F10.5//)
      WRITE(6,90)
   90 FORMAT(1H ,'UNSTEADY HEAT TRANSFER PARAMETER NU'//)
      WRITE(6,100) (NU(M),M=1,MM)
  100 FORMAT(1H ,5F26.8)
      WRITE(6,110)
  110 FORMAT(1H ,'INCREMENTAL HEAT TRANSFER PARAMETER'//)
      WRITE(6,100) (DNU(M),M=1,MM)
      WRITE(6,120) GW
  120 FORMAT(1HC,'UNSTEADY GPRIM FOR GW = 'F6.2//)
      WRITE(6,130) GW,GSPRIM
  130 FORMAT(1H0,'STEADY STATE GSPRIM FOR GW= 'F6.2,' IS 'F1
     *  0.4//)
      WRITE(6,140) PR
  140 FORMAT(1H1,'HEAT TRANSFER PARAMETER FROM EMPIRICAL DIS
     *  TRIBUTION FO
```

```
     1R PR = 'F6.2//)
      WRITE(6,100) (NE(M),M=1,MM)
      WRITE(6,110)
      WRITE(6,100) (DNE(M),M=1,MM)
      WRITE(6,150)
  150 FORMAT(1H1,'HEAT TRANSFER PARAMETER FROM CLOSED FORM S
     *  CLUTICN FOR
     1PR= 1'//)
      WRITE(6,160)
  160 FORMAT(1H ,'UNSTEADY HEAT TRANSFER PARAMETER NU1 FROM
     *  CLCSED FORM
     1SCLUTICN'//)
      WRITE(6,100) (NU1(M),M=1,MM)
      WRITE(6,110)
      WRITE(6,100) (DNU1(M),M=1,MM)
      WRITE(6,170) I2,I21
  170 FORMAT(1H1,'STEADY STATE INTEGRALS I2,I21 ARE '2F15.8/
     *  /)
      WRITE(6,180)
  180 FORMAT(1HO,'ITEGRALS I,I1,J,J1 ARE '//)
      WRITE(6,100) (I(M),M=1,MM)
      WRITE(6,100) (I1(M),M=1,MM)
      WRITE(6,100) (J(M),M=1,MM)
      WRITE(6,100) (J1(M),M=1,MM)
C     EVALUATION OF INTEGRAL DERIVATIVES DI AND DJ
      CALL DDET5(T,I,DI,MM,IER)
      CALL DDET5(T,J,DJ,MM,IER1)
      CALL DDET5(T,I1,DI1,MM,IER)
      CALL DDET5(T,J1,DJ1,MM,IER1)
      CALL DDET5(T,IE,DIE,MM,IERE)
      CALL DDET5(T,JE,DJE,MM,IERE)
      WRITE(6,190)
  190 FORMAT(1HO,'DERIVATIVES DI,DI1,DJ,DJ1 ARE '//)
      WRITE(6,100) (DI(M),M=1,MM)
      WRITE(6,100) (DI1(M),M=1,MM)
      WRITE(6,100) (DJ(M),M=1,MM)
      WRITE(6,100) (DJ1(M),M=1,MM)
C     EVALUATION OF TRANSIENT INDUCED PRESSURE
      K1=0
      K=0
  200 CONTINUE
      XI=0.0D0
      DO 210 M=1,MM
      P(M)=(GAMMA/(MACH*MACH))*(I2/A-A*(1.-XI)*(1.-XI)*DJ(M)
     *  -(1./A)*(I(M
     1)-2.*XI*(1.-XI)*DI(M)))
      P1(M)=(GAMMA/(MACH*MACH))*(A*(1.-XI)*(1.-XI)*DJ(M)+(1.
     *  /A)*(I(M)-2.
     1*XI*(1.-XI)*DI(M)))
      XI=XI+T
  210 CONTINUE
      WRITE(6,220) PR
```

```
  220 FORMAT(1H1,'INDUCED PRESSURE FUNCTION (P/PE)/CHI FOR P
     *  R='F6.2//)
      WRITE(6,100) (P(M),M=1,MM)
      WRITE(6,230) PR
  230 FORMAT(1H0,'INDUCED PRESSURE FUNCTION NOT REFERENCED T
     *  O FINAL STEA
     1DY STATE, FOR PR='F6.2//)
      WRITE(6,100) (P1(M),M=1,MM)
C     EVALUATION OF INDUCED PRESSURE FOR CHI=4.5 AND MACH NO
     *  .=10
C     (USING VECTOR SPACE J)
      DO 240 M=1,MM
      J(M)=CHI*P(M)
      P2(M)=CHI*P1(M)
  240 CONTINUE
      WRITE(6,250) CHI,MACH
  250 FORMAT(1H1,'INDUCED PRESSURE FOR CHI PARAMETER'F6.2,'
     *  AND MACH NO.
     1 'F6.2//)
      WRITE(6,100) (J(M),M=1,MM)
      WRITE(6,260) CHI,MACH
  260 FORMAT(1H0,'INDUCED PRESSURE NOT REFERENCED TO FINAL S
     *  TEADY STATE,
     1FOR CHI PARAMETER'F6.2,' AND MACH NO.'F6.2//)
      WRITE(6,100) (P2(M),M=1,MM)
      IF(K1.GE.1) STOP
      IF(K.GE.1) GO TO 270
      DO 280 M=1,MM
      I(M)=IE(M)
      DI(M)=DIE(M)
      DJ(M)=DJE(M)
  280 CONTINUE
      K=K+1
      GO TO 200
  270 K1=K1+1
      PR=1.
      DO 290 M=1,MM
      I(M)=I1(M)
      DI(M)=DI1(M)
      DJ(M)=DJ1(M)
  290 CONTINUE
      I2=121
      GO TO 200
   10 WRITE(6,300)
  300 FORMAT(' ERROR WHILE READING FROM TAPE')
      STOP
      END
```